UNIVERSITÀ
DEGLI STUDI
FIRENZE

## DOTTORATO DI RICERCA IN
## INGEGNERIA INDUSTRIALE

CICLO XXXII

COORDINATORE Prof. Maurizio De Lucia

# Design and characterization by using computational methodologies and life cycle assessment (LCA) of devices for energy production from renewable energy sources

Settore Scientifico Disciplinare CHIM/06

| **Dottorando** | **Tutore** |
|---|---|
| Dott.ssa Mohammadpourasl Sanaz | Prof.ssa Sinicropi Adalgisa |

**Coordinatore**
Prof. De Lucia Maurizio

Anni 2016/2019

# Acknowledgement

Firstly, I would like to express my sincere gratitude to my tutor Professor Adalgisa Sinicropi, for the motivation and encouraging my research and for allowing me to grow as a researcher. It has been an honor to be her PhD student. Your guidance helped me through each step of writing this thesis.

I would like to acknowledge Professor Riccardo Basosi, your advice all the time of these three years of research and especially in writing thesis has been priceless and thanks for your brilliant suggestions.

I would like to show my appreciation to Dr. Maria Laura Parisi, it was great to have the opportunity to participate your course as a part of my PhD.

I am also pleased to say thank you to Dr. Alessio Dessì and the experimental team in the CNR of Florence University for their collaboration.

A very special gratitude goes to the "La regione Toscana" for helping and providing the funding to make my PhD experience.

My sincere thanks go to Professor S. Shahab Naghavi and Professor Yavar Taghipour Azar who provided me to join their group at the University of Shahid Beheshti in Iran (Tehran), and special thanks to Professor Naghavi for your great comments on my thesis.

I would also like to thank my thesis committee members, thanks for your insightful comments.

A special thanks to my family. Words cannot express how grateful I am. Mom, dad, Elnaz thanks for your moral and emotional support, your prayer for me was what sustained me thus far. I would also like to thank my friends Elahe, Hedieh, Parisa, Samira for your spiritually supporting words. I want also to thank to my colleague Nahid at Shahid Beheshti University who has supported me

# Table of Contents

# List of Abbreviations

| | |
|---|---|
| APAC | Asia-Pacific |
| BIPV | Building-Integrated Photovoltaics |
| CdTe | Cadmium Telluride |
| CB | Conduction Band |
| CE | Counter electrode |
| CED | Cumulative Energy Demand |
| CIGS | Copper Indium Gallium Selenide |
| CSP | Concentrating Solar Power |
| CZTS | Copper Zinc Tin Sulfide |
| DFT | Density Functional Theory |
| D-π-A | Donor-bridge-Acceptor |
| DSSC | Dye Sensitized Solar Cell |
| EC | European Commission |
| EPFL | École Polytechnique Fédérale de Lausanne |
| FF | Fill Factor |
| FMO | Frontier Molecular Orbitals |
| FTO | Fluorine Doped Tin Oxide |
| GaAs | Gallium Arsenide |
| HOMO | Highest Occupied Molecular Orbital |
| ISO | International Standardization Organization |
| ITO | Indium Doped Tin Oxide |
| KS | Kohn-Sham |
| LCA | Life Cycle Assessment |
| LCI | Life Cycle Inventory |
| LCIA | Life Cycle Impact Assessment |
| LHE | Light Harvesting Efficiency |
| LUMO | Lowest Unoccupied Molecular Orbital |
| MEA | Middle East-Africa |
| NIR | Near-Infrared |
| NREL | National Renewable Energy Laboratory |

| | |
|---|---|
| OPV | Organic Photovoltaic |
| PCE | Power Conversion Efficiency |
| PES | Potential Energy Surface |
| PSC | Perovskite Solar Cell |
| Pt | Platinum |
| PV | Photovoltaic |
| QDPV | Quantum Dot Photovoltaic |
| QM | Quantum Mechanics |
| Ru | Ruthenium |
| SETAC | Society of Environmental Toxicology and Chemistry |
| Si | Silicon |
| TCO | Transparent Conductive Oxide |
| TDDFT | Time-Dependent Density Functional Theory |
| $TiO_2$ | Titanium Dioxide |
| UNEP | United Nations Environment Programme |

# CHAPTER I

## Introductory Remarks

# 1. Introductory Remarks

This thesis focuses on the design and characterization of more efficient components for Dye-Sensitized Solar Cells (DSSCs), an example of innovative latest generation photovoltaic systems. DSSCs are considered as a promising alternative to silicon solar cells due to their low cost, flexibility and facile fabrication. However, a low photo-electric conversion efficiency and stability of these cells are the main obstacles for their large-scale commercial applications. An emerging challenge is to find an optimum set of materials to improve the performance of DSSCs. One of the key components to optimize is the light absorbing dye (also referred as sensitizer) that is employed to enhance light harvesting of $TiO_2$ nanoparticles. Indeed, sensitizers are responsible for DSSCs photovoltaic performances, transparency and color.

In this context, purely organic dyes, not containing rare metals, such as ruthenium and other transition metals, and bearing potentially favorable properties, have been introduced. They can be easily prepared using potentially low-cost procedures, have large molar extinction coefficients and their molecular structure, mainly based on the "donor-bridge-acceptor" (D-π-A) structural motif, can be easily modified by means of appropriate molecular design and synthesis.

To this regards, computational chemistry methods can be used to predict the main optoelectronic and electrochemical properties of these sensitizers and thus allowing the design of novel and more efficient dyes for DSSCs applications. Indeed, using these methods, it is possible to compute molecular geometries, vertical excitation and emission maxima, frontier molecular orbitals energies and ground and excited redox potentials. These are key features to check, even prior to the synthesis, the efficiency of investigated sensitizers saving time, efforts and resources. In particular, to be a good dye-sensitizers, it has to: i) strongly absorb the incident photons in the visible to near-infrared region of the spectrum; ii) hold a correct "alignment" between its energy

levels and the other relevant electrochemical potentials of the cell, iii) show a charge transfer nature of its excited states; iv) possess a strong electron coupling of its excited state to the semiconductor manifold of unoccupied states to ensure an efficient electron injection into the $TiO_2$ conduction band. Moreover, if building integration and indoor applications are considered, sensitizers having a blue and green color would be of great interest both for their attractive colors and their capability to absorb in the red and near-infrared region of the spectrum.

Due to the desired large conjugation of the sensitizers and hence the large size of these molecules, the computational methods of choice are based on density functional theory (DFT) and its time-dependent extension (TDDFT), which have been proven to accurately reproduce optical and electrochemical properties of various D-π-A structures.

Considering all these issues, in this thesis, DFT and TDDFT have been applied to: i) the design of a new family of unsymmetrically substituted sensitizers containing the (E)-3,3′-bifuranylidene-2,2′-dione heterocyclic system (Pechmann lactone) for application in DSSCs with the aim of developing higher-performance devices and to increase their commercial appeal; ii) predict the ground state oxidation potential of organic dyes having a medium to large conjugation length which is of paramount importance for the rational design of novel organic sensitizers and greatly contribute to the development of more efficient devices.

Another scope of this thesis is the assessment of the environmental performances connected with the fabrication of DSSCs components, namely the sensitizer, through the application of the Life Cycle Assessment (LCA) methodology. Indeed, to evaluate the sustainability of photovoltaic devices, the investigation of the environmental impacts generated during their fabrication is essential in order to improve and optimize the energy and resource efficiency of manufacturing processes and, ultimately, the environmental footprint of the device. This assessment becomes of

3

paramount importance especially for photovoltaic devices based on innovative technologies that stand out for the use of alternative materials than traditional semiconductors.

LCA is a quantitative method, regulated by the ISO 14040 and 14044 Standards, that allows to calculate the potential impacts associated with a product, process or service. It is considered by the European Commission as the only tool with a scientific basis useful for understanding the environmental loads of a product or process as it provides verifiable quantitative data and allows the identification of the most critical environmental aspects on which to intervene to improve the environmental profile of the analyzed system.

In this thesis, LCA has been employed to investigate the environmental profile of alternative protocols for the synthesis, and eventually the production scale-up, of an organic dye bearing a thiazolo[5,4-d]thiazole ring as central unit, namely the TTZ5, that has been successfully proposed as a sensitizer for the manufacturing of DSSCs.

The remainder of this thesis is organized as follows: in Chapter 2, after a brief section on renewable energies (Section 2.1), the *state of the art* on photovoltaics technologies (Section 2.2) and DSSCs (Section 2.3) is presented. Chapter 3 collects details on the methodologies employed and in particular, Section 3.1 deals with computational chemistry methods and Section 3.2 with Life Cycle Assessment approach. The results obtained in this thesis's work are collected in three papers published or submitted to peer-reviewed international journals and they are inserted in Chapter 4, Sections 4.1-4.3.

# CHAPTER II

## State-of-the-Art

# 2. State-of-the-Art

## 2.1 Renewable Energy

One of the fundamental challenges that societies have faced in 21$^{st}$ century is the crisis of energy that ideally should be solved in an environmentally friendly way and using sustainable energy resources such as solar energy. The ever-increasing demand in energy supplies has accelerated fossil fuels depletion. The fossil fuels beside to the limited availability and non-renewability, severely cause an environmental pollution and consequently global warming. It is estimated that the reserves of fossil fuels around the world could last 40-55 years for oil, 55-70 years for natural gas and 110-160 years for coal, moreover for radioactive material such as uranium is projected for 40-45 years. [1].
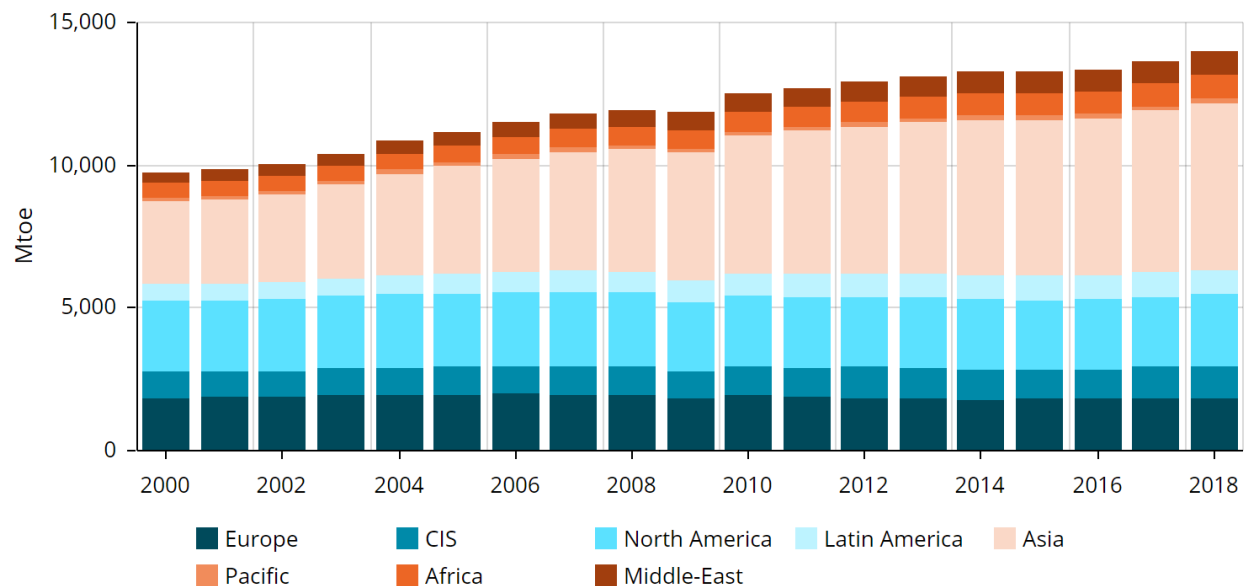


Figure 2.1. Total energy consumption 2000-2018 [2].

In the diagram above, the constantly increasing demand for energy around the world which leads to increasing in energy consumption *vs*. time is showed [2]. In 2018, energy consumption is speeding up by 2.3% which is caused by high demand for electricity and gas. China, which is the

world's largest energy consumer since 2009, had 3.7% growth rate in energy consumption in 2018. On the other hand, energy consumption in the European Union has decreased mostly due to the energy efficiency improvement and lower consumption in the power sector [2].

| | |
|---|---|
| China | 3,164 |
| United States | 2,258 |
| India | 929 |
| Russia | 800 |
| Japan | 424 |
| South Korea | 307 |
| Germany | 301 |
| Canada | 301 |
| Brazil | 290 |
| Iran | 265 |
| Indonesia | 251 |
| France | 243 |

Figure 2.2. Energy consumption 2018 (unit=Mtoe) [2].

In this scenario, unless we give renewable energy a serious thought, the problem of energy crisis cannot be solved. Currently, many countries are oriented to the broader exploration of renewable energy sources.
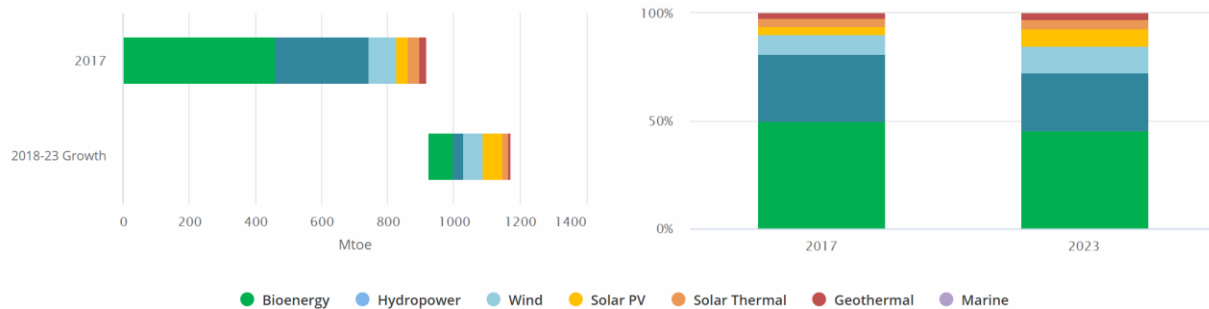
Figure 2.3. Renewable energy consumption by technology, 2017-2023 [3].

Bioenergy and hydropower are dominant renewable sources which are mainly exploited, but their share of total renewable consumption decrease from 2017 to 2023 as shown in the above diagram,

instead solar PV and wind are increasing from 2017 to 2023 [3]. Geothermal, Tidal and solar energy are other renewable energy sources.

Among renewable energy technologies, solar energy technologies have a great potential to produce energy and can improve rapidly as solar energy is one of the most abundant resources in the world. As well known, the sun strikes the earth in 1 hour providing more energy than all of the energy consumed by humans in an entire year [4]. Photovoltaic system (PV) is one of the four solar energy technologies, the others are concentrating solar power (CSP), solar thermal and solar fuels. PV is the field of technology related to the devices which directly convert sunlight into electricity. The basic building block of PV systems is PV solar cells. Solar cells are made of semiconductor materials, which are fundamental components that carry out the conversion of light into electricity.

## 2.2 Photovoltaics

Albert Einstein has explained the photovoltaic effect when he has published his famous paper in 1905 [5]. After that, the research in this area continued and developed to prepare solar cell materials that are currently used in PV technology. PV technology based on silicon wafer solar cells developed by the beginning of 20$^{th}$ century. Photovoltaic cells based on their primary active material are classified in three generations, which are named respectively traditional silicon solar cells, thin-film solar cells, and emerging solar cells.

### 2.2.1 Traditional Silicon Solar Cells

This technology is mainly based on a crystalline semiconductor which is silicon. They are the first commercially available photovoltaics technologies. This type of PV solar cell is currently dominant in the market due to their high efficiency ($\eta \approx 25\%$) and long durability (20-25 years),

This first generation of solar cells (see Figure 2.4) is well-matured in terms of their technology and fabrication process. These cells are based on two main types of silicon:

1- Monocrystalline

2- Polycrystalline

The monocrystalline is made from a single crystal of silicon, while polycrystalline is made from many silicon fragments melted together. The electrons that generate a flow of electricity have more room to move in a cell composed of a single crystal, thus monocrystalline silicon-based panels have higher efficiencies than polycrystalline options, therefore monocrystalline panel can produce more watt per hour using less materials, and thus less space. They have a darker black color while polycrystalline solar panels typically are bluer. Besides the crystalline silicon-based solar cells, also those cells which are made of GaAs wafer are classified in the first generation.
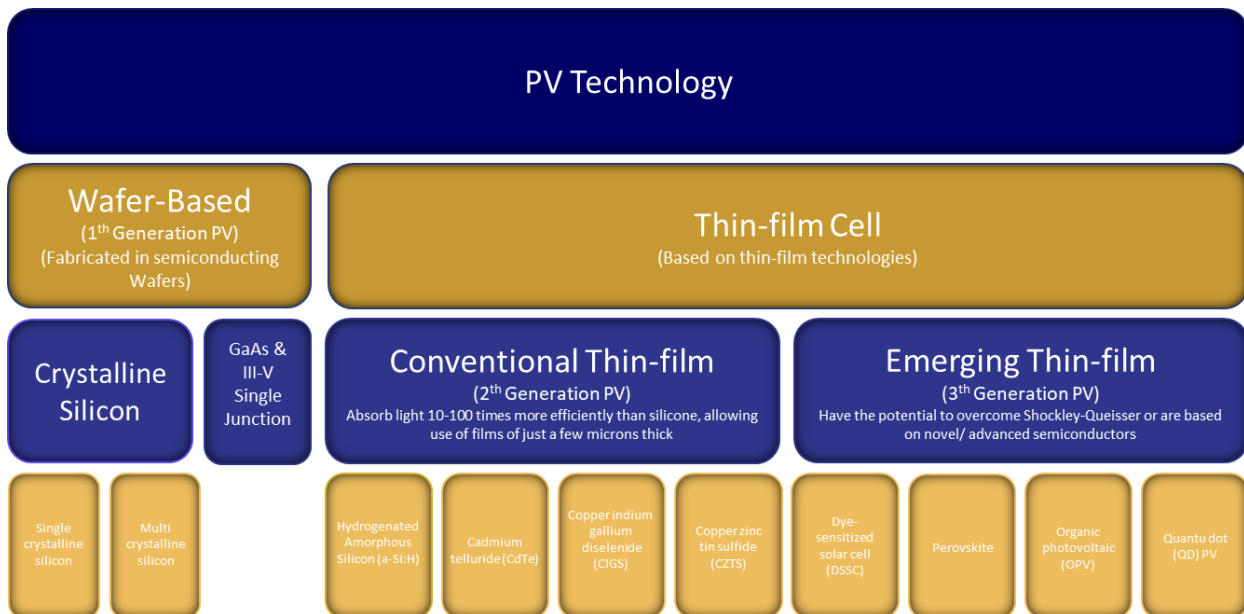


Figure 2.4. Main classes of PV technology.

## 2.2.2 Thin-Film Solar Cells

Second-generation solar cells were developed with the aim of reducing the costs of materials and manufacturing process through the utilization of thin-film technology, thus they are usually called thin-film solar cells. In fact, when compared to crystalline silicon-based cells, they are made from layers of semiconductor materials only a few micrometers thick. In this technology, the semiconductor of the most used cells is amorphous silicon [6], cadmium telluride (CdTe) [7], or copper indium gallium selenide (CIGS) [8]. As thin-film solar cells are semitransparent and flexible and lightweight they can be applied as window glazing for the building-integrated photovoltaics (BIPV) market.

## 2.2.3 Emerging Solar Cells

Third-generation technologies or emerging solar cells have tried to overcome the theoretical solar conversion efficiency limit which was calculated in 1961 by Shockley-Queisser [10]. They include Dye-sensitized solar cells (DSSCs), perovskites solar cells (PSCs), organic photovoltaic (OPV) and quantum dot (QDPV). They are considered as promising inexpensive alternative to traditional silicon-based PV. Most of the third-generation solar cells are still in research step by the aim of optimizing the energy conversion efficiency and stability, which are the two major challenges for the commercialization.

## 2.2.4 Solar Cell Efficiencies

Figure 2.5 shows the efficiency of solar cells evaluated by the National Renewable Energy Laboratory (NREL) [10]. The latest registered efficiency for DSSCs which are subjected in this thesis is 12.3% that is achieved by École Polytechnique Fédérale de Lausanne (EPFL).
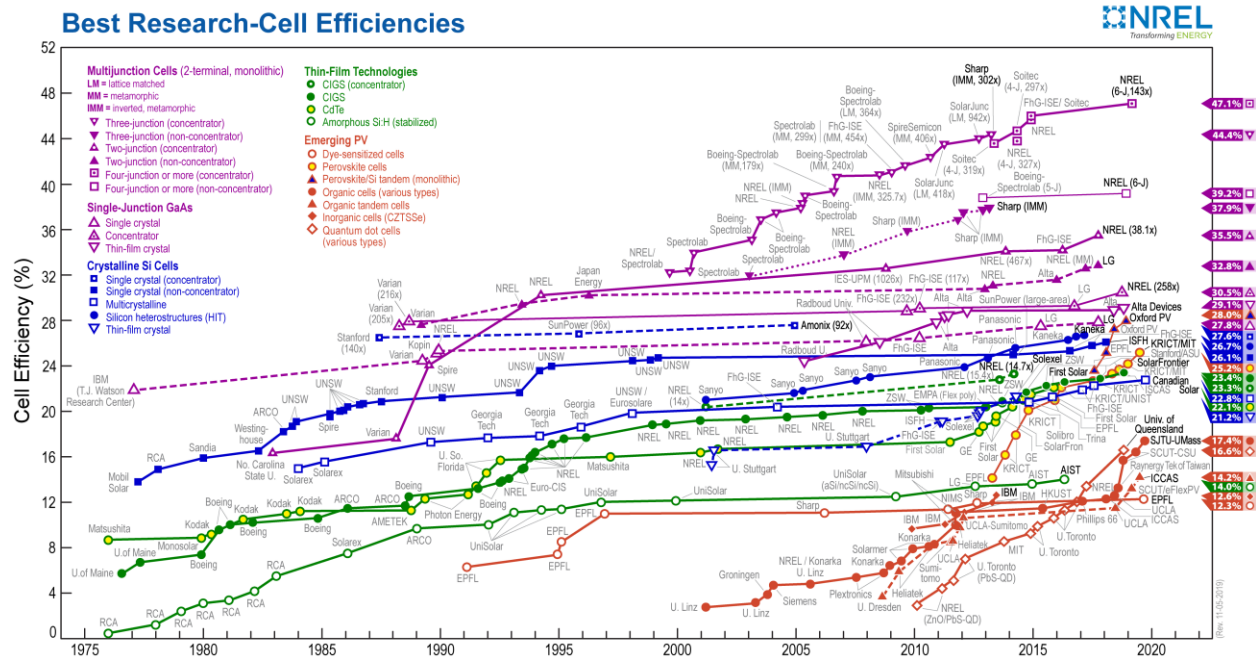
Figure 2.5. Efficiency chart for solar cells [10].

## 2.2.5 Global Installed Capacity

The total installed PV power capacity reached half a terawatt by the end of 2018 [11]. Since the beginning of the century total solar power has increased by nearly 320 times. One year earlier at the end of 2017, the total global solar power capacity reached to 400 GW, therefore in a year, the installed PV capacity improved 100 GW. More than half of the increased global power generation capacity in 2018 refers to the Asia-Pacific (APAC) region, Europe has the second position and the Americas has the world's third position. The world market share of the Middle East and Africa (MEA) have slightly increased.
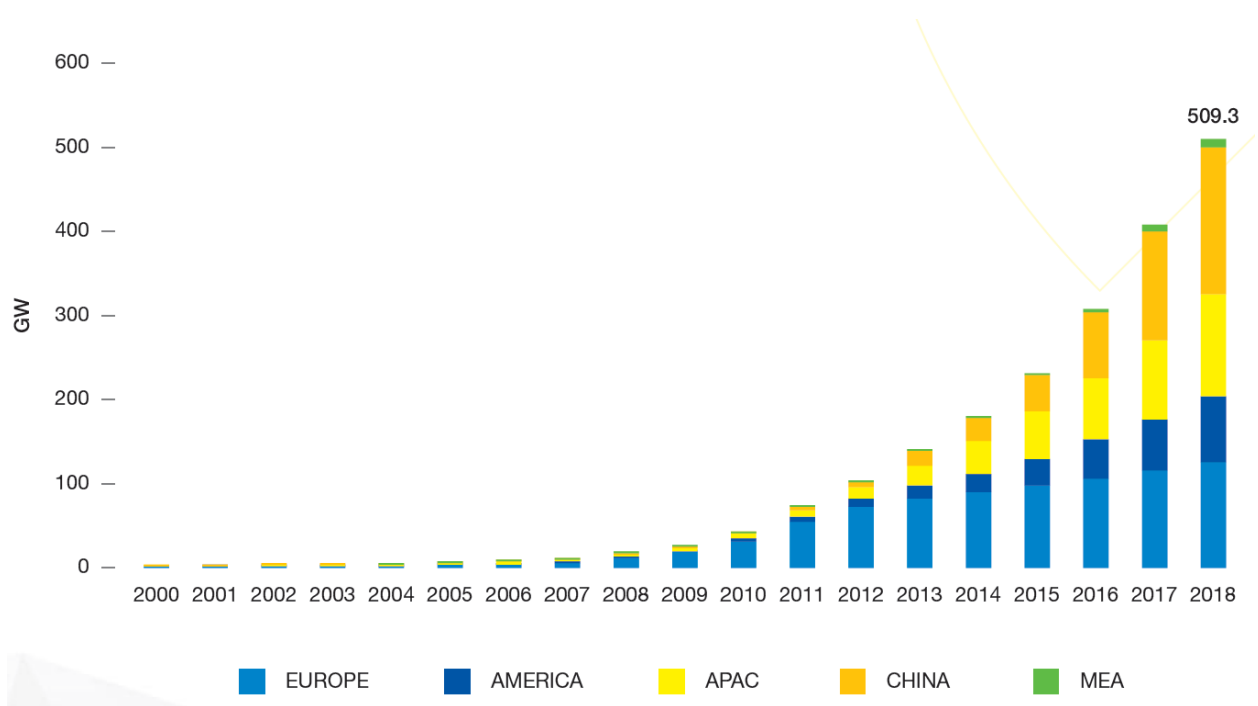
Figure 2.6. Global total solar PV installed capacity 2000-2018 [11].

## 2.3 Dye Sensitized Solar Cells

### 2.3.1 Initial Development

DSSCs were first invented by Grätzel and O'Regan in 1991 as a promising inexpensive alternative to traditional silicon-based PV cells [12-16]. There are several features that turn DSSCs to a promising candidate for solar cell applications such as easier production process compared to silicon cells, high transparency, tunable color, high mechanical flexibility and ability of working under diffused light [17-23]. Even though the conversion efficiency of dye-sensitized solar cells is lower than that of other solar cells, they can still play a role in the solar market, in particular because their aesthetic and transparency can allow their integration into building-integrated photovoltaic (BIPV) applications [20,24,25], moreover their high efficiency under indoor lighting is considerable [22]. Recently Cao and his coworkers introduced an advance structure of DSSCs

that achieved power conversion efficiency (PCE) over the best available silicon or GaAs based photovoltaics, they have reached 32% under artificial indoor light and 13.1% under sunlight illumination [23].

## 2.3.2 Components and Mechanism

**- Components of DSSCs**

The DSSCs contain a set of different layers (see Figure 2.7), including:

    I.    Glass substrate

    II.    Transparent conductive oxide (TCO)

    III.    Nanocrystalline semiconductor (generally $TiO_2$)

    IV.    Sensitizer (dye)

    V.    Electrolyte

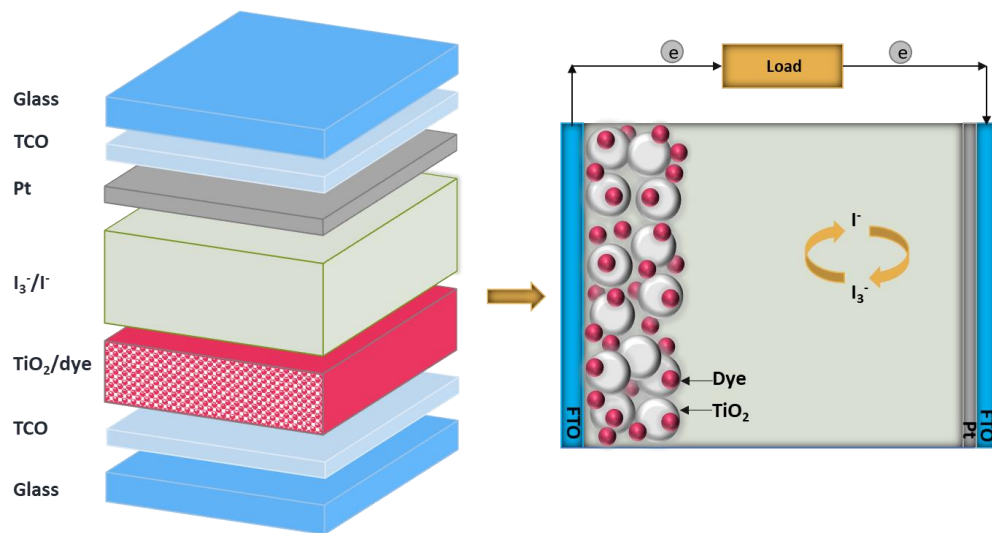    VI.    Counter electrode (generally Pt)



Figure 2.7. Schema of DSSC

Glass substrate and Transparent conductive oxide (TCO)

DSSCs are made up of two highly transparent glass sheets that are coated with a thin layer of conductive oxide. Conductivity and transparency are of course critical for this application as they let the sunlight pass to the effective area of solar cell. Conductive oxides are typically fluorine doped tin oxide (FTO) or indium doped tin oxide (ITO) [26].

Nanocrystalline semiconductor

Nanocrystalline Semiconductors perform as a scaffold for the dye sensitizer. A layer of mesoporous semiconductor oxide ($TiO_2$, ZnO or $SnO_2$) is deposited on a TCO to makes photo-anode. The deposition technique for the thin film preparation is screen printing. Among all semiconductor oxides, $TiO_2$ is the most common choice due to its appropriate properties: high porosity for dye loading, high conductivity, high stability, appropriate band alignment with respect to dye and electrolyte, nontoxicity, biocompatibility, abundance and low cost [26].

Sensitizer (dye)

Sensitizers are the key material of the DSSC since they harvest the solar energy. Sensitizer is covalently bonded to the semiconductor via anchoring group such as carboxylic group. A strong absorption of the dye molecules on the surface of semiconductor leads to a more efficient electron injection from an excited state of the dye to the conduction band (CB) of the semiconductor.

Electrolyte

Currently, the most common electrolyte is liquid containing iodide/triiodide, however in 2010 cobalt was used as redox mediator [27]. The ideal electrolyte is the one with low viscosity, high dielectric properties, high boiling point and environmental sustainability. The electrolyte

containing iodide/triiodide redox couple is convenient choice for DSSCs as it shows appropriate characteristics such as high thermal and chemical stability, high ionic conductivity and non-volatility. The durability and lifetime of DSSCs can be reduced by degradation mechanisms like the leakage, corrosion of the Pt counter electrode by the iodide/triiodide redox couple of electrolyte and detachment of dye of the semiconductor surface which can reduce the long-term stability of the cells [23,28,29]. For these reasons, solid state electrolytes have been developed [30].

Counter electrode (CE)

The Counter electrode (CE) consists of TCO sheets coated with Pt [31]. Pt is an appropriate material for the CE due to its good catalytic activity, excellent performance in reduction of $I_3^-$ and transparency.

**-Mechanism of DSSCs**

DSSCs have a process similar to natural photosynthesis. As shown in Figure 2.8, the absorption of solar energy by the sensitizer (dye) causes excited electrons to be injected to the CB of the semiconductor, generally $TiO_2$. The injected electrons diffuse through the nanocrystalline semiconductor to the photo-anode (FTO), then passing through the external circuit (generating an electric current) toward the counter electrode (cathode). These electrons are then collected by the electrolyte that contains redox couple ($I^-/I_3^-$). Finally, the oxidized dye molecules are reduced to their original ground state by reduced species of the electrolyte and the circuit is closed [32,33]. There are some undesirable recombination processes that should be avoided. Indeed, the injected electrons from the CB of $TiO_2$ may recombine either with the oxidized dyes or with the redox couple lowering the photovoltaic performances of DSSCs.
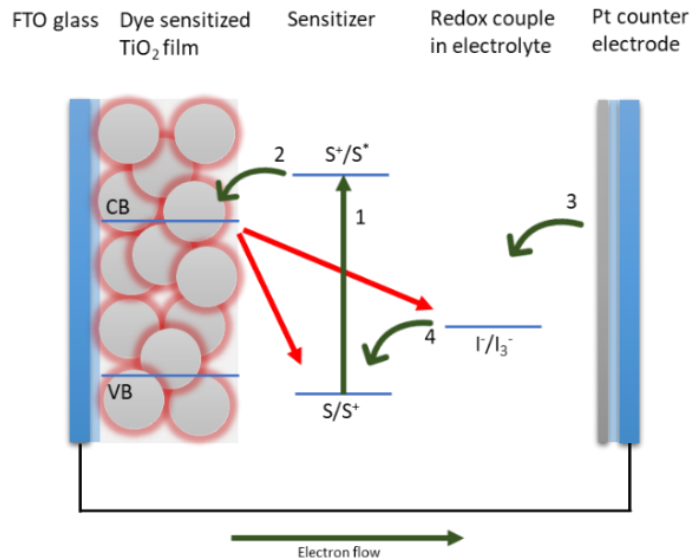
Figure 2.8. Electron transfer process in DSSC

### 2.3.3 Sensitizer (Dye)

Dye has essential role in absorbing and converting solar energy to electricity. An efficient photosensitizer should:

- Absorb strongly on the surface of the semiconductor by its anchoring group;

- Have a high extinction coefficient;

- Be stable enough in its oxidized state to be reduced by the electrolyte;

- Be stable long enough in its excited state to permit an efficient electron injection to the CB of semiconductor oxide;

- Absorb largely in the visible region of the spectrum and even in the near-infrared (NIR);

- Have LUMO energy levels higher than the CB of the semiconductor and HOMO energy levels lower than the redox potential of the electrolyte. These requirements (see Figure 2.9)

allow for an efficient electron injection and an efficient regeneration of the oxidized state of the sensitizer [34,35].
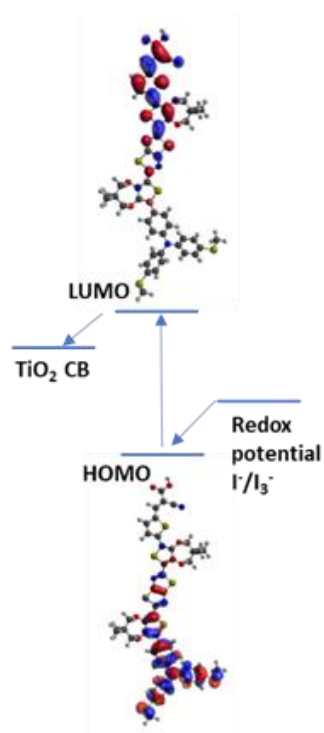


Figure 2.9. Alignment of semiconductor/dye/redox couple energy levels

In general, there are three main classes of photosensitizers:

**i) Metal complex sensitizers**

Among metal complexes, Ru(II)-polypyridyl complexes have been synthesized and have shown the best photovoltaic properties with a photoconversion of 11.7% [36] .

**ii) Natural sensitizers**

They can be extracted from flowers, fruits and vegetables in the form of anthocyanin, carotenoid, flavonoid and chlorophyll pigments. Although they have positive features such as easiness of extraction, low cost and toxicity, their low efficiency severely limits their application.

## iii) Metal free organic sensitizers

Metal free organic dyes have been developed as an alternative to metal-based complexes whose cost, low availability and toxicity limit the large-scale application. Metal free organic sensitizers have high molar extinction coefficient, tunable energy levels and low-cost preparation processes. The impressive performance of organic dyes has yielded an efficiency over 12.5% [37]. Efficient organic sensitizers have a D-π-A structure (see Figure 2.10) that is made of a donor (D), a conjugated linker (π) and an acceptor (A) [38-40]. In this system an electron-rich group role as the donor group (D), that could be linked through a conjugated linker (π) to the electron-deficient acceptor (A) which acts as the anchoring group linked directly to the semiconductor.
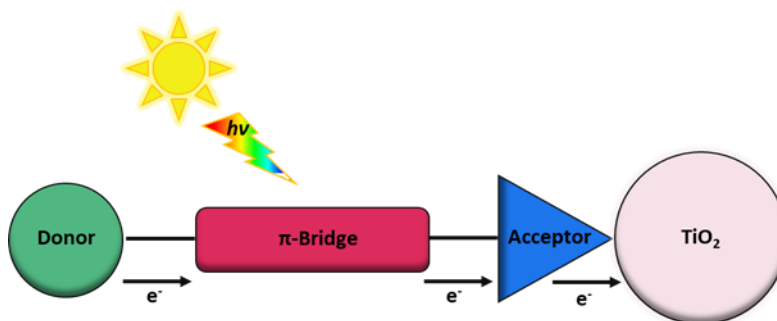


Figure 2.10. D-π-A structure

Two other successful structures are made of an auxiliary acceptor (D-A-π-A) or donor (D-D-π-A) added to the basic structure that can improve stability, facilitate the intramolecular electron transfer, inhibit dye aggregation and enhance photovoltaic performance [41-43].

The aggregation of dye molecules on the semiconductor surface should be avoided by incorporating long alkyl chains and aromatic groups into the dye structure.

The easily tunable D-π-A or D-A-π-A structure of the organic dye is a key to influence the level of HOMOs and LUMOs and thus to enhance their photovoltaic performances [44].

### 2.3.4 Photovoltaic Parameters

The solar energy-to-electricity conversion (power conversion efficiency) that mainly govern the performances of DSSCs is represented by the following equation [45,46]:

$$PCE = \frac{J_{sc} V_{oc} FF}{I_0} \tag{1}$$

$J_{sc}$ stands for the short-circuit current, and is the current which flows under illumination and is expressed as [45]:

$$J_{sc} = \int_{\lambda} LHE(\lambda) \Phi_{inject} \eta_{collect} d\lambda \tag{2}$$

Where $LHE(\lambda)$ is the light harvesting efficiency, $\Phi_{inject}$ is electron injection efficiency and $\eta_{collect}$ is the electron collection efficiency. In DSSC with only different dyes, the $\eta_{collect}$ can be reasonably considered constant, therefore the increasing of $J_{sc}$ depends on the $LHE(\lambda)$ and $\Phi_{inject}$.

The open circuit voltage $(V_{oc})$ is the voltage at the open terminals under illumination and is given by:

$$V_{oc} = E_F - E_{redox}$$

Where  $E_F = \frac{E_{cb}}{e} - \frac{kT}{e} \ln\left(\frac{n}{N_{cb}}\right)$ \tag{3}

Where $E_{cb}$ is the energy level of the TiO$_2$ CB, $k$ is the Boltzmann constant, $T$ is the temperature, $n$ is density of CB electrons in TiO$_2$ and $e$ is the elementary charge [47].

The $FF$ stands for the fill factor and is the ratio of the maximum power $P_{max}$ to the product of $J_{sc}$ and $V_{oc}$. $FF$ is described by the following equation:

$$FF = \frac{J_{max} V_{max}}{J_{sc} V_{oc}} \qquad (4)$$

And $I_0$ is the intensity of incident solar power on the cell (generally 100 mW cm$^{-2}$).

## 2.4 References

[1] R. Basosi, *Conference of Energy from the Principles of Thermodynamics to Sustainable Development*, Istanbul, 2014.

[2] "https://yearbook.enerdata.net."

[3] "https://www.iea.org/renewables2018."

[4] N. S. Lewis, "Toward Cost-Effective Solar Energy Use," *Science,* vol. 315, pp. 798–801, 2007.

[5] A. Einstein. "The Quantum Theory of Radiation," Physikalische Zeitschrift, vol. 18, pp. 121–128, 1917.

[6] C. R. Wronski, *Conference Record of the 28$^{th}$ IEEE Photovoltaic Specialists Conference, Anchorage, AK, IEEE:* New York, pp. 1–6, 2000.

[7] J. Britt and C. Ferekides, "Thin-film CdS/CdTe solar cell with 15.8% efficiency," *Appl. Phys. Lett.,* vol. 62, no. 22, pp. 2851–2852, 1993.

[8] M. A. Green, *Third Generation Photovoltaics: Advanced Solar Energy Conversion*, Springer-Verlag: Berlin, Heidelberg, 2003.

[9] W. Shockley and H. J. Queisser, "Detailed balance limit of efficiency of p-n junction solar cells," *J. Appl. Phys.,* vol. 32, no. 3, pp. 510–519, 1961.

[10] "https://www.nrel.gov/pv/assets/pdfs/best-research-cell-efficiencies.20191106.pdf"

[11] "https://www.solarpowereurope.org/wp-content/uploads/2019/05/SolarPower-Europe-Global-Market-Outlook-2019-2023.pdf."

[12] B. O'Regan and M. Grätzel, "A low-cost, high-efficiency solar cell based on dye-sensitized colloidal $TiO_2$ films," vol. 353, *Nature*., pp. 737–740, 1991.

[13] M. Grätzel, "Dye-sensitized solar cells," *J. Photoch. Photobio. C*., vol. 4, pp. 145–153, 2003.

[14] B. E. Hardin, H. J. Snaith, and M. D. McGehee, "The renaissance of dye-sensitized solar cells," *Nat. Photonics,* vol. 6, pp. 162–169, 2012.

[15] N. Robertson, "Optimizing dyes for dye-sensitized solar cells," *Angew. Chem. Int. Ed*., vol. 45, no 1, pp. 2338–2345, 2006.

[16] A. Hagfeldt, G. Boschloo, L. Sun, L. Kloo, and H. Pettersson, "Dye-Sensitized Solar Cells," *Chem. Rev*., pp. 6595–6663, 2010.

[17] D. Joly et al., "A robust organic dye for dye sensitized solar cells based on iodine/iodide electrolytes combining high efficiency and outstanding stability," *Sci. Rep.,* vol. 4, pp. 1–7, 2014.

[18] S. Mathew et al., "Dye-sensitized solar cells with 13% efficiency achieved through the molecular engineering of porphyrin sensitizers," *Nat. Chem.,* vol. 6, pp. 242-247, 2014.

[19] A. Fakharuddin, R. Jose, T. M. Brown, F. Fabregat-Santiago and J. Bisquert, "Environmental Science A perspective on the production of dye-sensitized solar modules," *E. Environ. Sci.,* vol. 7, pp. 3952–3981, 2014.

[20] M. Grätzel, "Photo-Electrochemical Cells ," *Nature.* vol. 414, pp. 338-344, 2001.

[21]    K. Kakiage, Y. Aoyama, T. Yano, K. Oya, J. Fujisawa and M. Hanaya., "Highly-efficient dye-sensitized solar cells with collaborative sensitization by silyl-anchor and carboxy-anchor dyes," *Chem. Commun.,* vol. 51, pp. 15894-15897, 2015.

[22]    M. Freitag *et al*., "Dye-sensitized solar cells for efficient power generation under ambient lighting," *Nat. Photonics*, vol. 11, pp. 372–378, 2017.

[23]    Y. Cao *et al*., "Direct Contact of Selective Charge Extraction Layers Enables High-Efficiency Molecular Photovoltaics" *Joule,* vol 2, pp. 1–10, 2018.

[24]    S. Sharma, B. Siwach, S. K. Ghoshal, and D. Mohan, "Dye sensitized solar cells: From genesis to recent drifts," *Renew. Sustain. Energy Rev*., vol. 70, pp. 529–537, 2017.

[25]    P. Selvaraj, A. Ghosh, T. K. Mallick, and S. Sundaram, "Investigation of semi-transparent dye-sensitized solar cells for fenestration integration," *Renew. Energy*, vol. 141, pp. 516–525, 2019.

[26]    W. Ghann et al., "Fabrication, Optimization and Characterization of Natural Dye Sensitized Solar Cell," *Sci. Rep.*, vol. 7,pp. 1–12, 2017.

[27]    S. M. Feldt, E. A. Gibson, E. Gabrielsson, and L. Sun, "Design of Organic Dyes and Cobalt Polypyridine Redox Mediators for High-Efficiency Dye-Sensitized Solar Cells," *J. Am. Chem. Soc*. pp. 16714–16724, 2010.

[28]    M. I. Asghar et al., "Review of stability for advanced dye solar cells," *Energy Environ. Sci.,* vol. 3, pp. 418–426, 2010.

[29]    H. Matsui, K. Okada, T. Kitamura, and N. Tanabe, "Thermal stability of dye-sensitized solar cells with current collecting grid," *Sol. Energy Mater. Sol. Cells,* vol. 93, pp. 1110–1115, 2009.

[30]    I. Benesperi, H. Michaels, and M. Freitag, "The researcher's guide to solid-state dye-sensitized solar cells," *J. Mater. Chem. C*, vol. 6, pp. 11903–11942, 2018.

[31]    J. Wu et al., "Counter electrodes in dye-sensitized solar cells," *Chem. Soc. Rev.*, vol. 46, pp. 5975–6023, 2017.

[32]    G. Hashmi et al., "Review of materials and manufacturing options for large area flexible dye solar cells," *Renew. Sustain. Energy Rev.,* vol. 15, pp. 3717–3732, 2011.

[33]    M. Z. H. Khan, M. R. Al-Mamun, P. K. Halder, and M. A. Aziz, "Performance improvement of modified dye-sensitized solar cells," *Renew. Sustain. Energy Rev.,* vol. 71, pp. 602–617, 2017.

[34]    M. Pastore and F. De Angelis, "Intermolecular interactions in dye-sensitized solar cells: A computational modeling perspective," *J. Phys. Chem. Lett.,* vol. 4, pp. 956–974, 2013.

[35]    N. Martsinovich and A. Troisi, "High-throughput computational screening of chromophores for dye-sensitized solar cells," *J. Phys. Chem. C*, vol. 115, pp. 11781–11792, 2011.

[36]    A. Carella, F. Borbone, and R. Centore, "Research progress on photosensitizers for DSSC," *Front. Chem.*, vol. 6, pp. 1–24, 2018.

[37]    Z. Yao, M. Zhang, H. Wu, L. Yang, R. Li, and P. Wang, "Donor/Acceptor Indenoperylene Dye for Highly Efficient Organic Dye-Sensitized Solar Cells," *J. Am. Chem. Soc.*, vol. 137, pp. 3799–3802, 2015.

[38]    R. Tarsang, V. Promarak, and T. Sudyoadsuk, "Journal of Photochemistry and Photobiology A : Chemistry Tuning the electron donating ability in the triphenylamine-based D- π -A architecture for highly efficient dye-sensitized solar cells," *J. Photochem. Photobiol. A. Chem.,* vol. 273, pp. 8–16,

2014.

[39]    Z. Chen, F. Li, and C. Huang, "Organic D- π -A Dyes for Dye-Sensitized Solar Cell," *Curr. Org. Chem.*,pp. 1241–1258, 2007.

[40]    F. Hajizadeh, A. Reisi-vanani, and Y. T. Azar, "Theoretical design of Zn-dithiaporphyrins as sensitizer for dye-sensitized solar cells," *Curr. Appl. Phys.,* vol. 18, pp. 1122–1133, 2018.

[41]    A. Dessì et al., "New Blue Donor-Acceptor Pechmann Dyes: Synthesis, Spectroscopic, Electrochemical, and Computational Studies," *ACS Omega,* vol. 4, pp. 7614–7627, 2019.

[42]    J. He et al., "Bithiazole-bridged dyes for dye-sensitized solar cells with high open circuit," *J. Mater. Chem.,* vol. 21, pp. 6054–6062, 2011.

[43]    W. Zhu et al., "Organic D-A- π -A Solar Cell Sensitizers with Improved Stability and Spectral Response," *Adv. Funct. Mater*., pp. 756–763, 2011.

[44]    S. Mandal, R. Vedarajan, and N. Matsumi, "Computational Investigation of the Influence of p - Bridge Conjugation Order of Thiophene and Thiazole Units in Triphenylamine Based Dyes in Dye-Sensitized Solar Cells," *ChemistrySelect.,* pp. 3582–3590, 2018.

[45]    A. Fitri, A. T. Benjelloun, M. Benzakour, M. McHarfi, M. Hamidi, and M. Bouachrine, "Theoretical investigation of new thiazolothiazole-based D-π-A organic dyes for efficient dye-sensitized solar cell," *Spectrochim. Acta - Part A. Mol. Biomol. Spectrosc.*, vol. 124, pp. 646–654, 2014

[46]    M. R. Narayan, "Review: Dye sensitized solar cells based on natural photosensitizers," *Renew. Sustain. Energy Rev.,* vol. 16, pp. 208–215, 2012.

[47]    A. Reinders, P. Verlinden, W. Sark, A. Freundlich, *Photovoltaic Solar Energy from Fundamentals to Applications*, Wiley & Sons, 2017.

# CHAPTER III

# Methods

# 3.Methods

## 3.1 Computational Chemistry Methods

In this paragraph, a brief introduction to the basis of density functional theory which has been used in this thesis is described.

### 3.1.1 Density Functional Theory

Density functional theory, as we know it today, was born in 1964 when a landmark paper was published by Hohenberg and Kohn in Physical Review. The theorems proved in this paper are the main theoretical pillars of the all density functional theories [1-5]. Each of the theorems are presented here.

#### 3.1.1.1 The Hohenberg–Kohn Theorems

Hohenberg and Kohn proved that for molecules with a non-degenerate ground state, the ground state energy and all other molecular electronic properties are uniquely determined by the ground state electronic probability density $\rho_0$ [1]. The ground state electronic energy $E_0$ is a functional of $\rho_0$, that is

$$E_0 = E_0[\rho_0] \tag{1}$$

Square brackets represent the functional relation. In fact, density functional theory attempts to calculate $E_0$ and other ground state molecular properties from ground state electronic density $\rho_0$. Electrons interact with each other through an external potential.

Suppose two different external potentials $v_a$ and $v_b$ correspond to a non-degenerate ground state density $\rho_0$. These two potentials have two Hamiltonian $H_a$ and $H_b$, respectively. Each of these Hamiltonian, will be associated with a ground state wave function, and its eigenvalue $E_0$. The

variation theorem of molecular orbital theory states that the expectation value of Hamiltonian $a$ over the wave function $b$ must be greater than the ground state energy $a$, i.e [1,4].

$$E_{0,a} < \langle \Psi_{0,b} | H_a | \Psi_{0,b} \rangle \tag{2}$$

We can rewrite this as follows

$$\begin{aligned} E_{0,a} &< \langle \Psi_{0,b} | H_a - H_b + H_b | \Psi_{0,b} \rangle \\ &< \langle \Psi_{0,b} | H_a - H_b | \Psi_{0,b} \rangle + \langle \Psi_{0,b} | H_b | \Psi_{0,b} \rangle \\ &< \langle \Psi_{0,b} | v_a - v_b | \Psi_{0,b} \rangle + E_{0,b} \end{aligned} \tag{3}$$

Since $v$ potentials are one-electron operators, we can write the last line integral as ground state density terms

$$E_{0,a} < \int [v_a(r) - v_b(r)] \rho_0(r) dr + E_{0,b} \tag{4}$$

We do not differentiate between $a$ and $b$, so we can write the same expression for $b$

$$E_{0,b} < \int [v_b(r) - v_a(r)] \rho_0(r) dr + E_{0,a} \tag{5}$$

By adding two inequalities we get

$$\begin{aligned} E_{0,a} + E_{0,b} &< \int [v_b(r) - v_a(r)] \rho_0(r) dr + \int [v_a(r) - v_b(r)] \rho_0(r) dr + E_{0,b} + E_{0,a} \\ &< \int [v_b(r) - v_a(r) + v_a(r) - v_b(r)] \rho_0(r) dr + E_{0,b} + E_{0,a} \\ &< E_{0,b} + E_{0,a} \end{aligned} \tag{6}$$

We came up with an impossible result, so we conclude that our initial assumption was wrong. Therefore, the density of the non-degenerate ground state must determine the external potential and therefore the Hamiltonian and wave function. Hamiltonian not only specifies the ground state wave function, but also all the wave functions of the excited states. Therefore, much information is hidden in density.

The Hohenberg–Kohn Variational Theorem

The first Hohenberg-Kohn theorem does not tell us how to predict the density of a system. Like molecular orbital theory, here we need something to help optimize our fundamental quantity [4].

Suppose we have a well-behaved density that gives the number of electrons N by integrating. The first theorem states that a density determines a wavefunction and a Hamiltonian. We can calculate an expectation value of energy. Therefore, we can choose different densities and know those that provide lower energies are more accurate. In their second theorem, Hohenberg and Kohn showed that density follows a variation principle. They proved that for any trial density function $\rho_{tr}$ that satisfies the following two conditions for all r [1]

$$\int \rho_{tr}(r)dr = n \quad and \quad \rho_{tr}(r) \geq 0 \tag{7}$$

the following inequality holds

$$E_0 \leq E_v[\rho_{tr}] \tag{8}$$

Since $E_0 = E_v[\rho_0]$, the true ground state electronic density minimizes the energy functional $E_v[\rho_{tr}]$. Hohenberg and Kohn proved their theorems only for non-degenerate ground states, but Levi also proved these for degenerate states [4].

So far, we have found a correspondence between density and Hamiltonian and wave function and therefore energy, but we have not presented any mathematical formalism for how density can determine energy in a variational equation without using the wave function. Such an approach was first introduced in 1965.

**3.1.1.2 The Kohn-Sham Equations**

The considerable step in developing the modern density functional theory was in 1965 when Kohn and Sham arranged a practical method for finding $\rho_0$ and, $E_0$ from $\rho_0$ [6]. The results of their formulation on DFT is known as the Kohn-Sham (KS) method, which is capable, in principle, of yielding the exact results, but due to the presence of an unknown term, it yields approximate results [1]. They assumed that the original many-body interacting system could be replaced by considering a fictitious system reference of non-interacting electrons with ground state density same as the original system [7]. The energy functional is described as [4],

$$E[\rho_{(r)}] = T_{ni}[\rho(r)] + V_{ne}[\rho(r)] + V_{ee}[\rho(r)] + \Delta T[\rho(r)] + \Delta V_{ee}[\rho(r)] \tag{9}$$

The components in the above equation refer to the kinetic energy of the non-interacting system $T_{ni}[\rho(r)]$, the nuclear-electron interaction ($V_{ne}[\rho]$), the electron-electron repulsion ($V_{ee}[\rho]$), the correction to the kinetic energy for the interaction of electrons $\Delta T[\rho(r)]$ and all non-classical corrections to electron-electron repulsion energy $\Delta V_{ee}[\rho(r)]$. Within an orbital expression for the density, we can rewrite the equation (9) as,

$$E[\rho(r)] = \sum_i^N \left( \left\langle \chi_i \left| -\frac{1}{2} \nabla_i^2 \right| \chi_i \right\rangle - \left\langle \chi_i \left| \sum_k^{nuclei} \frac{Z_k}{|r_i - r_k|} \right| \chi_i \right\rangle \right) \tag{10}$$

$$+ \sum_i^N \left\langle \chi_i \left| \frac{1}{2} \int \frac{\rho(\acute{r})}{|r_i - \acute{r}|} d\acute{r} \right| \chi_i \right\rangle + E_{xc}[\rho(r)]$$

where N is the number of the electrons and the density is defined as,

$$\rho = \sum_{i=1}^N \langle \chi_i | \chi_i \rangle \tag{11}$$

$E_{xc}$ is placed instead of complex terms $\Delta T[\rho(r)] + \Delta V_{ee}[\rho(r)]$ and is known as exchange-correlation energy.

The orbitals $\chi$ that minimize E in Eq. (11) must satisfy the Kohn-Sham equations

$$h_i^{KS}\chi_i = \varepsilon_i\chi_i \tag{12}$$

where the Kohn-Sham (KS) one electron operator described as

$$h_i^{KS} = -\frac{1}{2}\nabla_i^2 - \sum_k^{nuclei} \frac{Z_k}{|r_i - r_k|} + \int \frac{\rho(\acute{r})}{|r_i - \acute{r}|} d\acute{r} + V_{xc} \tag{13}$$

$$V_{xc} = \frac{\delta E_{xc}}{\delta\rho} \tag{14}$$

where $V_{xc}$ is functional derivative. Using the orbitals in Eq (12) we can write the slater determinantal form of Kohn-Sham equations as follows,

$$\sum_{i=1}^{N} h_i^{KS} |\chi_1\chi_2 \cdots \chi_N\rangle = \sum_{i=1}^{N} \varepsilon_i |\chi_1\chi_2 \cdots \chi_N\rangle \tag{15}$$

To calculate the KS orbitals in this method one uses an initial guess of the electron density. The Kohn-Sham orbitals are ones for the fictitious reference system of noninteracting electrons, thus provide the exact molecular ground-state ρ which can be calculated from.

**3.1.1.3 Time-Dependent Density Functional Theory**

Time-dependent DFT (TD-DFT) was developed by extension of DFT to calculate properties of excited electronic state. The formal foundation of TD-DFT is done by Runge-Gross Theorem [8], and described as:

$$\widehat{H}\Psi = i\frac{\partial}{\partial t}\Psi \tag{16}$$

The Hamiltonian and the wavefunction are a function of the spatial coordinates and the time. The wavefunction can be calculated at any time (t) by this equation. (considering $t_0$ the initial time for the system) [9].

### 3.1.1.4 Hybrid functional

Exchange in DFT is an approximation based on free-electron model and thus not suitable for the molecular systems where electrons are strongly localized. One the other hand, in Hartree-Fock (HF) method the definition of exchange is exact and come directly from the Slater-Determinant. Becke found that adding a portion of HF exact exchange to DFT can improve the accuracy of DFT for the molecular system. The new mixed functional is called Hybrid functional. He has developed one of popular exchange functionals, B3, which is twinned with Lee-Yang-Parr (LYP) functional to make B3LYP. One of the broadly used hybrid functional is B3LYP functional in molecular calculations [10]. This thesis uses hybrid functional B3LYP and MPW1K [11,12] as they were successfully applied in previous works [13].

### 3.1.2 Software Used

1. Avogadro: a molecular editor and a visualization tool that allows constructing and visualizing 3D molecules. It is also useful to visualize the molecular orbitals [14].

2. Gaussian 09: the computational software to run many kind of calculations. In order to perform a calculation, an input file with .com extension has to be specified and the program will generate an output file with .log extension [15].

3. PuTTY: the open source software that allows to manage with informatics remote systems [16].

4. WinSCP: the software that allows the file transfer between a local and a remote computer [17].

5. Molden: the program that allows the molecular and electronic structure pre- and post-processing [18].

## 3.2 Life Cycle Assessment

The origins of Life Cycle Assessment (LCA) dates back to the late 1960s and early 1970s, when the energy crisis had led companies to think of effective solutions for saving energy since their customers were demanding more energy-efficient products [19-22]. The evolution and strengthening of LCA concept have been largely supported by the activity of the Society of Environmental Toxicology and Chemistry (SETAC) in the following years [23]. In 1993, SETAC gave the first official definition of LCA as a strategic tool to evaluate the environmental burdens associated with a product, process, or activity thanks to its potential to analytically identify and quantify energy consumption, material usage and emissions to the environment. Beside the essential work of SETAC for LCA methodological development, the International Standardization Organization (ISO) [24], has been involved in LCA standardization since 1994. The methodological structure defined in the first edition of the ISO 14040 series organized the LCA approach in four phases, namely the (i) goal and scope definition, (ii) life cycle inventory, (iii) life cycle impact analysis and (iv) life cycle improvement analysis. This framework is still used in the LCA process method. Thanks to the synergy among SETAC, ISO and the United Nations Environmental Programme (UNEP) [25-26], environmental LCA had remarkable and fast growth over the last three decades [27].

Nowadays LCA is internationally acknowledged as a quantitative method, that allows to calculate the potential impacts associated with a product, process or service. It is considered by the European Commission as the only tool with a scientific basis useful for understanding the environmental loads of a product or process as it provides verifiable quantitative data and allows the identification of the most critical environmental aspects on which to intervene to improve the environmental profile of the analyzed system.

LCA could play an essential role in supporting environmental product policy and legislation. The impact of products on the environment has become one of the main elements of decision-making processes,
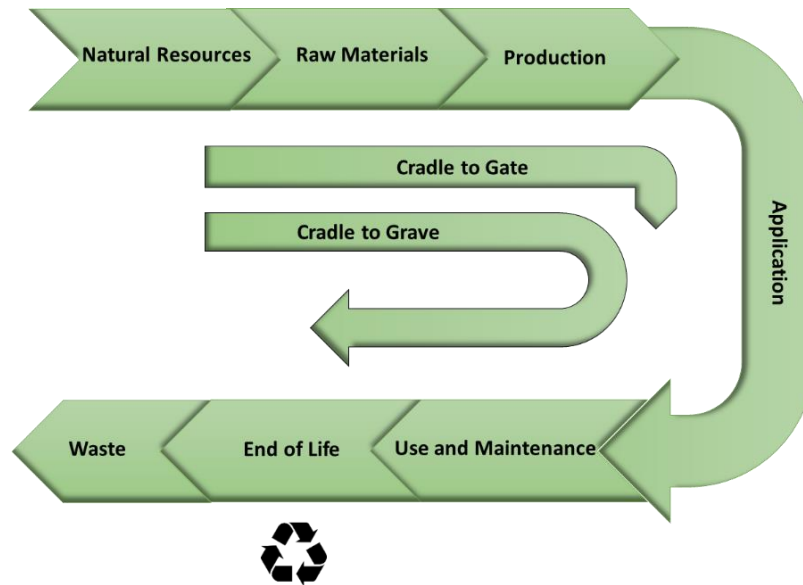


Figure 3.1 Life cycle assessment (LCA) process

The methodological framework and the guidelines of the LCA approach are reported in the 2006 edition of the international ISO 14040 and 14044 Standards [28-29].

LCA results allow for the identification of the environmental hotspots of the entire life cycle, highlighting the products or processes that have the highest load on the environment. These results and information are crucial for decision-makers, giving them proper support to implement policies related to the environmental impact mitigation and sustainable development.

According to the ISO standards, the application of LCA is performed through 4 main phases (Fig 3.2):

1. Goal and Scope Definition

2. Life Cycle Inventory Analysis

3. Life Cycle Impact Assessment

4. Interpretation
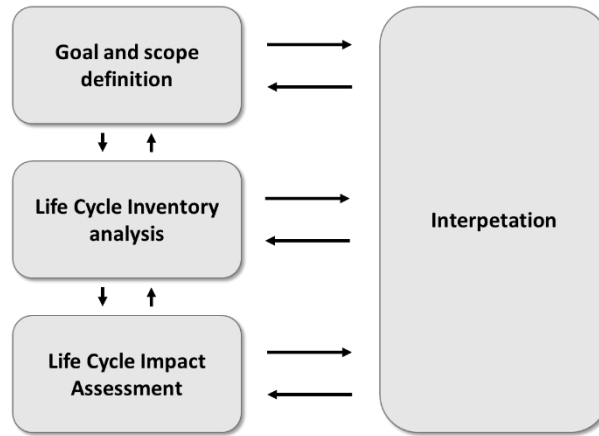


Figure 3.2 LCA methodological framework

### 3.2.1 Goal and Scope Definition

Goal and scope definition is the first step of LCA method and it represents the fundamental phase in which the study model is defined as well as the methodological framework of the study. Two basic elements for and LCA study are defined at this level: the functional unit and the system boundaries. The functional unit is the unit of measure on which all input and output flows are normalized. The system boundaries describe the system being studied, and which activities, the so-called process units, have to be included and investigated in the LCA analysis (Figure 3.3).
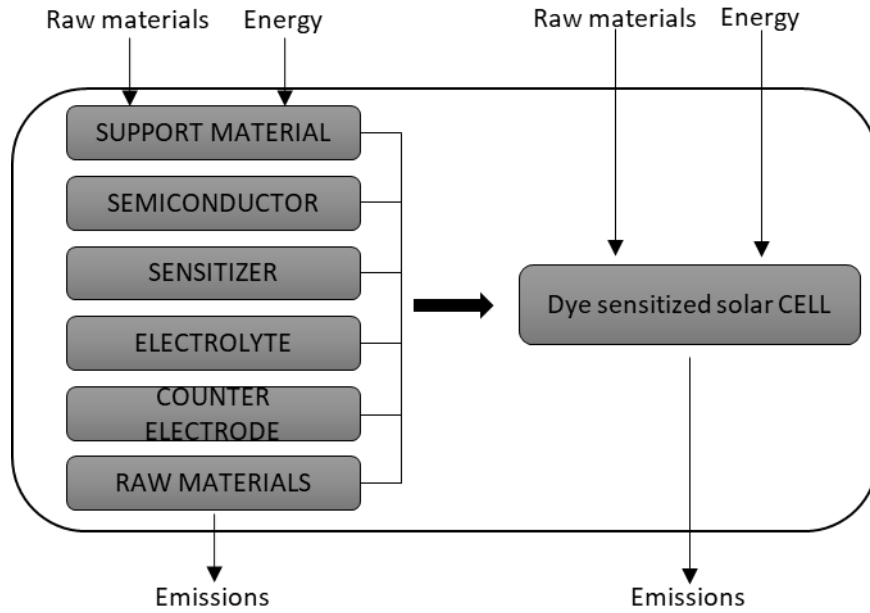
Figure 3.3. Sketch of the system boundaries of the Dye Sensitized Solar Cells production phase

Furthermore, during goal and scope definition the following items are considered too:

• Determining the reasons of the study;

• Intended audience and use of results;

• Data quality and requirements;

• Identifying study limitations and assumptions;

• Type of the report required for the study.

During the LCA study, changes may happen in goal and scope definition, as LCA is an iterative process. This step can guide the entire LCA procedure to confirm if the most related results are attained.

**3.2.2 Life Cycle Inventory Analysis (LCI)**

Life Cycle Inventory (LCI) consists of a list of the input and output material and energy flows characterizing the whole life cycle of the system as defined in the goal and scope phase. In this step the data collection is performed to develop a list, as much detailed as possible, of raw materials and energy amounts involved in all the process units included in the system boundaries.

**3.2.3 Life Cycle Impact Assessment (LCIA)**

In this step, the extent of environmental changes generated by the outflows to the environment and raw materials consumption produced by the case system is highlighted. Practically, the magnitude of the potential environmental impacts generated by the case system under investigation is calculated by linking life cycle inventory data to specific environmental impacts and expressing the results through related indicators. The LCIA phase is divided in different steps recommended by the ISO standards:

a) *Classification*: inventory data are assigned to impact categories. These categories show the environmental impacts caused by the emission and consumption of natural resources during the product's life cycle (obligatory step according to the ISO).

b) *Characterization*: after the LCI results are assigned to various impact categories, the characterization of the impacts must be performed. This task is accomplished using characterization factors that specify the relative load of LCI results to the pertinent environmental impact category by quantifying the contribution that a product or service has in each impact category (obligatory step according to the ISO).

c) *Normalization*: this step allows the calculation of the magnitude of the results of impact category indicators relative to some reference values (optional step according to the ISO).

d) *Weighting*: this step involves the conversion of the normalized results of each of the impact categories using weighting factors into values that expresses the relative importance of the impact category. The weighted results all have the same unit and can be added up to create one single score for the environmental impact of a product or scenario. This step mostly dedicated to complete information about ecosystem functions, where numerous environmental parameters are weighted and various environmental impact categories reflecting the comparative importance of the impacts are considered (optional step according to the ISO).

Several LCIA calculation methods have been developed to support in the implementation of the LCIA phase. Nowadays, there are several LCIA methods that can be used to assess the environmental impact of a system and the choice is mainly driven by the purpose of the study. Each method differs from the others in the way it performs the calculation and presents the final results.

### 3.2.4 Life Cycle Interpretation

Interpretation is the fourth phase of LCA in which the data from the inventory analysis and the impact assessment are evaluated together. The interpretation step should present results that are associated with the defined goal and scope, and it includes conclusions, explanation, and limitations and provides recommendations. The outcomes of this step can support the decision-making process.

## 3.3 Life Cycle Assessment Implementation

LCA has been demonstrated to be an effective and powerful tool for the evaluation of environmental burdens associated with the life cycle of PV systems [30-37]. The environmental impact of the PV systems is mainly associated with their production and disposal processes rather

than the operation phase, since the latter includes almost no greenhouse gas emission. Indeed, to evaluate the sustainability of PV devices, the investigation of the environmental impacts generated during their fabrication is essential in order to improve and optimize the energy and resource efficiency of manufacturing processes and, ultimately, the environmental footprint of the device. This assessment becomes of paramount importance especially for photovoltaic devices based on innovative technologies that stand out for the use of alternative materials than traditional semiconductors.

In this thesis, the assessment of the environmental performances connected with the fabrication of DSSCs components, namely the sensitizer, through the application of the LCA methodology has been performed. More in details, LCA has been employed to investigate the environmental profile of alternative protocols for the synthesis, and eventually the production scale-up, of an organic dye bearing a thiazolo[5,4-d]thiazole ring as central unit, namely the TTZ5, that has been successfully proposed as a sensitizer for the manufacturing of DSSCs [38].

Two LCIA method were employed for the analysis:

1 - the ILCD 2011 Midpoint+ method, developed by the Joint Research Centre - European Commission [39]. The primary objective of ILCD is to transform the long list of life cycle inventory data into a limited number of indicators based on midpoint and endpoint modeling thanks to specific characterization factors. At the midpoint level, 16 impact categories are included: climate change, ozone depletion, human toxicity non cancer effects, human toxicity cancer effects, particulate matter, ionizing radiation human health, ionizing radiation ecosystem, photochemical ozone formation, acidification, terrestrial eutrophication, freshwater eutrophication, marine eutrophication, freshwater ecotoxicity, land use, water resource depletion and mineral, fossil and renewable resource depletion.

2 - the Cumulative Energy Demand (CED) method [40] is employed to quantify the use of the direct and indirect energy requirement (in units of MJ) over the whole life cycle of the system. It quantifies the cumulative energy demand of fossil resources including hard coal, lignite, natural gas and crude oil, nuclear and other renewable resources like biomass, water, wind, and solar energy during the life cycle phases of the investigate system and it displays the energy demand as primary energy values.

## 3.4 References

[1]     I. N. Levine, *Quantum Chemistry*, Pearson Advanced Chemistry Series, 2014.

[2]     A. Szabo, N. S. Ostlund, *Modern Quantum Chemistry: Introduction to Advanced Electronic Structure Theory,* Dover Publication, 1982.

[3]     J. P. Lowe, K. A. Peterson*, Quantum Chemistry*, Elsevier, 2006.

[4]     C. J. Cramer, *Essentials of Computational Chemistry, Theories and Models*, Wiley, 2004.

[5]     W. Koch, and M. C. Holthausen, *A Chemist's Guide to Density Functional Theory*, 2001.

[6]     W. Kohn, and L. J. Sham, *Self-Consistent Equations Including Exchange and Correlation Effects,* vol. 140, no. 4A, pp. 1133-1138.

[7]     K. Burke, and L. O. Wagner, "DFT in a Nutshell," *Int. J. Quantum Chem.,* vol. 113, pp. 96–101, 2013.

[8]     E. Runge, and E. K. U. Gross, "Density-Functional Theory for Time-Dependent Systems," *A. Phys. Rev.,* vol. 52, no. 12, 1984.

[9]     M. Marques, *Time-Dependent Density-Functional Theory*, Springer, 2006.

[10]    A. D. Becke, "Density-functional thermochemistry. III. The role of exact exchange" *J. Chem. Phys.,* vol. 98, pp. 5648–5652, 1993.

[11]    Y. Zhao, B. J. Lynch, and D. G. Truhlar, "Development and Assessment of a New Hybrid Density Functional Model for Thermochemical Kinetics," *J. Phys. Chem. A,* vol. 108, pp. 2715–2719, 2004.

[12]    B. J. Lynch, P. L. Fast, M. Harris, and D. G. Truhlar, "Adiabatic Connection for Kinetics" *J. Phys. Chem. A,* vol. 104, pp. 4811–4815, 2000.

[13]    A. Dessì et al., "New Blue Donor-Acceptor Pechmann Dyes: Synthesis, Spectroscopic, Electrochemical, and Computational Studies," *ACS Omega,* vol. 4, no. 4, pp. 7614–7627, 2019.

[14]    "www.avogadro.cc"

[15]    "www.gaussian.com"

[16]    "www.putty.org."

[17]    "www.winscp.net."

[18]    "www.cmbi.ru.nl/molden."

[19]    G. Sundstro, "Investigation of energy requirements from raw material to garbage treatment for four Swedish beer and packaging alternatives," Malmö, Sweden, 1971.

[20]    I. Boustead, "Resource implications with particular reference to energy requirements for glass and plastic milk bottles," *Int. J. Dairy Technol*., vol. 27, pp. 159-165, 1974.

[21]    *Energy analysis workshop on methodology and conventions*, August 25-30, 1974; International Federation of Institutes for Advanced Study (IFIAS): Guldsmedshyttan, Sweden, 1974.

[22]    R. G. Hunt, W. E. Franklin, R. O. Welch, J. A. Cross, and A. E. Woodal, *Resource and environmental profile analysis of nine beverage container alternatives; U.S. Environmental*

*Protection Agency:* Washington, DC, 1974.

[23]    "http://www.setac.org/."

[24]    "http://www.iso.org/."

[25]    "http://www.unep.org/."

[26]    "https://www.lifecycleinitiative.org/."

[27]    J. B. Guinée, R. Heijungs, G. Huppes, A. Zamagni, P. Masoni, R. Buonamici, T. Ekvall, T. Rydberg, "Life Cycle Assessment: Past, Present, and Future," *Environ. Sci. Technol*., vol. 45, no. 1, pp. 90–96, 2011.

[28]    "https://www.iso.org/standard/37456.html."

[29]    "https://www.iso.org/standard/38498.html."

[30]    M. Bravi, M. L. Parisi, E. Tiezzi, and R. Basosi, "Life Cycle Assessment of Advanced Technologies for Photovoltaic Panels Production," *Int. J. Heat. Technol.,* vol. 28, pp. 133-139, 2010.

[31]    V. M. Fthenakis and H. C. Kim, "Photovoltaics: Life-cycle analyses," *Sol. Energy*, vol. 85, no. 8, pp. 1609–1628, 2011.

[32]    J. Peng, L. Lu, and H. Yang, "Review on life cycle assessment of energy payback and greenhouse gas emission of solar photovoltaic systems," *Renew. Sustain. Energy Rev*., vol. 19, pp. 255–274, 2013.

[33]    M. L. Parisi, S. Maranghi, A. Sinicropi, and R. Basosi, "Development of dye sensitized solar cells: A life cycle perspective for the environmental and market potential assessment of a renewable energy technology," *Int. J. Heat Technol.,* vol. 31, no. 2, pp. 143–148, 2013.

[34]    M. L. Parisi, S. Maranghi, and R. Basosi, "The evolution of the dye sensitized solar cells from Grätzel prototype to up-scaled solar applications: A life cycle assessment approach," *Renew. Sustain. Energy Rev.,* vol. 39, pp. 124–138, 2014.

[35]    V. Fthenakis, *Life Cycle Assessment of Photovoltaic: From Fundamental to applications,* Wiley & Sons, vol. 14044, pp. 646–657, 2017.

[36]    S. Cucurachi, C. Van Der Giesen, and J. Guinée, "Ex-ante LCA of Emerging Technologies," *Procedia CIRP*, vol. 69, pp. 463–468, 2018.

[37]    N. A. Ludin *et al.,* "Prospects of life cycle assessment of renewable energy from solar photovoltaic technologies: A review," *Renew. Sustain. Energy Rev.,* vol. 96, pp. 11–28, 2018.

[38]    A. Dessì *et al.,* "Organic dyes with intense light absorption especially suitable for application in thin-layer dye-sensitized solar cells," *Chem. Commun.,* vol. 50, no. 90, pp. 13952–13955, 2014.

[39]    European Commission. ILCD., "*International Reference Life Cycle Data System (ILCD) handbook: Framework and Requirements for Life Cycle Impact Assessment Models and Indicators*," 2010.

[40]    R. Frischknecht et al., "Implementation of Life Cycle Impact Assessment Methods," *ecoinvent report, Swiss Centre for Life Cycle Inventories* vol. 2.0, no. 3, pp. 1–151, 2007.

# CHAPTER IV

## Results and Discussion

# 4. Results and Discussion

This thesis is based on three papers that are included in this Chapter 4. In the following, a brief introduction to the three manuscripts along with a comment to specify candidate's contribution is presented:

## 4.1 New Blue Donor–Acceptor Pechmann Dyes: Synthesis, Spectroscopic, Electrochemical, and Computational Studies

In this paper that is published in the ACS Omega journal, a new class of blue-colored Pechmann dyes having a D-A-π-A configuration are designed and their synthesis and characterization are reported. These organic compounds could have a great interest for application as photosensitizers in DSSCs due to their particular characteristics such as light absorption in one of the most photon-dense region of the solar spectrum and their blue color. The presence of Pechmann unit (which is a strong electron withdrawing unit) as an auxiliary acceptor in the π bridge allows to obtain the desired optical and electrochemical properties.

The candidate's contribution to this paper refers to the application of computational chemistry methods based on DFT and TDDFT for the prediction of main optoelectronic properties of these metal free organic dyes. In particular, as for an efficient dye is necessary to have, among other features, LUMO energy levels higher than the CB of the TiO$_2$ and HOMO energy levels lower than redox couple, FMOs energies are computed and compared to those of the semiconductor and redox couple and also to those of previous known dye as reference. Moreover, the absorption maxima ($\lambda_{max}$), excitation energy ($E_{exc}$) and oscillator strength ($f$))and related LHE, $\Delta G_{inject}$, $E_{ox}^{dye}$ and $E_{ox}^{dye^*}$ are evaluated including solvent effects via implicit methods. On the basis of the in silico results, the most promising dyes were proposed and thus synthesized.

**4.2 Ground state redox potentials calculations of organic dyes for DSSC and Visible-Light-Driven Hydrogen Production**

In this paper that is submitted to the Molecules journal, the *in silico* prediction of ground state redox potential (GSRP) of 16 organic dyes is reported. They are computed in terms of Gibbs free energy changes of the redox reaction using DFT, and in particular the MPW1K functional, which have been shown to give the best accuracy in previous works, and a polarizable continuum model (PCM) to take into account solvent effects. The prediction of GSRP is fundamental for a successful design of more efficient novel organic sensitizers to be employed in DSSCs but also in photocatalytic systems for the production of $H_2$.

The DFT predicted values have been compared to the available experimental data showing that the employed strategy allows to reproduce the GSRP with a mean absolute error $< 0.2$ eV.

The Ph.D. candidate is first author of the paper and mainly contributed to the computational data collection, analysis and interpretation.

**4.3 Combined LCA and green metrics approach for the sustainability assessment of organic TTZ5 dye synthesis at lab scale**

The development of emerging solar cells based on innovative materials such as DSSCs needs an evaluation of their environmental impact profile specifically regarding the synthesis of sensitizers. This paper that is submitted to the Frontiers journal reports the environmental profile of alternative synthetic protocols for preparation of the metal free organic dye TTZ5, that has been successfully proposed as a sensitizer for DSSCs The methodology applied relies on a mass-based green metrics and LCA combined approach to obtain a gate-to-gate assessment. The outcomes of the present

study clearly show that the LCA results should be carefully taken into account to guide the preparation of new photosensitizers.

In the context of this manuscript, the candidate contributed to carry out the LCA analysis and its interpretation.

# New Blue Donor−Acceptor Pechmann Dyes: Synthesis, Spectroscopic, Electrochemical, and Computational Studies

Alessio Dessì,*,[†] Adalgisa Sinicropi,[§,†,#] Sanaz Mohammadpourasl,[§,#] Riccardo Basosi,[§,†,#] Maurizio Taddei,[§,†] Fabrizia Fabrizi de Biani,[§] Massimo Calamante,[†,‡] Lorenzo Zani,[†] Alessandro Mordini,[†,‡] Pamela Bracq,[†] Daniele Franchi,[†,‡] and Gianna Reginato*,[†]

[†]Istituto di Chimica dei Composti Organometallici (CNR-ICCOM), Via Madonna del Piano 10, 50019 Sesto Fiorentino, Italy

[‡]Dipartimento di Chimica "U. Schiff", Università degli Studi di Firenze, Via della Lastruccia 13, 50019 Sesto Fiorentino, Italy

[§]Dipartimento di Biotecnologia, Chimica e Farmacia, Università degli Studi di Siena, Via A. Moro 2, 53100 Siena, Italy

[#]CSGI, Consorzio per lo Sviluppo dei Sistemi a Grande Interfase, via della Lastruccia 3, 50019 Sesto Fiorentino, Italy

ⓢ *Supporting Information*

**ABSTRACT:** The design, synthesis, and characterization of a new class of blue-colored thiophene-substituted Pechmann dyes are reported. Due to a distinguishing blue coloration and the capability to absorb light in one of the most photon-dense regions of the solar spectrum, such compounds are of great interest for application as photoactive materials in organic optoelectronics, in particular, in dye-sensitized solar cells. To achieve fine tuning of the optical and electrochemical properties, the electron-poor thiophene-bis-lactone moiety has been decorated with donor (D) and acceptor groups (A), targeting fully conjugated D−A−π−A structures. The designed structures have been investigated by means of DFT and time-dependent DFT calculations, and the most promising dyes have been synthesized. These molecules represent the very first preparation of unsymmetrical Pechmann derivatives. Optical and electrochemical properties of the new dyes have been studied by cyclic voltammetry and UV−vis and fluorescence spectroscopy. In two cases, test cells were built proving that a photocurrent can indeed be generated when using electrolytes especially formulated for narrow-band-gap dyes, although with a very low efficiency.
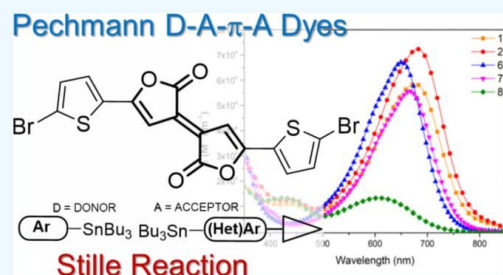
## ■ INTRODUCTION

Among new generation photovoltaic technologies, dye-sensitized solar cells (DSSC) are considered a promising option for the efficient conversion of solar energy to electricity.[1] The working principle[2] of a DSSC is inspired by natural photosynthesis as light harvesting is carried out by a dye, which is absorbed on a thin-layer of a mesoporous semiconductor (usually $TiO_2$). Thanks to photoexcitation, an electron is promoted from the HOMO of the dye to its LUMO and from there is transferred to the conduction band of the semiconductor. Traveling through an external circuit (thus generating an electric current), the electron can be collected at the cathode, where the reduction of a redox couple, such as iodide/triiodide, takes place. The original state of the dye can be finally restored by electron donation from the electrolyte, closing the circuit. Clearly, the photosensitizer represents a key component of a DSSC, being responsible not only for its photovoltaic performances but also for its appearance and for some peculiar properties, such as transparency and color. Accordingly, a large number of metal-free organic dyes have been designed, synthesized, and tested for this kind of application,[3] and in particular, donor−π bridge−acceptor

(D−π−A) structures showed desirable characteristics, including tunable optoelectronic and electrochemical properties, simple molecular design, high molar extinction coefficients, low cost, and simple synthetic and purification methods. However, although very good power conversion efficiencies (PCEs) have been reached,[4,5] with record values exceeding 14%,[6] further efforts are required to find colorful, stable, and highly efficient organic dyes, especially when aiming to increase the commercial appeal of DSSC technology for building integration and indoor applications. In particular, blue and green dyes would be of high commercial interest due to their lovely colors, in turn derived from their ability to absorb the incident photons in the red and near-infrared region (NIR) of the spectrum.[7] Nevertheless, although the efficient conversion of low energy photons ($\lambda > 700$ nm) is crucial for increasing the overall PCE in a DSSC, only a few blue sensitizers have been reported so far. In particular, some blue devices have been reported using squaraine[8] or diketopyrrolopyrrole

(DPP)-based sensitizers. Above all, the latter were able to give a satisfying efficiency of 7.3% when assembled with the cobalt bipyridine-based electrolytes, a value which was further increased to 8.7% using a co-sensitization strategy with a red dye[9] and even exceeded 10% in the presence of very bulky indoline donors.[10] Very recently, a blue dye featuring an electron-rich polycyclic aromatic hydrocarbon (PAH) scaffold has also been reported achieving a PCE of 12.6%.[11] Clearly, there are still significant possibilities of introducing structural modifications in the sensitizers, in particular, in the search of new building blocks capable of extending the range of available panchromatic dyes. In this context, we have been intrigued by the possibility of introducing the (E)-3,3′-bifuranylidene-2,2′-dione heterocyclic systems (Pechmann lactone, Figure 1) in the π scaffold of the dye.
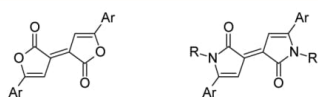


Figure 1. Pechmann and aza-Pechmann molecular structures.

Actually, the Pechmann moiety is characterized by a planar and conjugated structure, which is a known requirement to promote charge transport in organic electronic frameworks. Accordingly, Pechmann bis-lactone and aza-Pechmann bis-lactam units have been exploited to prepare conjugated systems of potential interest for organic electronics,[12,13] for instance, as semiconductors in organic field-effect transistors (OFET).[14] Furthermore, quadrupolar D−A−D systems based on Pechmann-lactone analogues were reported to show highly intense and red-shifted visible−NIR absorption and fluorescence,[15] whereas the aza-Pechmann moiety can be found, together with diketopyrrolopyrrole, in photoactive donor−acceptor polymers suitable for organic photovoltaic devices[16] and also in small molecules that were used to build OFETs with excellent hole mobilities.[17]

In this paper, we report the design of a new family of unsymmetrically substituted Pechmann dyes for application in DSSCs. The dyes studied differ both for the electron-rich substituents on the donor and for the anchoring group (Figure 2). Using an approach which was successfully applied in previous studies,[18] the dyes were investigated by means of
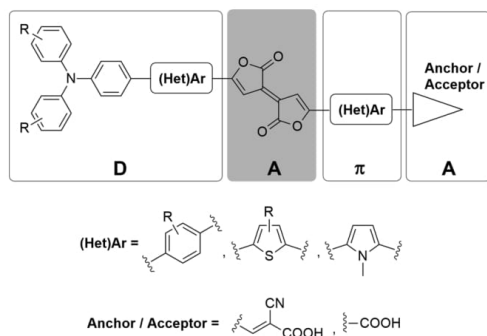


Figure 2. General structure of dyes containing the Pechmann lactone moiety.

density functional theory (DFT) and time-dependent DFT (TD-DFT) calculations, those with the most promising features were synthesized, and their spectroscopic and electrochemical properties were experimentally verified.

## ■ RESULTS AND DISCUSSION

Dyes 1−13 (Figure 3) were designed with the aim to rationalize the effect of decorating the central Pechmann scaffold with different donor and acceptor groups. We mainly focused on thiophene-derived Pechmann lactones (dyes 1−10) because the thienyl substituent is ubiquitous in the structure of organic semiconductors and photosensitizers. However, to have better insight, some other aromatic and heteroaromatic rings such as xylenyl (11), fluorenyl (12), and pyrrolyl-(13) were considered (Figure 3), and the effect of conjugated spacers with different electron densities was evaluated by placing phenyl (5 and 6), ethynylphenyl (7), and 3,4-ethylenedioxythiophenyl (EDOT) (9 and 10) moieties between the anchoring group and the central core. In addition, hydrophobic alkyl chains were inserted to improve the solubility, reduce aggregation,[19] and simplify the handling of the final compounds. All the structures were endowed with triarylamine donor groups, differing in terms of the presence of electron-rich substituents in the para position. In particular, unsubstituted triarylamine compounds (1 and 8) were compared with p-hexyloxy- (3) and p-thiohexyl-substituted ones (2, 5, 6, 7, 9, and 10) because the latter are known to have a beneficial reducing effect on aggregation and enhancing effect on regeneration of the dyes.[19a,b,20,21] Finally, the Pechmann lactone scaffold was substituted with the aza-Pechmann one in compounds 4 and 8.

**Computational Studies.** To assess the optoelectronic properties of the selected Pechmann-based structures and verify that their energy levels match the semiconductor conduction band and the redox couple potential, it was essential to model the relative energies of their frontier molecular orbitals (FMOs) and their UV−vis absorption maxima. All quantum mechanics (QM) calculations were performed using the Gaussian 09 program package.[22] Geometry optimizations of Pechmann-based dyes (1−13, Figure 3) were carried out by DFT calculations using the Becke three-parameter-Lee−Yang−Parr (B3LYP) hybrid-DFT exchange-correlation functional[23] in combination with the standard 6-31G* basis set in the gas phase. The values of the HOMO−LUMO energy gaps for all the computed structures are reported along with the wave function plots of corresponding FMOs. Vertical excitation energies ($E_{exc}$), absorption maxima ($\lambda_{max}$), and oscillator strengths (f) were computed at the time-dependent DFT (CAMB3LYP/6-31G*) level on all the optimized structures. To include the effect of the solvent ($CHCl_3$), the polarized continuum model (PCM) was employed.[24] Finally, methyl groups have been used in place of the alkyl chains to reduce the computational cost. The energy and shape of FMOs for 1−13 are shown in Figure 4, along with the known D−π−A sensitizer DF15,[25] which was used as reference. As we expected, and in comparison to DF15, the introduction of the Pechmann unit, which is an auxiliary acceptor group in the π bridge of the molecules, lowered the energy of the LUMO orbitals, consequently reducing the HOMO−LUMO gaps, which were in the range of 1.45−1.78 eV. Similarly to other D−A−π−A dyes,[26] the HOMO/LUMO orbitals of compounds 1−13 were mostly localized on the donor and acceptor, respectively, but both also stretched onto
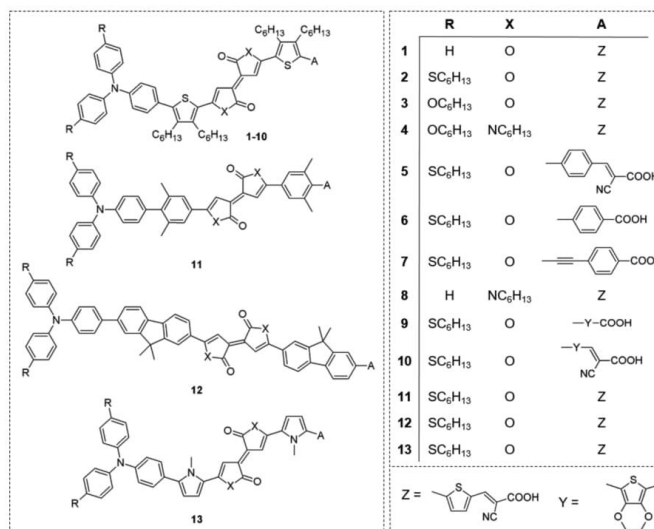
47

**Figure 3.** Structures of the designed Pechmann dyes **1–13**.

the Pechmann unit, giving rise to an extended superimposition, suggesting strong intramolecular charge transfer upon photo-excitation. Comparing the different structures, it appears that the substitution of the lactone moiety with the less electron-withdrawing lactam (**4** vs **3** and **8** vs **1**) raised the energy of both frontier molecular orbitals, even if the consequent increase of the HOMO–LUMO gap (from 1.49 eV for dye **3** to 1.72 eV for dye **4** and from 1.62 eV for dye **1** to 1.78 eV for dye **8**; see Figure 4) was especially due to the larger positive shift of the LUMO orbital.

As expected, the introduction of a stronger donor group (dyes **2** and **3** vs dye **1**) raised the energy of the HOMO orbital, lowering the HOMO–LUMO gap, whereas the presence of different spacers between the anchoring unit and the central core (dyes **5** and **10** vs dye **2**) affected the energy of the LUMO orbital, with a slight increase of the HOMO–LUMO gap. The same effect was produced by the substitution of the cyanoacrylic acid with a simple carboxylic acid (dyes **6** and **7** vs dye **5**; dye **9** vs dye **10**). In the case of dyes **6** and **7**, the shape of the LUMO was also different, with a smaller contribution of the actual anchoring group, probably as a consequence of the less electron-withdrawing nature of the acceptor. Finally, substitution of the thienyl rings with different aromatic and heteroaromatic moieties (dyes **11–13** vs dye **2**) changed the energy levels of both the frontier molecular orbitals, without altering the HOMO–LUMO gap dramatically. Also, in the case of dyes **11** and **12**, we observed a more limited localization of the LUMO on the anchoring group; however, because in this case the latter was the same as those of dyes **1–4** and **8**, the reason could not be ascribed to its weaker electron-accepting ability but rather to the smaller planarity of the conjugated system, especially between the $\pi$ bridge and the acceptor moiety (see Figure S25).

In Table 2, ground- ($E^{dye}$) and excited ($E^{dye*}$)-state oxidation potentials, electron injection free energies ($\Delta G^{inject}$), and light-harvesting efficiencies (LHE) associated with the oscillator strength ($f$) of each dye molecule at the maximum

absorption wavelength are presented. These photovoltaic properties have been calculated according to the following equations[26]

$$E^{dye} = -E_{HOMO} \tag{1}$$

$$E^{dye*} = E^{dye} - E_{exc} \tag{2}$$

$$\Delta G^{inject} = E^{dye*} - E_{CB} \tag{3}$$

where $E_{CB} = -4.0$ eV is the conduction band energy of TiO$_2$.

$$LHE = 1 - 10^{-f} \tag{4}$$

where $f$ is the oscillator strength of the dye.

Assuming that the commonly accepted value is −4.0 eV for the energy of the TiO$_2$ conduction band,[1] $\Delta G^{inject}$ values were negative for all sensitizers, indicating that electron injection from the dye to TiO$_2$ is predicted to be thermodynamically favored.

The most negative $\Delta G^{inject}$ values belong to dyes **11** and **12**, which have also the lowest computed absorption maxima ($\lambda_{max}$ = 576–585 nm), due to the fact that the most influential electronic transition occurs from the HOMO−1 to LUMO level and to dyes **4**, **6**, and **8**, whose LUMO orbitals have the least negative values. The high and similar values (0.98−0.99) for LHE suggest that all dyes are, in principle, able to maximize the photocurrent response. We can thus conclude that the computational design suggested that almost all of dyes **1−13** are suitable sensitizers for DSSC application. In particular, there is an appropriate alignment of the dyes' energy levels: vertical absorption maxima ranging from 600 to 800 nm (except for dyes **11** and **12**) confirm their red to infrared light absorption, high oscillator strength values suggest large molar extinction coefficients, and wave function plots of frontier molecular orbitals involved in the excitation process are in favor of an intramolecular charge-transfer nature of the excitation.
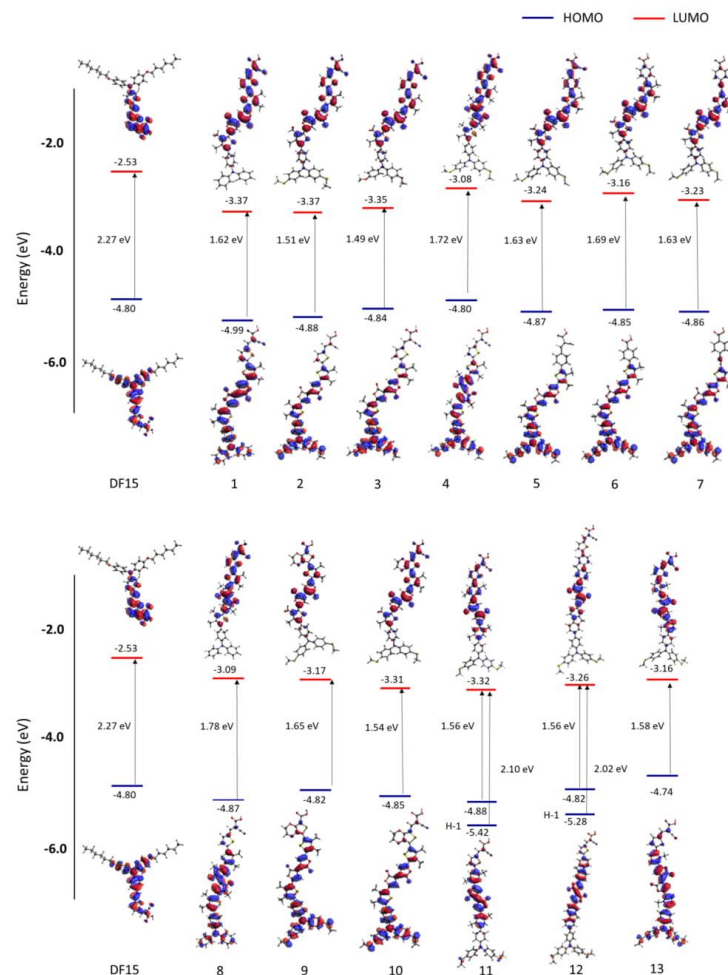
48

**Figure 4.** Energy levels and electron density distributions of FMOs of compounds **1−13**.

**Synthesis of the Pechmann Dyes.** Not all the thirteen calculated dyes were synthesized. Taking into account the computational results, we decided to exclude dyes **11** and **12** due to their insufficient NIR light absorption. Among the remaining dyes, we selected compounds **1**, **2**, **6**, **7**, and **8** (see Figure 3). Compound **1** was selected as a reference, and compound **2** was preferred over compound **3** to take advantage of the possible beneficial enhancing effect of thiohexyl chains on dye regeneration.[19b,21] Similarly, between dyes **4** and **8**, where the bis-lactone unit is substituted with the aza-Pechmann core, we selected only compound **8** to be compared with **1**. Finally, we focused on dyes **6** and **7**, having a simple carboxylic anchoring group and less electron-rich phenyl or ethynylphenyl spacers, to be compared with **2**. As mentioned above, in the case of dyes **6** and **7**, the contribution of the actual anchoring groups to their LUMO orbitals was inferior to those shown by the corresponding cyanoacrylic dyes. Never-

theless, we still decided to prepare and test them based on the following considerations: (a) They had more negative calculated $\Delta G^{\text{inject}}$ values and higher LUMO levels than dyes **1** and **2**, and therefore, we supposed that they could still display a significant charge injection capability owing to a larger driving force. (b) Charge injection into $TiO_2$ was previously demonstrated also in cases where the LUMO orbital of the dye was spatially separated from the semiconductor surface: an example is the highly performing **ADEKA-1** dye described by Kakiage et al.[6] (for which efficiencies up to 12.5% were reported when used alone).[27] Furthermore, electron transfer to a semiconductor was observed also for dyes (both organic and organometallic) whose main chromophore was separated from the anchoring group by a saturated carbon chain, albeit at a reduced rate compared to the fully conjugated compounds.[28]

49

**Table 1. TD-DFT (CAM-B3LYP/6-31G\*)-Computed Absorption Maxima ($\lambda_{max}^{a}$)[a]**

| dyes | $\lambda_{max}^{a}$ (nm) | $E_{exc}$ (eV) | $f$ | composition (%) H → L |
|---|---|---|---|---|
| 1 | 675 | 1.84 | 2.23 | 83 |
| 2 | 692 | 1.79 | 2.26 | 72 |
| 3 | 685 | 1.81 | 2.27 | 67 |
| 4 | 639 | 1.94 | 1.77 | 67 |
| 5 | 640 | 1.94 | 1.96 | 65 |
| 6 | 630 | 1.97 | 1.79 | 67 |
| 7 | 652 | 1.90 | 2.01 | 70 |
| 8 | 638 | 1.94 | 1.74 | 79 |
| 9 | 661 | 1.88 | 1.91 | 77 |
| 10 | 684 | 1.81 | 2.25 | 73 |
| 11 | 576 | 2.15 | 1.92 | 72 (H−1 → L) |
| 12 | 585 | 2.12 | 2.59 | 75 (H−1 → L) |
| 13 | 700 | 1.77 | 2.41 | 88 |

[a]Excitation energy ($E_{exc}$) and oscillator strengths ($f$) in CHCl$_3$.

**Table 2. TD-DFT (CAM-B3LYP/6-31G\*)-Computed $\Delta G^{inject}$, LHE, and Ground- ($E^{dye}$) and Excited ($E^{dye*}$)-State Oxidation Potential Energies**

| dyes | $E^{dye}$ (eV) | $E^{dye*}$ (eV) | $\Delta G^{inject}$ (eV) | LHE |
|---|---|---|---|---|
| 1 | 4.99 | 3.16 | −0.84 | 0.99 |
| 2 | 4.88 | 3.09 | −0.91 | 0.99 |
| 3 | 4.84 | 3.03 | −0.97 | 0.99 |
| 4 | 4.80 | 2.86 | −1.14 | 0.98 |
| 5 | 4.87 | 2.93 | −1.07 | 0.99 |
| 6 | 4.85 | 2.88 | −1.12 | 0.98 |
| 7 | 4.86 | 2.95 | −1.05 | 0.99 |
| 8 | 4.87 | 2.93 | −1.07 | 0.98 |
| 9 | 4.82 | 2.94 | −1.06 | 0.98 |
| 10 | 4.85 | 3.04 | −0.96 | 0.99 |
| 11 | 4.88 | 2.73 | −1.27 | 0.99 |
| 12 | 4.82 | 2.71 | −1.29 | 0.99 |
| 13 | 4.74 | 2.96 | −1.04 | 1.00 |

The synthetic approach to all the dyes started with the preparation of the common intermediate dibromide **17**, which can be obtained, following our optimized procedure,[29] by bromination of thienyl lactone **16**, in turn obtained by reaction of 2,4-dihexylthiophene (**14**) and maleic anhydride (see Scheme 1) and subsequent cyclization of the resulting 4-oxobut-2-enoic acid **15**. Except for a recent polymerization study,[14a] the synthetic elaboration of Pechmann lactones has not been previously reported. In addition, all derivatives described so far are symmetrical, and the desymmetrization of the central Pechmann chromophore to obtain nonsymmetrical D−π−A or similar structures has never been attempted. Very recently, we described the preparation of some symmetrically functionalized Pechmann lactones following a procedure entailing Stille−Migita cross-coupling between dibromide **17**

and a suitable stannane.[29] The experimental procedure we used, being performed in very mild conditions and without bases, proved a suitable tool for the synthetic elaboration of the very sensitive bis-lactone scaffold, and thus we decided to use a similar approach also to prepare compounds **1** and **2**. We started with the introduction of the donor groups, which implies the desymmetrization of the central Pechmann scaffold **17**. Reaction with stannanes **18a,b** was then performed, following a slightly modified version of our cross-coupling procedure.[29] Accordingly, the Stille−Migita reactions were carried out using a stoichiometric amount of the stannanes and stopped before the complete conversion of the starting material, to avoid the formation of the symmetric double-coupling product. For this reason, the desired products **19a,b** could be obtained only in 25−27% yield, even though the starting dibromide **17** could always be partially recovered after chromatographic purification, and recycled for further use. The acceptor group was then introduced by a second Stille−Migita reaction using organostannane **20**. In both cases, the desired aldehydes **21a,b** were obtained in good yields. The last step of the synthesis required Knoevenagel condensation to obtain cyanoacrylic acids. Considering that the Pechmann core proved to be quite sensitive to the presence of excess acetic acid, we needed to modify the standard reaction conditions, which commonly require using a mixture of toluene and acetic acid as the solvent and a large excess of cyanoacetic acid and ammonium acetate.[30] Instead, we decided to use a stoichiometric amount of piperidine[25] as the base and a mixture of toluene and acetonitrile as the solvent. In this way, provided that the reaction is stopped before the complete conversion of the starting materials to minimize degradation, we have been able to recover the desired dyes **1** and **2** in 37 and 62% isolated yield, respectively (Scheme 2).[1]

Advanced intermediate **19b** was also used to prepare the two dyes **6** and **7** (Scheme 3). Following the usual procedure, reaction with organostannane **22**[31] gave compound **6** in good yield after purification (Scheme 3). On the other hand, compound **7** was prepared by coupling **19b** with the unprotected 4-ethynylbenzoic acid **23**, following standard Sonogashira conditions, that is, Pd(PPh$_3$)$_4$ as the catalyst, CuI as the co-catalyst, and Et$_3$N as the base.[32]

Finally, to synthesize compound **8**, lactone **16** was reacted overnight with a 4-fold excess of $n$-C$_6$H$_{13}$NH$_2$ and 20% DMAP in DCM, followed by acidification with TsOH·H$_2$O (Scheme 4)[13a] to obtain lactam **25**. Unfortunately, attempts to prepare dibromide **24** by standard bromination of **25** failed, and only decomposition products were recovered even after a very short reaction time. Therefore, we decided to convert directly dibromo bis-lactone **17** into bis-lactam **24**. Using the same amidation conditions, pure intermediate **24** was indeed recovered after chromatography, although in moderate yield. To end the synthesis, the usual approach was followed,

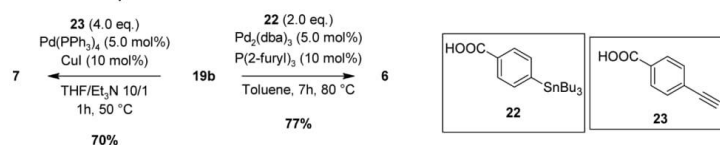**Scheme 1. Synthetic Pathway for the Preparation of the Pechmann Scaffold**
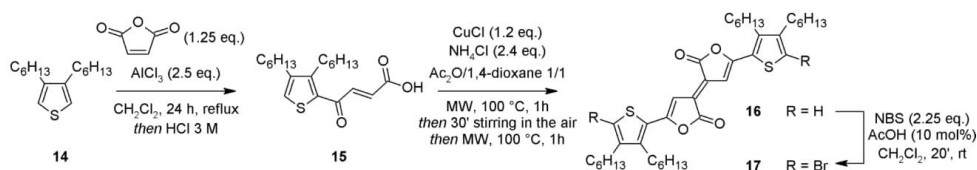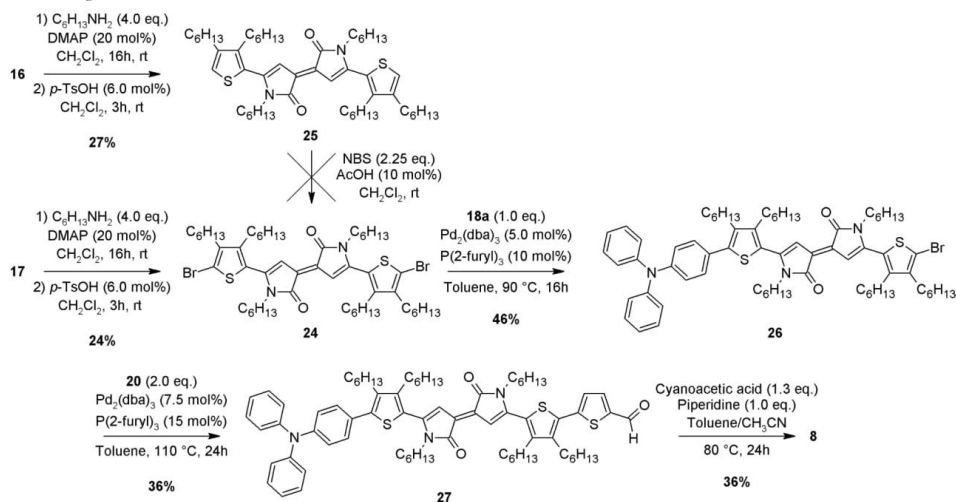
**Scheme 2. Preparation of Nonsymmetrical Pechmann Derivatives 1 and 2**
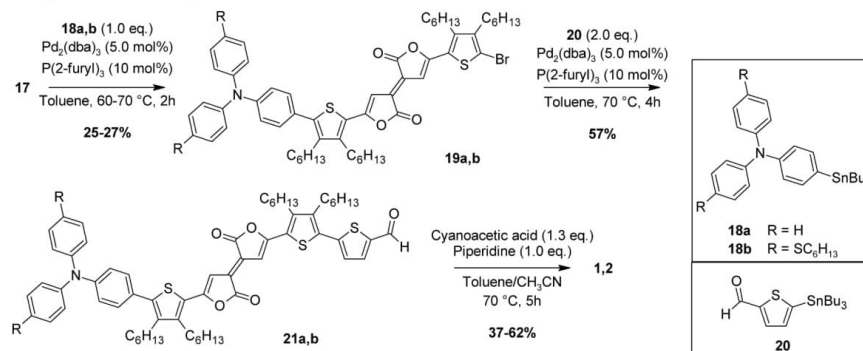


**Scheme 3. Preparation of Nonsymmetrical Pechmann Derivatives 6 and 7**



**Scheme 4. Preparation of Aza-Pechmann Derivative 8**



performing two subsequent cross-coupling reactions, using stannane **18a** first and then stannane **20**. Although in both cases, lactam derivatives showed a lower reactivity compared to their lactone analogues and higher reaction temperature and longer times were required, the desired dye **8** was indeed obtained in a pure form and with a reasonable overall yield. Surprisingly, dye **8** was quite unstable, rapidly turning from green (see below) to pale yellow upon dissolution in the most common solvents. We tentatively attribute such behavior to the ring opening of the lactam moiety (possibly followed by ring closure to a different isomer), which has been reported to

yield species characterized by weaker and blue-shifted absorption spectra compared to the Pechmann chromophore.[12,13]

**Spectroscopic and Electrochemical Data.** The optical properties of all the new dyes were studied. First of all, the UV−vis spectra of dye **1** and all its synthetic intermediates containing the Pechmann moiety (namely, **16**, **17**, **19a**, and **21a**) were recorded in CHCl$_3$ solution (Figure 5a). The comparison clearly shows the red shift and widening of the absorption bands, due to the elongation of the conjugated skeleton and the formation of the alternating D−A structure,
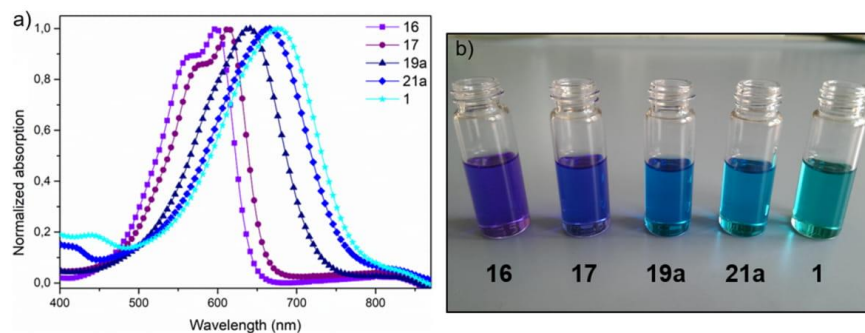
**Figure 5.** (a) UV−vis absorption spectra of intermediates **16**, **17**, **19a**, and **21a** and of dye **1** in CHCl$_3$: **16**, violet squares; **17**, purple circles; **19a**, navy blue triangles; **21a**, blue diamonds; and **1**, cyan stars. (b) Photograph of CHCl$_3$ solutions of compounds **16**, **17**, **19a**, **21a**, and **1** (approximate concentration of 1−2 × 10$^{-5}$ M).
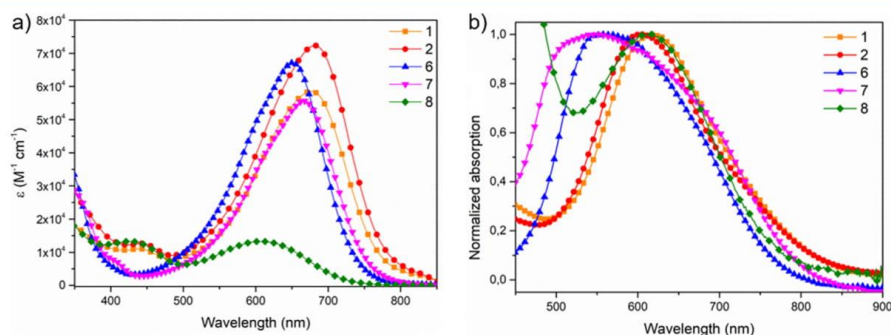


**Figure 6.** (a) UV−vis absorption spectra of compounds **1**, **2**, **6**, **7**, and **8** in CHCl$_3$ solution. (b) Normalized UV−vis absorption spectra of compounds **1**, **2**, **6**, **7**, and **8** adsorbed on a TiO$_2$ thin film: **1**, orange squares; **2**, red circles; **6**, blue upside triangles; **7**, purple downside triangles; and **8**, green rhombi.

**Table 3. Spectroscopic and Electrochemical Data for Dyes 1, 2, 6, 7, and 8**

| compound | $\lambda_{abs.}$ (nm)$^a$ | $\varepsilon$ (× 10$^4$) [M$^{-1}$ cm$^{-1}$] | $\lambda_{abs.}$ (nm) on TiO$_2$ | $\lambda_{emi}$ (nm)$^a$ | $E_{0-0}$ (eV)$^b$ | $E_{S+/S}$ (V)$^c$ | $E_{S+/S*}$ (V)$^d$ | $\Gamma$ (× 10$^{-7}$) [mol cm$^{-2}$] |
|---|---|---|---|---|---|---|---|---|
| **1** | 676 | 5.9 | 617 | 799 | 1.68 | 1.10 | −0.58 | 1.88 |
| **2** | 681 | 7.2 | 604 | 788 | 1.69 | 1.05 | −0.64 | 2.47 |
| **6** | 651 | 6.8 | 558 | 754 | 1.78 | 1.03 | −0.75 | 0.50 |
| **7** | 666 | 5.6 | 550 | 766 | 1.75 | 1.02 | −0.73 | 1.02 |
| **8**$^e$ | 608 (433) | 1.6 (2.0) | 612 (413) | 742 | 1.80 | | | 0.82 |

$^a$In CHCl$_3$ solution. $^b$Estimated from the intersection of normalized absorption and emission spectra. $^c$Measured in 0.1 M CH$_2$Cl$_2$/TBAPF$_6$ on a glassy carbon electrode. Values are reported against NHE. $^d$Obtained by means of the following expression: $E_{S+/S*} = E_{S+/S} - E_{0-0}$. $^e E_{S+/S}$ and $E_{S+/S*}$ were not measured due to decomposition of compound **8**.

with the color of the compounds progressively shifting from violet to cyan (Figure 5b). This trend was finely predicted by the TD-DFT study (see Supporting Information, Table S2). UV−vis spectra of dyes **1**, **2**, **6**, **7**, and **8** were then recorded, both in CHCl$_3$ solution and after adsorption on TiO$_2$ (Figure 6a,b and Table 3). Again, the values we found are in very good agreement with those obtained from the DFT/TD-DFT study (Table 1). As expected, **1**, **2**, **6**, and **7** showed an intense cyan color in solution due to their broad absorption of red/NIR light. In particular, dyes **1** and **2** showed the most red-shifted absorption with a maximum value of $\lambda$ = 681 nm registered for **2**, due to the strong electron-donating character of the thioalkyl substituent. On the other hand, the presence of less

electron-withdrawing anchoring groups such as for dyes **6** and **7** resulted in a blue shift of the absorption maxima, which is more pronounced in the case of **6** probably because of a loss of planarity, which might hamper conjugation between the thienyl group of the central scaffold and the benzoic acid substituent. Finally, bis-lactam-based compound **8** presented a blue-shifted and much less intense low-energy absorption band compared to its bis-lactone analogue **1** (1.6 × 10$^4$ vs 5.9 × 10$^4$ M$^{-1}$ cm$^{-1}$), which was accompanied by a higher energy absorption band of similar intensity (2.0 × 10$^4$ M$^{-1}$ cm$^{-1}$) at 433 nm. As a consequence, the corresponding CHCl$_3$ solution displayed an intense green rather than cyan color (Figure 6a).

All dyes exhibited fluorescence in CHCl$_3$ solution (Figures S26−S30); therefore, optical band gaps ($E_{0-0}$) could be obtained from the intersection of the normalized absorption and emission spectra and were found in the 1.68−1.80 eV range (Table 3), with **1** and **2** having the smallest $E_{0-0}$ values. A very wide absorption band (500−850 nm) was observed when the dyes were adsorbed on the TiO$_2$ layer. This was accompanied by a moderate blue shift of the maximum absorption peak, probably due to partial aggregation.[33] Interestingly, the only exception was observed for dye **8**, for which a slight red shift was observed (612 vs 608 nm in CHCl$_3$ solution), possibly due to the presence of two additional linear hexyl chains (bonded to the lactam nitrogen atoms) on its molecular structure, which might have a limiting effect on the incidence of aggregation phenomena.[19a,b] As already outlined, in the case of dye **8**, we observed a rapid change in color from green to pale yellow after dissolution in most of the common solvents or adsorption on TiO$_2$ which hampered any further analysis. The ground-state oxidation potentials ($E_{S+/S}$) of the dyes were then measured by means of cyclic voltammetry (CV), which was carried out in dichloromethane solutions in the presence of 0.1 M Bu$_4$NPF$_6$ as the electrolyte (Figures S31−S34 and Table 3).

$E_{S+/S}$ values ranging from 1.02 to 1.10 V versus the normal hydrogen electrode (NHE) were found, and consequently, driving forces for the regeneration from the I$^-$/I$_3^-$ redox couple ($\Delta G_{reg}$) were over 670 mV.

Because overpotentials of approximately 500 mV are required for efficient dye regeneration from the iodide/triiodide electrolyte,[34] the electron transfer from the redox shuttle to the oxidized dyes is expected to work well. Indeed, the excited-state oxidation potential ($E_{S+/S*}$) is a crucial parameter to assess the electron injection efficiency from the excited state of the dye to the conduction band (CB) of titania and was calculated using the following equation

$$E_{S+/S*} = E_{S+/S} - E_{0-0}$$

All the calculated $E_{S+/S*}$ values are in the range −0.58 to −0.75 V versus NHE (Table 3). In Figure 7, the comparison of ground-state and excited-state oxidation potentials of dyes **1** and **2** and **6** and **7** with the TiO$_2$ CB (−0.50 V vs NHE) and the iodide/triiodide redox couple (0.35 V vs NHE)[35] potentials is reported, together with that of the **DF15** reference dye.[25] Clearly, the driving force for electron injection ($\Delta G^{inject}$) ranges from ~80 to 250 mV, values that are lower than 300 mV, which is the optimal driving force to have fast kinetics of electron injection in the TiO$_2$ layer,[7,34] but are comparable or superior to the minimum overpotential, which is estimated to be ~100 to 100 mV (Figure 7).[34,36]

This situation is unfortunately common in narrow-band-gap dyes, especially those containing strong electron-deficient π bridges (see for instance thieno[3,4-b]pyrazine-based dyes),[18d,37] resulting in low efficiency of the corresponding devices. Very often, in these cases, the $\Delta G^{inject}$ can be increased by using special precautions in fabricating solar cells.

**Photovoltaic Measurements.** To assess the capability of the new compounds to yield working DSSCs, we decided to carry out a preliminary study and built some solar devices using dyes **6** and **7**. We selected these two dyes because, relying on the values of excited state potentials ($E_{S+/S*}$), they were the only ones able to guarantee the minimum required overpotential with respect to the TiO$_2$ conduction layer, with
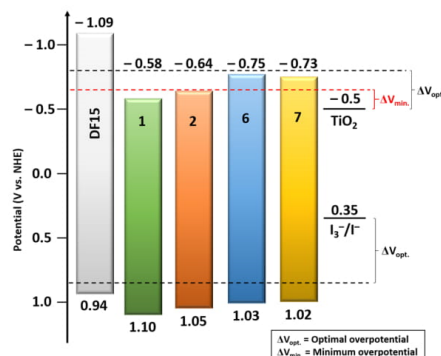


**Figure 7.** Energy level diagram of ground-state and excited-state oxidation potentials of dyes **DF15**, **1**, **2**, **6**, and **7** compared with TiO$_2$ CB (−0.50 V) and iodide/triiodide redox couple (0.35 V) potentials. Black dotted lines mark the optimal $E_{S+/S}$ (0.85 V) and $E_{S+/S*}$ (−0.80 V) values for a sensitizer with fast electron transfer kinetics. The red dotted line defines the limit potential (−0.65 V) to guarantee electron injection.

dye **8** being too unstable to be used in the experimental conditions required.

Initially, we built test cells using standard conditions: photoanodes of different thicknesses were sensitized with compound **6**, and a standard high-performance electrolyte[38] was used. No photocurrent was recorded in such conditions. However, the electrolyte we used contains special additives (i.e., *tert*-butyl pyridine and guanidinium isothiocyanate GuSCN), which are usually present with the aim of increasing $V_{oc}$ by enhancing the TiO$_2$ CB potential. This feature is not compatible with dyes having a low injection overpotential; thus, we decided to try to investigate different electrolyte compositions. In particular, six different electrolytes were tested, sensitizing the electrodes with dye **6**, and the three best-performing compositions were also tested using dye **7**. The power conversion efficiency, $\eta$, was calculated using the following equation

$$\eta = J_{sc} V_{oc} FF / I_0 \qquad (5)$$

where $J_{sc}$ is the short-circuit photocurrent density, $V_{oc}$ is the open-circuit photovoltage, FF is the fill factor, and $I_0$ is the energy of incident sunlight (100 mW cm$^{-2}$). The results obtained are summarized in Table 4. It is evident that for all the cells prepared, a very low efficiency was recorded; however, in the case of dye **6**, even with a simple electrolyte containing only the redox couple (A), a low photocurrent was observed. LiI and guanidinium thiocyanate were then added, which are often used to increase both $V_{oc}$ and the short-circuit photocurrent ($J_{sc}$).[39,40] Indeed, a moderate concentration of guanidinium thiocyanate (B) increased $V_{oc}$ values without affecting the photocurrent, whereas a higher concentration of guanidinium thiocyanate (C) was detrimental to both. Addition of the bulky cation 1-butyl-3-methylimidazolium (BMI$^+$) and the innocent anion ClO$_4^-$ (D), as expected, slowed down the recombination processes increasing the photovoltage;[41] however, it did not give a better efficiency. Increasing the concentration of Li$^+$ to 1.025 M (E) and 1.625 M (F) gave, as we expected, higher photocurrents, with the best results occurring with electrolyte E, corresponding also

53

**Table 4. Photovoltaic Characteristics of the DSSC Sensitized with Dyes 6 and 7 under AM 1.5 Simulated Solar Illumination**

| dye | E[a] | $J_{sc}$ (mA cm$^{-2}$) | $V_{oc}$ (mV) | FF | $\eta$ (%)[b] |
|-----|------|-------------------------|---------------|------|---------------|
| 6 | A | 0.86 | 386.0 | 52.0 | 0.17 |
| 7 |   | 0.63 | 412.6 | 53.4 | 0.14 |
| 6 | B | 0.84 | 400.6 | 54.0 | 0.18 |
| 7 |   | 0.54 | 408.1 | 43.4 | 0.10 |
| 6 | C | 0.65 | 362.9 | 40.7 | 0.10 |
| 6 | D | 0.68 | 430.6 | 57.2 | 0.17 |
| 6 | E | 1.19 | 420.8 | 48.9 | 0.24 |
| 7 |   | 0.53 | 387.4 | 44.7 | 0.10 |
| 6 | F | 0.95 | 414.3 | 44.2 | 0.17 |

[a]Electrolyte: A: I$_2$ (0.04 M), LiI (0.625 M); B: I$_2$ (0.04 M), LiI (0.625 M), guanidinium thiocyanate (0.1 M); C: I$_2$ (0.04 M), LiI (0.625 M), guanidinium thiocyanate (0.3 M); D: I$_2$ (0.04 M), N-methyl-N-butylimidazolium iodide (0.625 M), LiClO$_4$ (0.625 M), guanidinium thiocyanate (0.1 M); E: I$_2$ (0.04 M), LiI (0.625 M), guanidinium thiocyanate (0.1 M), LiClO$_4$ (0.4 M); F: I$_2$ (0.04 M), LiI (0.625 M), guanidinium thiocyanate (0.1 M), LiClO$_4$ (1.0 M). In all cases, the solvent was acetonitrile/valeronitrile (85/15, v/v). [b]Data refer to the best results obtained for at least three devices for each configuration.

with the best efficiency recorded. When electrodes were sensitized with dye 7, the effect of the additives was detrimental in all cases, and cells built using the simple electrolyte A resulted in the best performing ones. This different behavior of dye 7 might be due to its lower excited state potential (see Table 3), which makes any attempt to enhance the electron injection process ineffective. Representative J/V curves for the best devices built with dyes 6 and 7 are reported in Figure S35.

In any case, the low efficiencies recorded were mostly due to low photocurrents. Recalling the results of our computational analysis, it is possible that the scarce delocalization of the LUMO orbitals of dyes 6 and 7 on their actual anchoring groups, coupled with the abovementioned small driving forces, limited their charge injection efficiency, reducing its rate and making it competitive with recombination reactions as well as unproductive intermolecular energy transfer processes.

## ■ CONCLUSIONS

Thirteen new thiophene-substituted Pechmann dyes have been designed, intended to evaluate the effect of decorating the central scaffold with different donor (D) and acceptor (A) groups on their physico- and electrochemical properties. Such an approach was aimed at preparing new D−A−π−A structures suitable for application as sensitizers for DSSCs because increased knowledge in choosing an appropriate combination of D/A moieties and exploitation of new building blocks are essential for the development of high-performance devices.

The designed structures were investigated by means of DFT and TD-DFT calculations to evaluate the red to NIR absorption maxima, the proper alignment of their FMO energies compared to the CB of TiO$_2$ and the I$^-$/I$_3^-$ redox potential, and the intramolecular charge-transfer nature of the excitation. Calculations suggested that almost all the designed dyes were suitable for application in DSSCs. Five of these new dyes were prepared using an approach that was based on bromination of the central Pechmann core and desymmetrization by running Stille−Migita cross-coupling in strictly stoichiometric conditions and stopping the reaction before

complete consumption of the starting material. Further elaboration of the resulting intermediates led to the preparation of D−A−π−A compounds constituting, to the best of our knowledge, the first example of synthesis of unsymmetrical Pechmann (or aza-Pechmann) derivatives. In agreement with DFT computational studies, the new dyes showed intense absorption of light in the NIR region of the spectrum, accompanied by a significant degree of intramolecular charge transfer. Unfortunately, the driving force for electron injection ($\Delta G^{inject}$) of such dyes was found to be too low to have fast kinetics of electron injection. This is in agreement with the very low efficiencies given by test cells built using two representative dyes (6 and 7), whose charge injection capabilities were also probably hampered by insufficient LUMO delocalization, caused by the weak electron-withdrawing nature of their anchoring groups. Nevertheless, a photocurrent increase could still be observed in the presence of electrolytes especially formulated for narrow-band-gap dyes with low $E_{S+/S*}$. The results of these preliminary investigations provide a basic understanding of the properties of D−A−π−A dyes based on the Pechmann chromophore and should be useful to stimulate further research directed toward structural refinement of the sensitizers and optimization of device characteristics.

## ■ EXPERIMENTAL SECTION

Unless otherwise stated, all reagents were purchased from commercial suppliers and used without purification. Dibromide 17 and stannanes 18a, 18b, 20,[29] and 22[31a] were prepared as reported. All air-sensitive reactions were performed using Schlenk techniques. Solvents used in cross-coupling reactions were previously degassed by means of the "freeze−pump−thaw" method. Tetrahydrofuran (THF) was freshly distilled immediately before use from sodium/benzophenone. CH$_2$Cl$_2$ and triethylamine were distilled over CaH$_2$, and toluene and acetonitrile were dried on a resin exchange solvent purification system. Petroleum ether, unless specified, is the 40−70 °C boiling fraction. Reactions were monitored by TLC on SiO$_2$ plates, and detection was made using a KMnO$_4$ basic solution or a UV lamp. The organic phase derived from aqueous workup was dried over Na$_2$SO$_4$. Flash column chromatography was performed using glass columns (10−50 mm wide) and SiO$_2$ (230−400 mesh).$^1$H-NMR spectra recorded at 300 or 400 MHz and $^{13}$C-NMR spectra were recorded at 75.5 or 100.6 MHz, respectively. Chemical shifts were referenced to the residual solvent peak (CDCl$_3$, $\delta$ 7.26 ppm for $^1$H-NMR and $\delta$ 77.16 ppm for $^{13}$C-NMR; THF-$d_8$, $\delta$ 1.72 and 3.58 ppm for $^1$H-NMR and $\delta$ 67.21 and 25.31 ppm for $^{13}$C-NMR; C$_6$D$_6$, $\delta$ 7.16 ppm for $^1$H-NMR and $\delta$ 128.06 ppm for $^{13}$C-NMR). Coupling constants ($J$) were reported in Hz. ESI-MS analyses were recorded with an LCQ-Fleet ion-trap mass spectrometer. HR-MS analyses were performed using a LTQ Orbitrap FT-MS spectrometer. FT-IR spectra were recorded with a Perkin-Elmer Spectrum BX instrument in the range 4000−400 cm$^{-1}$ with 2 cm$^{-1}$ resolution. UV−vis spectra were recorded with a Varian Cary 400 spectrometer and a Shimadzu 2600 series spectrometer, and fluorescence spectra were recorded with a Varian Eclipse instrument, irradiating the sample at the wavelength corresponding to the maximum absorption in the UV spectrum. In all electrochemical experiments, N$_2$-saturated solutions of the compound under study were used with [Bu$_4$N][PF$_6$] (0.1 M) as the supporting electrolyte (Fluka, electrochemical grade) and

freshly distilled dichloromethane. Cyclic voltammetry was performed in a three-electrode cell using a glassy carbon working electrode, a platinum counter electrode, and a AgCl/Ag (NaCl 3 M) reference electrode. A BAS 100 W electrochemical analyzer was used as the polarizing unit. All the potential values are referred to the NHE ([$E$ vs NHE] = [$E$ vs Ag/AgCl (NaCl 3 M) +0.21] V). Typical analyte concentration was $10^{-3}$ M. Ferrocene was used as the external standard (+0.44 V vs Ag/AgCl).

**General Procedure for Preparation of Compounds 19a,b.** Dibromide **17** (1.0 equiv) was dissolved in toluene, and then a solution of Pd$_2$dba$_3$ (5 mol %) and P(2-furyl)$_3$ (10 mol %) in toluene and the appropriate stannane (**18**, 1.0 equiv) were added. The resulting mixture was heated to 70 °C, stirred for 2 h, then allowed to cool to rt, and diluted with H$_2$O (50 mL) and ethyl acetate (100 mL). The organic layers were washed with brine and dried. After filtration and evaporation of the solvent, the crude product was purified by flash column chromatography.

*(3E)-5-(5-(4-(Diphenylamino)phenyl)-3,4-dihexylthio-phen-2-yl)-5′-(5-bromo-3,4-dihexylthiophen-2-yl)-3,3′-bifuranyl idene-2,2-dione (19a).* Dibromide **17** (185 mg, 0.23 mmol) in toluene (15 mL) was dissolved and reacted with Pd$_2$(dba)$_3$ (12 mg, 0.011 mmol), P(2-furyl)$_3$ (5.2 mg, 0.022 mmol), and 4-tributylstannyl-*N,N*-diphenylaniline (**18a**, 120 mg, 0.23 mmol) at 70 °C. Flash column chromatography (petroleum ether/toluene gradient of 6:1 to 2:1) gave pure product **19a** (56 mg, 0.056 mmol, 25% yield) as a dark-blue amorphous solid. $^1$H-NMR (400 MHz, CDCl$_3$): $\delta$ = 7.27–7.33 (m, 7H), 7.23 (s, 1H), 7.15 (d, $J$ = 7.5 Hz, 4H), 7.06–7.10 (m, 4H), 2.81–2.85 (m, 4H), 2.51–2.62 (m, 4H), 1.47–1.66 (m, 12H), 1.24–1.43 (m, 20H), 0.79–0.91 (m, 12H) ppm; $^{13}$C-NMR (75 MHz, CDCl$_3$): $\delta$ = 167.2, 166.9, 155.0, 152.8, 148.7, 148.3, 147.4, 145.8, 145.5, 144.5, 141.0, 129.9, 129.6, 127.3, 126.3, 125.3, 125.2, 124.0, 123.8, 123.5, 122.5, 116.6, 104.1, 104.0, 31.7, 31.6, 31.5, 31.0, 30.2, 30.0, 29.9, 29.7, 29.6, 29.5, 29.4, 28.5, 27.4, 22.7, 14.2 ppm; IR (KBr): $\tilde{\nu}$ = 3029, 2924, 2853, 1762, 1559, 1199 cm$^{-1}$; ESI-MS: $m/z$ = 987.28 [M+1]$^+$

*(3E)-5-(5-(4-(Di-4-(hexylthio)phenyl)amino)phenyl)-3,4-dihexylthiophen-2-yl)-5′-(5-bromo-3,4-dihexyl thiophen-2-yl)-3,3′-bifuranylidene-2,2′-dione (19b).* Dibromide **17** (180 mg, 0.22 mmol) was dissolved in toluene (12 mL) and reacted with Pd$_2$(dba)$_3$ (11 mg, 0.011 mmol), P(2-furyl)$_3$ (5.1 mg, 0.021 mmol), and 4-tributylstannyl-*N,N*-(4-hexylthiophenyl) aniline (**18b**, 168 mg, 0.22 mmol) at 60 °C. Flash column chromatography (petroleum ether/toluene gradient of 6:12 to 2:1) gave pure product **19b** (72 mg, 0.059 mmol, 27% yield) as a blue gummy solid. $^1$H-NMR (300 MHz, C$_6$D$_6$): $\delta$ = 7.47 (s, 1H), 7.31–7.38 (m, 3H), 7.25 (d, $J$ = 8.7 Hz, 4H), 7.06 (d, $J$ = 8.6 Hz, 2H), 6.98 (d, $J$ = 8.6 Hz, 4H), 2.81–2.92 (m, 2H), 2.58–2.76 (m, 8H), 2.40–2.49 (m, 2H), 1.70–1.82 (m, 2H), 1.05–1.68 (m, 46H), 0.95–1.02 (m, 6H), 0.79–0.94 (m, 12H) ppm; $^{13}$C-NMR (75 MHz, C$_6$D$_6$): $\delta$ = 166.8, 166.5, 155.0, 153.0, 148.4, 148.3, 145.6, 145.4, 145.3, 144.5, 141.0, 132.6, 131.4, 131.0, 130.4, 125.8, 125.5, 125.0, 124.8, 124.0, 122.8, 116.7, 104.43, 104.39, 34.4, 31.94, 31.87, 31.76, 31.66, 31.3, 30.4, 30.2, 30.1, 30.0, 29.9, 29.8, 29.7, 29.6, 28.8, 28.6, 27.7, 23.13, 23.07, 23.0, 22.9, 14.39, 14.36, 14.31, 14.25 ppm; IR (KBr): $\tilde{\nu}$ = 3014, 2927, 2855, 1762, 1560, 1199 cm$^{-1}$. ESI-MS: $m/z$ = 1220.32 [M+1]$^+$

**General Procedure for Preparation of Compounds 21a,b.** Bromide (**19a,b**, 1.0 equiv) was dissolved in toluene

and reacted with a solution of Pd$_2$dba$_3$ (5 mol %), P(2-furyl)$_3$ (10 mol %), and 2-tributylstannyl-5-formylthiophene (**20**, 2.0 equiv) in toluene. The resulting mixture was heated to 70 °C and stirred for 4 h, and then it was cooled to rt and diluted with H$_2$O (50 mL) and ethyl acetate (100 mL). The organic layer was washed with brine and dried. After filtration and evaporation of the solvent, the crude product was purified by flash column chromatography.

*(3E)-5-(5-(4-(Diphenylamino)phenyl)-3,4-dihexylthio-phen-2-yl)-5′-(5-(5-formylthiophen-2-yl)-3,4-dihexylthio-phen-2-yl)-3,3′- bifuranylidene-2,2′-dione (21a).* Bromide **19a** (73 mg, 0.074 mmol) was dissolved in toluene (9 mL) and reacted with Pd$_2$(dba)$_3$ (3.8 mg, 0.004 mmol, 5 mol %), P(2-furyl)$_3$ (1.7 mg, 0.007 mmol, 10 mol %), and 2-tributylstannyl-5-formylthiophene (**20**, 59 mg, 0.148 mmol). Flash column chromatography (petroleum ether/toluene gradient, 2:1 to 1:3) gave pure aldehyde **21a** (43 mg, 0.042 mmol, 57% yield) as an amorphous black solid. $^1$H-NMR (400 MHz, CDCl$_3$): $\delta$ = 9.91 (s, 1H), 7.73 (d, $J$ = 4.0 Hz, 1H), 7.34 (s, 1H), 7.27–7.33 (m, 8H), 7.15 (d, $J$ = 7.7 Hz, 4H), 7.06–7.10 (m, 4H), 2.66–2.88 (m, 6H), 2.57–2.64 (m, 2H), 1.48–1.66 (m, 16H), 1.25–1.42 (m, 16H), 0.85–0.94 (m, 12H) ppm; $^{13}$C-NMR (100 MHz, CDCl$_3$): $\delta$ = 182.7, 167.1, 166.9, 155.3, 152.7, 149.0, 148.4, 147.6, 147.4, 145.9, 145.2,143.6, 143.5, 141.1, 136.7, 134.6, 129.9, 129.6, 127.4, 127.2, 126.5, 125.6, 125.3, 124.0, 123.8, 123.2, 122.4,105.3, 104.2, 31.7, 31.64, 31.61, 31.5, 31.0, 30.5, 30.2, 30.0, 29.9, 29.8, 29.7, 29.5, 29.4, 29.1, 28.2, 27.5, 22.79, 22.77, 22.74, 22.72, 14.2 ppm; IR (KBr): $\tilde{\nu}$ = 3062, 2924, 2854, 1757, 1661, 1551, 1201 cm$^{-1}$; ESI-MS: $m/z$ = 1063.70 [M+C$_2$H$_6$O]$^+$.

*(3E)-5-(5-(4-(bis(4-(Hexylthio)phenyl)amino)phenyl)-3,4-dihexylthiophen-2-yl)-5′-(5-(5-formylthiophen-2-yl)-3,4-di-hexylthiophen-2-yl)-3,3′-bifuranylidene-2,2′-dione (21b).* Bromide **19b** (90 mg, 0.074 mmol) was dissolved in toluene (10 mL) and reacted with Pd$_2$(dba)$_3$ (3.8 mg, 0.004 mmol, 5 mol %), P(2-furyl)$_3$ (1.7 mg, 0.007 mmol, 10 mol %), and 2-tributylstannyl-5-formylthiophene (**20**, 59 mg, 0.148 mmol). Flash column chromatography (petroleum ether/toluene, gradient 2:1 to 1:3) gave pure aldehyde **21b** (52 mg, 0.042 mmol, 57% yield) as a blue gummy solid. $^1$H-NMR (300 MHz, C$_6$D$_6$): $\delta$ = 9.46 (s, 1H), 7.49 (s, 1H), 7.48 (s, 1H), 7.35 (d, $J$ = 8.3 Hz, 2H), 7.25 (d, $J$ = 8.3 Hz, 4H), 7.07 (d, $J$ = 8.6 Hz, 2H), 6.98 (d, $J$ = 8.4 Hz, 4H), 6.93 (d, $J$ = 3.8 Hz, 1H), 6.84 (d, $J$ = 3.8 Hz, 1H), 2.82–2.94 (m, 2H), 2.56–2.79 (m, 10H), 1.68–1.82 (m, 2H), 1.05–1.68 (m, 46H), 0.95–1.02 (m, 6H), 0.79–0.94 (m, 12H) ppm; $^{13}$C-NMR (75 MHz, C$_6$D$_6$): $\delta$ = 181.8, 166.8, 166.6, 155.2, 153.1, 148.7, 148.3, 147.7, 145.6, 145.4, 144.3, 144.1, 143.4, 141.1, 136.1, 135.2, 132.7, 131.0, 130.4, 127.4, 126.8, 125.9, 125.7, 124.9, 123.8, 122.8, 105.6, 104.5, 34.4, 32.0, 31.9, 31.74, 31.66, 31.3, 30.5, 30.4, 30.2, 30.1, 29.8, 29.6, 29.3, 28.8, 28.3, 27.7, 23.1, 23.0, 22.9, 14.4, 14.3, 14.2 ppm (one of the aromatic signals is covered due to the solvent); IR (KBr): $\tilde{\nu}$ = 3027, 2925, 2853, 1752, 1655, 1552, 1203 cm$^{-1}$; ESI-MS: $m/z$ = 1251.42 [M+1]$^+$.

**General Procedure for Preparation of Compounds 1 and 2.** Aldehyde (**21a,b**, 1.0 equiv) was dissolved in toluene, and then a solution of cyanoacetic acid (1.3 equiv) and piperidine (1.0 equiv) in MeCN was added. The resulting mixture was heated to 70 °C and stirred for 5 h, and then chloroform (100 mL) and a 3 M aqueous solution of HCl (100 mL) were added. The organic phase was separated, and the solvent was evaporated. The resulting solid was purified by

consecutive washes with pentane, diethyl ether, methanol, and ethyl acetate and dried under vacuum.

*2-Cyano-3-(5-(5-((3E)-3-(2-oxo-5-(5-(4-(diphenylamino) phenyl)-3,4-dihexylthiophen-2-yl)-furan-3(2H)-ylidene)-furan-2(3H)-on-5-yl)-3,4-dihexylthiophen-2-yl)thiophen-2-yl)acrylic acid (1).* Aldehyde **21a** (30 mg, 0.029 mmol) was dissolved in toluene (4 mL) and reacted with cyanoacetic acid (3.2 mg, 0.038 mmol) and piperidine (2.5 mg, 0.029 mmol, 2.9 $\mu$L) in MeCN (2.0 mL). Workup and purification afforded compound **1** (12 mg, 0.011 mmol, 37% yield) as an amorphous dark solid. $^1$H-NMR (300 MHz, THF-$d_8$): $\delta$ = 8.37 (s, 1H), 7.80−7.91 (m, 1H), 7.43−7.52 (m, 1H), 7.22−7.41 (m, 8H), 6.99−7.19 (m, 8H), 2.81−2.97 (m, 6H), 2.61−2.74 (m, 2H), 1.51−1.68 (m, 12H), 1.21−1.49 (m, 20H), 0.79−0.98 (m, 12H) ppm; $^{13}$C−NMR (75 MHz, THF-$d_8$): $\delta$ = 166.8, 166.6, 163.7, 155.5, 153.3, 149.2, 149.0, 148.2, 148.1, 146.1, 145.9, 144.6, 144.2, 141.5, 139.9, 139.1, 137.5, 135.6, 130.4, 130.1, 128.0, 127.8, 126.9, 125.8, 124.6, 124.4, 123.9, 122.8, 116.4, 105.6, 104.3, 100.5, 32.4, 32.3, 32.2, 31.5, 31.2, 30.6, 30.48, 30.46, 30.41, 30.3, 30.1, 29.8, 29.5, 28.9, 27.9, 23.4, 23.34, 23.30, 14.3 ppm; IR (KBr): $\tilde{\nu}$ = 3421, 3067, 2923, 2853, 2211, 1759, 1552, 1201 cm$^{-1}$; ESI-MS: $m/z$ = 1084.93 [M]$^+$; HRMS (ESI) C$_{66}$H$_{72}$O$_6$N$_2$S$_3$ ([M]$^+$), calcd 1084.4547, found 1084.4527.

*2-Cyano-3-(5-(5-((3E)-3-(2-oxo-5-(5-(4-(bis(4-(Hexylthio) phenyl)amino)phenyl)-3,4-dihexylthiophen-2-yl)-furan-3(2H)-ylidene)-furan-2(3H)-on-5-yl)-3,4-dihexylthiophen-2-yl) thiophen-2-yl)acrylic acid (2).* Aldehyde **21b** (50 mg, 0.040 mmol) was dissolved in toluene (6.0 mL) and reacted with cyanoacetic acid (4.4 mg, 0.052 mmol) and piperidine (3.4 mg, 0.040 mmol, 4.0 $\mu$L) in MeCN (3.0 mL). Workup and purification afforded compound **2** (33 mg, 0.025 mmol, 62% yield) as a dark gummy solid. $^1$H-NMR (300 MHz, THF-$d_8$): $\delta$ = 8.34 (s, 1H), 7.83 (d, $J$ = 3.9 Hz, 1H), 7.45 (d, $J$ = 3.9 Hz, 1H), 7.19−7.41 (m, 8H), 6.98−7.13 (m, 6H), 2.79−2.98 (m, 10H), 2.60−2.74 (m, 2H), 1.54−1.68 (m, 12H), 1.22−1.48 (m, 36H), 0.83−0.98 (m, 18H) ppm; $^{13}$C-NMR (75 MHz, THF-$d_8$): $\delta$ = 166.7, 166.5, 163.6, 155.4, 153.3, 149.0, 148.7, 148.3, 145.90, 145.87, 145.7, 144.6, 144.2, 141.5, 139.1, 137.5, 135.6, 132.9, 131.1, 130.5, 128.00, 127.96, 126.9, 126.1, 125.8, 124.7, 123.9, 122.8, 116.4, 105.6, 104.3, 100.4, 34.5, 32.4, 32.3, 32.2, 30.51, 30.47, 30.43, 30.3, 30.1, 30.0, 29.2, 23.43, 23.41, 23.36, 23.32, 23.29, 14.3, 14.2 ppm; IR (KBr): $\tilde{\nu}$ = 3435, 2924, 2853, 2212, 1760, 1522, 1201 cm$^{-1}$; ESI-MS: $m/z$ = 1316.41 [M]$^+$. HRMS (ESI) C$_{78}$H$_{96}$O$_6$N$_2$S$_5$ ([M]$^+$), calcd 1316.5866, found 1316.5862.

**Preparation of Compound 6.** *4-(5-((3E)-3-(2-Oxo-5-(5-(4-(bis(4-(hexylthio)phenyl)amino) phenyl)-3,4-dihexylthiophen-2-yl)-furan-3(2H)-ylidene)-furan-2(3H)-on-5-yl)-3,4-dihexyl thiophen-2-yl)benzoic acid (6).* Bromide **19b** (55 mg, 0.045 mmol, 1.0 equiv) and 4-(tributyltin)benzoic acid (**22**, 37 mg, 0.090 mmol, 2.0 equiv) were dissolved in toluene (2.0 mL) and stirred with a solution of Pd$_2$dba$_3$ (2.3 mg, 0.0023 mmol, 5 mol %) and P(2-furyl)$_3$ (1.0 mg, 0.0045 mmol, 10 mol %) in toluene (2 mL) at 80 °C for 7 h. After cooling to room temperature, the solvent was evaporated under reduced pressure. The crude product was first purified by flash column chromatography (dichloromethane, then ethyl acetate, and then ethyl acetate + 2% acetic acid). The solid obtained was dissolved in dichloromethane (20 mL), washed with 3 M aq HCl (25 mL), and dried with Na$_2$SO$_4$. After filtration and removal of the solvent, the solid residue was washed with small portions of pentane (3 × 5 mL) and methanol (2 × 5 mL) to

give dye **6** (45 mg, 0.036 mmol, 79% yield) as a blue gummy solid. $^1$H-NMR (400 MHz, CDCl$_3$): $\delta$ = 8.18 (d, $J$ = 7.9 Hz, 2H), 7.57 (d, $J$ = 7.9 Hz, 2H), 7.24−7.32 (m, 8H), 7.03−7.10 (m, 6H), 2.76−2.95 (m, 8H), 2.56−2.72 (m, 4H), 1.19−1.82 (m, 48H), 0.85−1.00 (m, 18H); $^{13}$C-NMR (100 MHz, CDCl$_3$): $\delta$ = 170.8, 167.2, 167.1, 154.7, 153.6, 148.5, 147.8, 147.6, 145.2, 145.1, 142.3, 142.1, 141.0, 139.8, 131.5, 130.8, 130.0, 129.3, 127.6, 126.0, 125.4, 125.0, 124.1, 123.7, 122.6, 104.5, 104.0, 34.5, 31.6, 31.5, 31.0, 30.2, 29.8, 29.5, 29.3, 28.6, 27.4, 22.8, 22.7, 14.2, 14.1 (two of the aromatic signals are absent due to overlapping); IR (KBr): $\tilde{\nu}$ = 3418, 2958, 2924, 2855, 1762, 1694, 1557, 1464, 1200 cm$^{-1}$; ESI-MS: $m/z$ = 1260.72 [M+1]$^+$. HRMS (ESI) C$_{77}$H$_{97}$NO$_6$S$_4$ ([M]$^+$), calcd 1259.6199, found 1259.6189.

**Preparation of Compound 7.** *4-((5-((3E)-3-(2-Oxo-5-(5-(4-(bis(4-(hexylthio)phenyl) amino)phenyl)-3,4-dihexylthiophen-2-yl)-furan-3(2H)-ylidene)-furan-2(3H)-on-5-yl)-3,4-di-hexylthiophen-2-yl)ethynyl) benzoic acid (7).* A solution of bromide **21b** (75 mg, 0.061 mmol, 1.0 equiv) in THF (9.0 mL) was degassed, and then 4-ethynylbenzoic acid (**23**, 36 mg, 0.246 mmol, 4.0 equiv), Pd(PPh$_3$)$_4$ (6.1 mg, 0.0061 mmol, 10 mol %), copper (I) iodide (1.2 mg, 0.0061 mmol, 10 mol %), and triethylamine (0.35 mL) were added. The resulting mixture was stirred at 50 °C for 1 h, and then after cooling to room temperature, the solvent was removed under reduced pressure. The reaction crude was suspended in dichloromethane (25 mL) and 3 M aq HCl (25 mL) and filtered over Celite. The organic phase was washed again with 3 M aq HCl (25 mL) and dried. The crude obtained after solvent removal was filtered by flash column chromatography (dichloromethane, then ethyl acetate, and then ethyl acetate + 2% acetic acid). The solid obtained was dissolved in dichloromethane (25 mL), and the organic phase was washed with 3 M aq HCl (25 mL) and dried. After filtration and removal of the solvent, the residue was washed with pentane (3 × 5 mL) and methanol (2 × 5 mL) to give dye **7** (55 mg, 0.043 mmol, 70% yield) as a blue gummy solid. $^1$H-NMR (400 MHz, CDCl$_3$): $\delta$ = 8.06 (d, $J$ = 8.0 Hz, 2H), 7.56 (d, $J$ = 8.0 Hz, 2H), 7.22−7.30 (m, 8H), 7.02−7.08 (m, 6H), 2.89 (t, $J$ = 7.3 Hz, 4H), 2.78−2.86 (m, 4H), 2.69−2.78 (m, 2H), 2.57−2.63 (m, 2H), 1.21−1.72 (m, 48H), 0.82−1.01 (m, 18H); $^{13}$C-NMR (100 MHz, CDCl$_3$): $\delta$ = 170.8, 167.0, 166.9, 154.8, 152.7, 150.4, 148.8, 147.8, 145.6, 145.4, 145.2, 141.0, 131.6, 131.3, 130.8, 130.3, 129.9, 128.8, 128.3, 127.5, 127.3, 125.4, 125.2, 124.1, 123.3, 122.9, 122.5, 105.1, 104.2, 98.9, 86.4, 34.5, 31.7, 31.6, 31.5, 31.0, 30.4, 30.1, 29.9, 29.8, 29.5, 29.4, 28.7, 22.8, 22.7, 14.2; IR (KBr): $\tilde{\nu}$ = 3418, 2954, 2921, 2853, 2189, 1756, 1694, 1555, 1416, 1201 cm$^{-1}$. ESI-MS: $m/z$ = 1283.80 [M]$^+$. HRMS (ESI) C$_{79}$H$_{97}$NO$_6$S$_4$ ([M]$^+$), calcd 1283.6199, found 1283.6194.

**Preparation of Aza-Pechmann Derivative 8.** *(3E)-5,5′-(5-Bromo-3,4-dihexylthiophen-2-yl)-1,1′-dihexyl-3,3′-bipyr-rolylidene-2,2′-dione (24).* A solution of dibromide **17** (0.200 g, 0.243 mmol, 1.0 equiv), hexylamine (0.098 g, 0.972 mmol, 128 $\mu$L, 4.0 equiv), and DMAP (6.0 mg, 0.049 mmol, 20 mol %) in dichloromethane (15 mL) was stirred at room temperature for 16 h, and then *p*-toluenesulfonic acid monohydrate (0.277 g, 1.458 mmol, 6.0 equiv) was added and let to react for 3 h at room temperature. The organic phase was washed with 0.3 M aq HCl (25 mL), NaHCO$_3$-saturated aqueous solution (25 mL), and brine (25 mL) and then dried. After evaporation of the solvent and flash column chromatography (petroleum ether/toluene = 3/1, then 2/1), compound **24** (76 mg, 0.077 mmol, 31% yield) was obtained as a viscous

56

purple oil. $^1$H-NMR (400 MHz, CDCl$_3$): $\delta$ = 6.87 (s, 2H), 3.55 (t, $J$ = 7.3 Hz, 4H), 2.62 (t, $J$ = 7.6 Hz, 4H), 2.56 (t, $J$ = 7.6 Hz, 4H), 1.17−1.53 (m, 48H), 0.82−0.93 (m, 18H); $^{13}$C-NMR (100 MHz, CDCl$_3$): $\delta$ = 170.4, 145.3, 143.8, 142.7, 128.6, 126.5, 112.6, 105.4, 41.1, 31.7, 31.6, 31.4, 30.9, 29.6, 29.4, 29.2, 29.0, 28.7, 26.5, 22.7, 22.6, 14.2; IR (KBr): $\tilde{\nu}$ = 3036, 2955, 2925, 2855, 1674, 1493, 1278 cm$^{-1}$; ESI-MS: $m/z$ = 989.56 [M+1]$^+$.

*(3E)-5-(5-(4-(Diphenylamino)phenyl)-3,4-dihexylthiophen-2-yl)-5'-(5-bromo-3,4-dihexylthiophen-2-yl)-1,1'-dihexyl-3,3'-bipyrrolylidene-2,2'-dione (26).* Dibromide **24** (203 mg, 0.21 mmol, 1.0 equiv) was dissolved in toluene (5.0 mL) and reacted with a solution of Pd$_2$dba$_3$ (0.011 g, 0.010 mmol, 5 mol %), P(2-furyl)$_3$ (4.8 mg, 0.021 mmol, 10 mol %), and 4-tributylstannyl-*N,N*-diphenylaniline (**18a**, 109 mg, 0.21mmol, 1.0 equiv) in toluene (5.0 mL). The mixture was heated to 85 °C, stirred for 7 h, and then after cooling to rt, diluted with H$_2$O (30 mL) and ethyl acetate (50 mL). The organic layers were washed with brine (30 mL) and dried. After filtration, evaporation of the solvent gave a dark-purple crude which was purified by flash column chromatography (petroleum ether/toluene 4:1 to 3:2) to give pure product **26** (67 mg, 0.058 mmol, 28% yield) as a dark-purple gummy solid. $^1$H-NMR (400 MHz, CDCl$_3$): $\delta$ = 7.26−7.31 (m, 6H), 7.14 (d, $J$ = 7.6 Hz, 4H), 7.04−7.11 (m, 4H), 6.94 (s, 1H), 6.88 (s, 1H), 3.65 (t, $J$ = 7.4 Hz, 2H), 3.56 (t, $J$ = 7.4 Hz, 2H), 2.68 (t, $J$ = 7.7 Hz, 2H), 2.62 (t, $J$ = 7.7 Hz, 4H), 2.56 (t, $J$ = 7.8 Hz, 2H), 1.17−1.51 (m, 48H), 0.78−0.93 (m, 18H); $^{13}$C-NMR (100 MHz, CDCl$_3$): $\delta$ = 170.8, 170.4, 147.7, 147.6, 146.9, 145.3, 144.4, 143.6, 142.6, 141.1, 139.0, 130.1, 129.5,129.1, 128.0, 127.8, 126.7, 124.9, 124.6, 123.5, 123.0, 112.3, 105.5, 104.9, 41.2, 41.0, 31.7, 31.6, 31.5, 31.4, 31.1, 30.9, 29.9, 29.63, 29.58, 29.5, 29.4, 29.3, 29.2, 29.0, 28.8, 28.7, 27.6, 26.5, 22.8, 22.7, 22.6, 14.2, 14.1; IR (KBr): $\tilde{\nu}$ = 3033, 2956, 2926, 2855, 1673, 1494, 1279 cm$^{-1}$; ESI-MS: $m/z$ = 1153.76 [M]$^+$.

*(3E)-5-(5-(4-(Diphenylamino)phenyl)-3,4-dihexylthiophen-2-yl)-5'-(5-(5-formylthiophen-2-yl)-3,4-dihexylthiophen-2-yl)-1,1'-dihexyl-3,3'-bipyrrolylidene-2,2'-dione (27).* Bromide **26** (67 mg, 0.058 mmol, 1.0 equiv) was dissolved in toluene (2.0 mL) and then reacted with a solution of Pd$_2$dba$_3$ (4.7 mg, 4.3 $\mu$mol, 7.5 mol %), P(2-furyl)$_3$ (2.0 mg, 8.7 $\mu$mol, 15 mol %), and 2-tributylstannyl-5-formylthiophene (**20**, 47 mg, 0.12 mmol, 2.0 equiv) in toluene (3.0 mL). The reaction mixture was heated to 110 °C under stirring for 24 h, then cooled, and diluted with water (30 mL) and dichloromethane (30 mL). The organic phase was washed with brine (30 mL) and dried. After removal of the solvent under vacuum, purification by flash column chromatography (petroleum ether/toluene 1:1, then toluene) gave pure aldehyde **27** (35 mg, 0.030 mmol, 51% yield) as a dark-blue gummy solid. $^1$H-NMR (400 MHz, CDCl$_3$): $\delta$ = 9.91 (s, 1H), 7.73 (d, $J$ = 3.9 Hz, 1H), 7.26−7.31 (m, 6H), 7.14 (d, $J$ = 7.7 Hz, 4H), 7.04−7.11 (m, 5H), 6.97 (s, 1H), 6.96 (s, 1H), 3.61−3.69 (m, 4H), 2.79 (t, $J$ = 7.9 Hz, 2H), 2.60−2.71 (m, 6H), 1.15−1.53 (m, 48H), 0.80−0.92 (m, 18H); $^{13}$C-NMR (100 MHz, CDCl$_3$): $\delta$ = 182.8, 170.8, 170.5, 147.7, 147.6, 147.1, 145.8, 145.6, 145.4, 144.3, 143.0, 142.3, 141.2, 139.1, 136.9, 132.0, 130.1, 129.5, 129.2, 127.9, 127.7, 127.5, 126.9, 124.9, 124.6, 123.5, 122.9, 105.7, 105.0, 41.2, 31.6, 31.5, 31.4, 31.1, 31.0, 30.9, 30.6, 29.8, 29.7, 29.6, 29.5, 29.3, 29.2, 28.8, 28.6, 28.4, 27.6, 26.5, 22.7, 22.6, 14.2, 14.1; IR (KBr): $\tilde{\nu}$ = 2956, 2927, 2857, 1668, 1629, 1494, 1464, 1279 cm$^{-1}$; ESI-MS: $m/z$ = 1184.82 [M+1]$^+$; 1201.37 [M+H$_2$O]$^+$.

*2-Cyano-3-(5-(5-((3E)-1-hexyl-3-(1-hexyl-2-oxo-5-(5-(4-(diphenylamino)phenyl)-3,4-dihexylthiophen-2-yl)-pyrrol-3(2H)-ylidene)-pyrrol-2(3H)-on-5-yl)-3,4-dihexylthiophen-2-yl)thiophen-2-yl)acrylic acid (8).* Aldehyde **27** (20 mg, 0.017 mmol, 1.0 equiv) was dissolved in toluene (2.0 mL), and then a solution of cyanoacetic acid (4.3 mg, 0.051 mmol, 3.0 equiv) and piperidine (4.3 mg, 0.051 mmol, 5.0 $\mu$L, 3.0 equiv) in MeCN (1.0 mL) was added. The resulting mixture was heated to 75 °C and stirred for 4 h. The solvent was evaporated under vacuum, and the residue was dissolved in dichloromethane (50 mL) and washed with a 3 M aqueous solution of HCl (2 × 50 mL). Evaporation of the solvent gave a green solid, which was purified by consecutive washes with pentane, diethyl ether, and methanol and dried under vacuum to afford acid **8** (17 mg, 0.014 mmol, 81% yield) as a dark-green gummy solid. $^1$H-NMR (400 MHz, THF-$d_8$): $\delta$ = 8.39 (s, 1H), 7.84−7.90 (m, 1H), 7.40−7.44 (m, 1H), 7.35 (d, $J$ = 8.2 Hz, 2H), 7.21−7.31 (m, 5H), 6.94−7.14 (m, 9H), 3.64−3.75 (m, 4H), 2.84−2.98 (m, 2H), 2.65−2.82 (m, 6H), 1.20−1.62 (m, 48H), 0.81−0.95 (m, 18H)$^{13}$C-NMR (100 MHz, THF-$d_8$): $\delta$ = 170.6, 170.4, 163.7, 148.7, 148.3, 147.2, 146.3, 146.1, 145.8, 145.1, 144.9, 142.9, 141.9, 139.6, 139.0, 137.0, 133.0, 130.6, 130.0, 129.1, 128.4, 128.3, 127.6, 125.5, 125.2, 124.1, 123.7, 123.3, 116.4, 106.0, 105.2, 100.2, 41.3, 32.3, 32.2, 32.0, 31.7, 31.6, 31.5, 31.3, 30.5, 30.2, 30.1, 29.8, 29.4, 29.2, 29.0, 28.0, 27.0, 23.3, 23.2, 14.2, 14.1; IR (KBr): $\tilde{\nu}$ = 3459, 2953, 2923, 2851, 2209, 1671, 1632, 1493, 1372, 1259 cm$^{-1}$; ESI-MS: $m/z$ = 1250.66 [M]$^+$. HRMS (ESI) C$_{78}$H$_{98}$O$_4$N$_4$S$_3$ ([M]$^+$), calcd 1250.6750, found 1250.6756.

## ■ ASSOCIATED CONTENT

**Ⓢ Supporting Information**

The Supporting Information is available free of charge on the ACS Publications website at DOI: 10.1021/acsomega.8b03560.

> $^1$H- and $^{13}$C-NMR spectra of compounds **19a**, **19b**, **21a**, **21b**, **1**, **2**, **6**, **7**, **24**, **26**, **27**, **8**; UV−vis absorption spectra, fluorescence emission spectra ,and cyclic voltammograms of compounds **1**, **2**, **6**, **7**, and **8**; TD-DFT (CAM-B3LYP/6-31G*)-computed absorption maxima ($\lambda_{max}^a$), excitation energy ($E_{exc}$), and oscillator strengths ($f$) of reaction intermediates **16**, **17**, **19a**, and **21a** and dye **1**; and fabrication details and characterization of dye-sensitized solar cells (PDF)

## ■ AUTHOR INFORMATION

**Corresponding Authors**
*E-mail: a.dessi@iccom.cnr.it (A.D.).
*E-mail: gianna.reginato@iccom.cnr.it (G.R.).
**ORCID** Ⓞ
Alessio Dessì: 0000-0003-2358-227X
Gianna Reginato: 0000-0002-7712-3426

**Notes**
The authors declare no competing financial interest.

## ■ ACKNOWLEDGMENTS

57

■ ADDITIONAL NOTE

[1]The moderate yield of compound **1** could be ascribed to its low solubility, which hampered its final purification.

■ REFERENCES

(1) Hagfeldt, A.; Boschloo, G.; Sun, L.; Kloo, L.; Pettersson, H. Dye-Sensitized Solar Cells. *Chem. Rev.* **2010**, *110*, 6595.

(2) O'Regan, B.; Grätzel, M. A low-cost, high-efficiency solar cell based on dye-sensitized colloidal TiO₂ films. *Nature* **1991**, *353*, 737.

(3) Mishra, A.; Fischer, M. K. R.; Bäuerle, P. Metal-Free Organic Dyes for Dye-Sensitized Solar Cells: From Structure: Property Relationships to Design Rules. *Angew. Chem., Int. Ed.* **2009**, *48*, 2474.

(4) Bessho, T.; Zakeeruddin, S. M.; Yeh, C.-Y.; Diau, E. W.-G.; Grätzel, M. Highly Efficient Mesoscopic Dye-Sensitized Solar Cells Based on Donor−Acceptor-Substituted Porphyrins. *Angew. Chem., Int. Ed.* **2010**, *49*, 6646.

(5) Yao, Z.; Zhang, M.; Wu, H.; Yang, L.; Li, R.; Wang, P. Donor/Acceptor Indenoperylene Dye for Highly Efficient Organic Dye-Sensitized Solar Cells. *J. Am. Chem. Soc.* **2015**, *137*, 3799.

(6) Kakiage, K.; Aoyama, Y.; Yano, T.; Oya, K.; Fujisawa, J.-i.; Hanaya, M. Highly-efficient dye-sensitized solar cells with collaborative sensitization by silyl-anchor and carboxy-anchor dyes. *Chem. Commun.* **2015**, *51*, 15894.

(7) Brogdon, P.; Cheema, H.; Delcamp, J. H. Near-Infrared-Absorbing Metal-Free Organic, Porphyrin, and Phthalocyanine Sensitizers for Panchromatic Dye-Sensitized Solar Cells. *ChemSusChem* **2018**, *11*, 86.

(8) (a) Burke, A.; Schmidt-Mende, L.; Ito, S.; Grätzel, M. A novel blue dye for near-IR 'dye-sensitised' solar cell applications. *Chem. Commun.* **2007**, 234. (b) Paek, S.; Choi, H.; Kim, C.; Cho, N.; So, S.; Song, K.; Nazeeruddin, M. K.; Ko, J. Efficient and stable panchromatic squaraine dyes for dye-sensitized solar cells. *Chem. Commun.* **2011**, *47*, 2874. (c) Shi, Y.; Hill, R. B. M.; Yum, J.-H.; Dualeh, A.; Barlow, S.; Gratzel, M.; Marder, S. R.; Nazeeruddin, M. K. A high-efficiency panchromatic squaraine sensitizer for dye-sensitized solar cells. *Angew. Chem., Int. Ed.* **2011**, *50*, 6619. (d) Jradi, F. M.; Kang, X.; O'Neil, D.; Pajares, G.; Getmanenko, Y. A.; Szymanski, P.; Parker, T. C.; El-Sayed, M. A.; Marder, S. R. Near-Infrared Asymmetrical Squaraine Sensitizers for Highly Efficient Dye Sensitized Solar Cells: The Effect of π-Bridges and Anchoring Groups on Solar Cell Performance. *Chem. Mater.* **2015**, *27*, 2480.

(9) Hao, Y.; Saygili, Y.; Cong, J.; Eriksson, A.; Yang, W.; Zhang, J.; Polanski, E.; Nonomura, K.; Zakeeruddin, S. M.; Gratzel, M.; Hagfeldt, A.; Boschloo, G. Novel Blue Organic Dye for Dye-Sensitized Solar Cells Achieving High Efficiency in Cobalt-Based Electrolytes and by Co-Sensitization. *ACS Appl. Mater. Interfaces* **2016**, *8*, 32797.

(10) Yum, J.-H.; Holcombe, T. W.; Kim, Y.; Rakstys, K.; Moehl, T.; Teuscher, J.; Delcamp, J. H.; Nazeeruddin, M. K.; Grätzel, M. Blue-Coloured Highly Efficient Dye-Sensitized Solar Cells by Implementing the Diketopyrrolopyrrole Chromophore. *Sci. Rep.* **2013**, *3*, 2446.

(11) Ren, Y.; Sun, D.; Cao, Y.; Tsao, H. N.; Yuan, Y.; Zakeeruddin, S. M.; Wang, P.; Grätzel, M. A Stable Blue Photosensitizer for Color Palette of Dye-Sensitized Solar Cells Reaching 12.6% Efficiency. *J. Am. Chem. Soc.* **2018**, *140*, 2405.

(12) (a) Norsten, T. B.; Kantchev, E. A. B.; Sullivan, M. B. Thiophene-Containing Pechmann Dye Derivatives. *Org. Lett.* **2010**, *12*, 4816. (b) Kantchev, E. A. B.; Norsten, T. B.; Tan, M. L. Y.; Ng, J. J. Y.; Sullivan, M. B. Thiophene-Containing Pechmann Dyes and Related Compounds: Synthesis, and Experimental and DFT Characterisation. *Chem. - Eur. J.* **2012**, *18*, 695.

(13) (a) Kantchev, E. A. B.; Norsten, T. B.; Sullivan, M. B. Time-dependent density functional theory (TDDFT) modelling of Pechmann dyes: from accurate absorption maximum prediction to

virtual dye screening. *Org. Biomol. Chem.* **2012**, *10*, 6682. (b) Hashimoto, H.; Shiratori, K.; Kawakita, K.; Tanaka, T.; Sekine, R.; Irikawa, H. Preparation and Properties of Dehydrotrichotomine-type Dyes: A New Near-Infrared Absorbing Indigoid. *Heterocycles* **2005**, *65*, 1385.

(14) (a) Efrem, A.; Courté, M.; Wang, K.; Fichou, D.; Wang, M. Synthesis and characterization of γ-lactone-Pechmann dye based donor-acceptor conjugated polymers. *Dyes Pigm.* **2016**, *134*, 171. (b) Cai, Z.; Luo, H.; Qi, P.; Wang, J.; Zhang, G.; Liu, Z.; Zhang, D. Alternating Conjugated Electron Donor−Acceptor Polymers Entailing Pechmann Dye Framework as the Electron Acceptor Moieties for High Performance Organic Semiconductors with Tunable Characteristics. *Macromolecules* **2014**, *47*, 2899. (c) Cai, Z.; Liu, Z.; Luo, H.; Qi, P.; Zhang, G.; Zhang, D. π-Extented Conjugated Polymers Entailing Pechmann Dye Moieties for Solution-Processed Ambipolar Organic Semiconductors. *Chin. J. Chem.* **2014**, *32*, 788.

(15) Hayashi, M.; Toshimitsu, F.; Sakamoto, R.; Nishihara, H. Double Lactonization in Triarylamine-Conjugated Dimethyl Diethynylfumarate: Formation of Intensely Colored and Luminescent Quadrupolar Molecules Including a Missing Structural Isomer of Pechmann Dyes. *J. Am. Chem. Soc.* **2011**, *133*, 14518.

(16) Qi, P.; Wang, Z.; Liu, Z.; Yang, S.; Yang, Y.; Yao, J.; Zhang, G.; Zhang, D. Conjugated donor−acceptor terpolymers entailing the Pechmann dye and dithienyl-diketopyrrolopyrrole as co-electron acceptors: tuning HOMO/LUMO energies and photovoltaic performances. *Polym. Chem.* **2016**, *7*, 3838.

(17) (a) Cai, Z.; Guo, Y.; Yang, S.; Peng, Q.; Luo, H.; Liu, Z.; Zhang, G.; Liu, Y.; Zhang, D. New Donor−Acceptor−Donor Molecules with Pechmann Dye as the Core Moiety for Solution-Processed Good-Performance Organic Field-Effect Transistors. *Chem. Mater.* **2013**, *25*, 471. (b) Luo, H.; Dong, X.; Cai, Z.; Wang, L.; Liu, Z. Pechmann Dye-Based Molecules Containing Fluorobenzene Moieties for Ambipolar Organic Semiconductors. *Asian J. Org. Chem.* **2018**, *7*, 592.

(18) (a) Zhu, W.; Wu, Y.; Wang, S.; Li, W.; Li, X.; Chen, J.; Wang, Z. S.; Tian, H. Organic D-A-π-A Solar Cell Sensitizers with Improved Stability and Spectral Response. *Adv. Funct. Mater.* **2011**, *21*, 756. (b) Wu, Y.; Zhu, W. H.; Zakeeruddin, S. M.; Grätzel, M. Insight into D−A−π−A Structured Sensitizers: A Promising Route to Highly Efficient and Stable Dye-Sensitized Solar Cells. *ACS Appl. Mater. Interfaces* **2015**, *7*, 9307. (c) Gao, Y.; Li, X.; Hu, Y.; Fan, Y.; Yuan, J.; Robertson, N.; Hua, J.; Marder, S. R. Effect of an auxiliary acceptor on D−A−π−A sensitizers for highly efficient and stable dye-sensitized solar cells. *J. Mater. Chem. A* **2016**, *4*, 12865. (d) Liyanage, P. N.; Yella, A.; Nazeeruddin, M.; Grätzel, M.; Delcamp, J. H. Thieno[3,4-*b*]pyrazine as an Electron Deficient π-Bridge in D−A−π−A DSCs. *ACS Appl. Mater. Interfaces* **2016**, *8*, 5376.

(19) (a) Dessì, A.; Calamante, M.; Mordini, A.; Peruzzini, M.; Sinicropi, A.; Basosi, R.; de Biani, F. F.; Taddei, M.; Colonna, D.; di Carlo, A.; Reginato, G.; Zani, L. Thiazolo[5,4-*d*]thiazole-based organic sensitizers with strong visible light absorption for transparent, efficient and stable dye-sensitized solar cells. *RSC Adv.* **2015**, *5*, 32657. (b) Dessì, A.; Calamante, M.; Mordini, A.; Peruzzini, M.; Sinicropi, A.; Basosi, R.; de Biani, F. F.; Taddei, M.; Colonna, D.; Di Carlo, A.; Reginato, G.; Zani, L. Organic dyes with intense light absorption especially suitable for application in thin-layer dye-sensitized solar cells. *Chem. Commun.* **2014**, *50*, 13952. (c) Bernini, C.; Zani, L.; Calamante, M.; Reginato, G.; Mordini, A.; Taddei, M.; Basosi, R.; Sinicropi, A. Excited State Geometries and Vertical Emission Energies of Solvated Dyes for DSSC: A PCM/TD-DFT Benchmark Study. *J. Chem. Theory Comput.* **2014**, *10*, 3925.

(20) Otsuka, A.; Funabiki, K.; Sugiyama, N.; Mase, H.; Yoshida, T.; Minoura, H.; Matsui, M. Design and Synthesis of Near-infrared-active Heptamethine−Cyanine Dyes to Suppress Aggregation in a Dye-sensitized Porous Zinc Oxide Solar Cell. *Chem. Lett.* **2008**, *37*, 176.

(21) Robson, K. C. D.; Hu, K.; Meyer, G. J.; Berlinguette, C. P. Atomic Level Resolution of Dye Regeneration in the Dye-Sensitized Solar Cell. *J. Am. Chem. Soc.* **2013**, *135*, 1961.

58

(22) Frisch, M. J.; Trucks, G. W.; Schlegel, H. B.; Scuseria, G. E.; Robb, M. A.; Cheeseman, J. R.; Scalmani, V.; Barone, V.; Mennucci, B.; Petersson, G. A.; Nakatsuji, H.; Caricato, M.; Li, X.; Hratchian, H. P.; Izmaylov, A. F.; Bloino, J.; Zheng, G.; Sonnenberg, J. L.; Hada, M.; Ehara, M.; Toyota, K.; Fukuda, R.; Hasegawa, J.; Ishida, M.; Nakajima, T.; Honda, Y.; Kitao, O.; Nakai, H.; Vreven, T.; Montgomery, J. A., Jr.; Peralta, J. E.; Ogliaro, F.; Bearpark, M.; Heyd, J. J.; Brothers, E.; Kudin, K. N.; Staroverov, V. N.; Kobayashi, R.; Normand, J.; Raghavachari, K.; Rendell, A.; Burant, J. C.; Iyengar, S. S.; Tomasi, J.; Cossi, M.; Rega, N.; Millam, N. J.; Klene, M.; Knox, J. E.; Cross, J. B.; Bakken, V.; Adamo, C.; Jaramillo, J.; Gomperts, R.; Stratmann, R. E.; Yazyev, O.; Austin, A. J.; Cammi, R.; Pomelli, C.; Ochterski, J. W.; Martin, R. L.; Morokuma, K.; Zakrzewski, V. G.; Voth, G. A.; Salvador, P.; Dannenberg, J. J.; Dapprich, S.; Daniels, A. D.; Farkas, Ö.; Foresman, J. B.; Ortiz, J. V.; Cioslowski, J.; Fox, D. J., *Gaussian 09*. Gaussian, Inc., Wallingford CT, 2009, (Revision C.01).

(23) (a) Becke, A. D. Density-functional thermochemistry. III. The role of exact exchange. *J. Chem. Phys.* 1993, 98, 5648. (b) Lee, C.; Yang, W.; Parr, R. G. Development of the Colle-Salvetti correlation-energy formula into a functional of the electron density. *Phys. Rev. B* 1988, 37, 785.

(24) Tomasi, J.; Mennucci, B.; Cammi, R. Quantum Mechanical Continuum Solvation Models. *Chem. Rev.* 2005, 105, 2999.

(25) Franchi, D.; Calamante, M.; Reginato, G.; Zani, L.; Peruzzini, M.; Taddei, M.; de Biani, F. F.; Basosi, R.; Sinicropi, A.; Colonna, D.; Di Carlo, A.; Mordini, A. A comparison of carboxypyridine isomers as sensitizers for dyesensitized solar cells: assessment of device efficiency and stability. *Tetrahedron* 2014, 70, 6285.

(26) Fitri, A.; Benjelloun, A. T.; Benzakour, M.; Mcharfi, M.; Hamidi, M.; Bouachrine, M. Theoretical investigation of new thiazolothiazole-based D-π-A organic dyes for efficient dye-sensitized solar cell. *Spectrochim. Acta, Part A* 2014, 124, 646.

(27) Kakiage, K.; Aoyama, Y.; Yano, T.; Otsuka, T.; Kyomen, T.; Unno, M.; Hanaya, M. An achievement of over 12 percent efficiency in an organic dye-sensitized solar cell. *Chem. Commun.* 2014, 50, 6379.

(28) (a) Anderson, N. A.; Ai, X.; Chen, D.; Mohler, D. L.; Lian, T. Bridge-Assisted Ultrafast Interfacial Electron Transfer to Nanocrystalline SnO$_2$ Thin Films. *J. Phys. Chem. B* 2003, 107, 14231. (b) Wang, L.; Ernstorfer, R.; Willig, F.; May, V. Absorption Spectra Related to Heterogeneous Electron Transfer Reactions: The Perylene TiO$_2$ System. *J. Phys. Chem. B* 2005, 109, 9589. (c) Ernstorfer, R.; Felber, S.; Storck, W.; Galoppini, E.; Wei, Q.; Willig, F. Distance dependence of heterogeneous electron transfer probed in ultra-high vacuum with femtosecond transient absorption. *Res. Chem. Intermed.* 2005, 31, 643.

(29) Dessì, A.; Bartolini, M.; Calamante, M.; Zani, L.; Mordini, A.; Reginato, G. Extending the conjugation of Pechmann lactone thienyl derivatives: a new class of small molecules for organic electronics application. *Synthesis* 2018, 50, 1284.

(30) Dessì, A.; Consiglio, G. B.; Calamante, M.; Reginato, G.; Mordini, A.; Peruzzini, M.; Taddei, M.; Sinicropi, A.; Parisi, M. L.; de Biani, F. F.; Basosi, R.; Mori, R.; Spatola, M.; Bruzzi, M.; Zani, L. Organic chromophores based on a fused bis-thiazole core and their application in dye-sensitized solar cells. *Eur. J. Org. Chem.* 2013, 1916.

(31) (a) Fujinaga, M.; Yamasaki, T.; Maeda, J.; Yui, J.; Xie, L.; Nagai, Y.; Nengaki, N.; Hatori, A.; Kumata, K.; Kawamura, K.; Zhang, M.-R. Development of N-[4-[6-(Isopropylamino)pyrimidin-4-yl]-1,3-thiazol-2-yl]-N-methyl-4-[$^{11}$C]methylbenzamide for Positron Emission Tomography Imaging of Metabotropic Glutamate 1 Receptor in Monkey Brain. *J. Med. Chem.* 2012, 55, 11042. (b) Tang, P.; Furuya, T.; Ritter, T. Silver-Catalyzed Late-Stage Fluorination. *J. Am. Chem. Soc.* 2010, 132, 12150.

(32) (a) Chinchilla, R.; Nájera, C. The Sonogashira Reaction: A Booming Methodology in Synthetic Organic Chemistry. *Chem. Rev.* 2007, 107, 874. (b) Chinchilla, R.; Nájera, C. Recent advances in Sonogashira reactions. *Chem. Soc. Rev.* 2011, 40, 5084.

(33) (a) Chen, R.; Yang, X.; Tian, H.; Sun, L. Tetrahydroquinoline dyes with different spacers for organic dye-sensitized solar cells. *J.*

*Photochem. Photobiol., A* 2007, 189, 295. (b) Tian, H.; Yang, X.; Chen, R.; Pan, Y.; Li, L.; Hagfeldt, A.; Sun, L. Phenothiazine derivatives for efficient organic dye-sensitized solar cells. *Chem. Commun.* 2007, 3741. (c) Zhang, L.; Cole, J. M. Dye aggregation in dye-sensitized solar cells. *J. Mater. Chem. A* 2017, 5, 19541−19559.

(34) Hardin, B. E.; Snaith, H. J.; McGehee, M. D. The renaissance of dye-sensitized solar cells. *Nat. Photonics* 2012, 6, 162.

(35) Boschloo, G.; Hagfeldt, A. Characteristics of the Iodide/Triiodide Redox Mediator in Dye-Sensitized Solar Cells. *Acc. Chem. Res.* 2009, 42, 1819−1826.

(36) Koops, S. E.; O'Regan, B. C.; Barnes, P. R. F.; Durrant, J. R. Parameters Influencing the Efficiency of Electron Injection in Dye-Sensitized Solar Cells. *J. Am. Chem. Soc.* 2009, 131, 4808.

(37) (a) Peddapuram, A.; Cheema, H.; Adams, R. E.; Schmehl, R. H.; Delcamp, J. H. A Stable Panchromatic Green Dual Acceptor, Dual Donor Organic Dye for Dye-Sensitized Solar Cells. *J. Phys. Chem. C* 2017, 121, 8770. (b) Wu, J.; Li, G.; Zhang, L.; Zhou, G.; Wang, Z.-S. Energy level engineering of thieno[3,4-b]pyrazine based organic sensitizers for quasi-solid-state dye-sensitized solar cells. *J. Mater. Chem. A* 2016, 4, 3342.

(38) Hagberg, D. P.; Yum, J.-H.; Lee, H.; De Angelis, F.; Marinado, T.; Karlsson, K. M.; Humphry-Baker, R.; Sun, L.; Hagfeldt, A.; Grätzel, M.; Nazeeruddin, M. K. Molecular Engineering of Organic Sensitizers for Dye-Sensitized Solar Cell Applications. *J. Am. Chem. Soc.* 2008, 130, 6259.

(39) Kopidakis, N.; Neale, N. R.; Frank, A. J. Effect of an Adsorbent on Recombination and Band-Edge Movement in Dye-Sensitized TiO$_2$ Solar Cells: Evidence for Surface Passivation. *J. Phys. Chem. B* 2006, 110, 12485.

(40) Lee, K.-M.; Suryanarayanan, V.; Ho, K.-C.; Thomas, K. R. J.; Lin, J. T. Effects of co-adsorbate and additive on the performance of dye-sensitized solar cells: A photophysical study. *Sol. Energy Mater. Sol. Cells* 2007, 91, 1426.

(41) (a) Boschloo, G.; Häggman, L.; Hagfeldt, A. Quantification of the Effect of 4-tert-Butylpyridine Addition to I$^-$/I$_3^-$ Redox Electrolytes in Dye-Sensitized Nanostructured TiO$_2$ Solar Cells. *J Phys. Chem. B* 2006, 110, 13144. (b) Becerril, V. S.; Franchi, D.; Abrahamsson, M. Ionic Liquid-Induced Local Charge Compensation: Effects on Back Electron-Transfer Rates in Dye-Sensitized TiO$_2$ Thin Films. *J. Phys. Chem. C* 2016, 120, 20016.

59

# 2 Ground state redox potentials calculation of organic
# 3 dyes for DSSC and Visible-Light-Driven Hydrogen
# 4 Production

5  **Sanaz Mohammadpourasl[1], Fabrizia Fabrizi de Biani[2], Carmen Coppola[1,3], Maria Laura Parisi[1,3,4],**
6  **Lorenzo Zani[4], Alessio Dessì[4], Massimo Calamante[4], Gianna Reginato[4], Riccardo Basosi[1,3,4] and**
7  **Adalgisa Sinicropi[1,3,4]\***

8   [1]  R2ES Lab, Department of Biotechnology, Chemistry and Pharmacy, University of Siena, 53100 Siena, Italy
9   [2]  Department of Biotechnology, Chemistry and Pharmacy, University of Siena, 53100 Siena, Italy
10  [3]  Center for Colloid and Surface Science (CSGI), 50019 Sesto Fiorentino, Italy
11  [4]  National Research Council, Institute for the Chemistry of OrganoMetallic Compounds (CNR-ICCOM),
12      50019 Sesto Fiorentino, Italy
13  \*  Correspondence: adalgisa.sinicropi@unisi.it

15  **Abstract:** The prediction of ground state redox potentials by quantum chemical methods has a
16  prominent role in the rational design of novel organic photosensitizers both for dye-sensitized solar
17  cells and photocatalytic systems for the production of $H_2$. Indeed, the ground state redox potential
18  of the photosensitizers is one of the key parameters to identify the most promising candidates for
19  such applications. Here, the ground state redox potentials of 16 organic D-π-A and D-A-π-A dyes
20  having a medium to large size of the conjugated scaffold are evaluated, using the methods of the
21  Density Functional Theory, in terms of free energy differences between their neutral and oxidized
22  state. These results are also compared to computed -ε(HOMO) values as approximation of ground
23  state redox potentials according to Koopmans' theorem. Using the MPW1K functional in
24  combination with the 6-31G\* basis set, the strategy based on the free energy cycle including solvent
25  effects reproduces with a good level of accuracy the observed values and trend of redox potentials
26  within related families of dyes. On the other hand, the computed -ε(HOMO) values are clearly
27  against an uncritical use of Koopmans' theorem.

30  _____

## 31 1. Introduction

32      Organic dyes having a donor-π-acceptor (D-π-A) or donor-acceptor-π-acceptor (D-A-π-A)
33  architecture have been extensively used as photosensitizers in dye-sensitized solar cells (DSSCs) [1–
34  3] and, more recently, as sensitizers in photocatalytic systems for the production of $H_2$ [4–7]. In both
35  devices, visible-light absorbing dyes are employed to enhance light harvesting of semiconductor
36  nanoparticles of $TiO_2$.
37      In DSSCs, the dye absorbs light and, upon excitation, it transfers an electron to the conduction
38  band of the semiconductor, which carries it to a glass electrode (TCO layer); at the same time, in the
39  oxide, the resulting hole is transferred from the dye/sensitizer to the redox mediator (usually a $I^-/I_3^-$
40  redox couple) which, through an oxidation-reduction interchange, carries it to the counter-electrode,
41  thereby closing the circuit and generating a current (See Figure 1a).
42      The photocatalytic systems, on the other hand, are dye-sensitized $Pt/TiO_2$ photocatalysts in
43  which the dye, as in DSSCs, harvests visible light and injects the electron in the $TiO_2$ conduction band
44  (See Figure 1b). Electrons are then transferred to $Pt^0$ nanoparticles which are adsorbed on the $TiO_2$

45  surface and here protons are reduced to $H_2$. The regeneration of the oxidized dye occurs by using a
46  sacrificial electron donor (SED) agent. Triethanolamine (TEOA), ethylenediaminetetraacetic acid
47  (EDTA), ascorbic acid (AA) and, more recently, ethanol have been employed as SEDs [4].
48
49
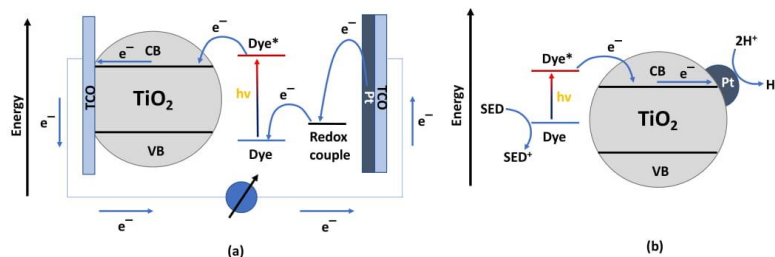


50

51  **Figure 1.** Energy levels and working mechanisms of: (a) Dye-sensitized solar cells and (b) dye-
52  sensitized Pt/TiO$_2$ photocatalysts.

53

54  Among other requirements, the correct alignment of the relative energy levels of the dye and the
55  redox couple in DSSCs or the SED in the Pt/TiO$_2$ photocatalysts is a key issue that affects the overall
56  efficiency of both dye-sensitized systems. Indeed, the effective regeneration of the oxidized dye is
57  pivotal for both devices to obtain good performances in terms of efficiency. Thus, a key parameter
58  for an efficient dye to be employed is the ground state redox potential (GSRP) since this value,
59  especially when compared to the redox couple or SED energy levels, is a measure of the dye
60  regeneration driving force.
61  The prediction of GSRP by quantum chemical methods is of outstanding importance for the
62  rational design of novel organic sensitizers and greatly contributes to the development of more
63  efficient devices. Indeed, the calculations of these photoelectrochemical properties along with the
64  modeling of other key parameters such as the excited state redox potential, the vertical excitation and
65  emission energies, the charge transfer nature of the excitation process and the electronic coupling
66  between the dye and the semiconductor, would give an indication of the most promising dye
67  candidates for solar energy and fuel (H$_2$) devices. This strategy has been intensely applied in literature
68  for the molecular engineering of the organic sensitizer for DSSC [8–14], essentially using the methods
69  of the density functional theory (DFT) and its time dependent extension (TDDFT).
70  The accurate evaluation of GSRP is hard to achieve especially because it has been shown that the
71  accuracy deteriorates as the conjugation length of the molecule increases [15]. In the present study,
72  the GSRP of 16 organic dyes having a medium to large conjugation length (see molecules in Chart 1)
73  have been computed using DFT, and in particular the MPW1K functional [16,17], which has been
74  shown to give the best accuracy before [15], and a polarizable continuum model (PCM) [18] to take
75  into account solvent effects. To the best of our knowledge, this is the first work dealing with the
76  calculations of GSRP of a relatively large set of organic dyes having a medium to large size of the
77  conjugated scaffold. The DFT predicted values have been compared to the available experimental
78  data showing that the employed strategy allows to reproduce the GSRP with a mean absolute error
79  < 0.2 eV.
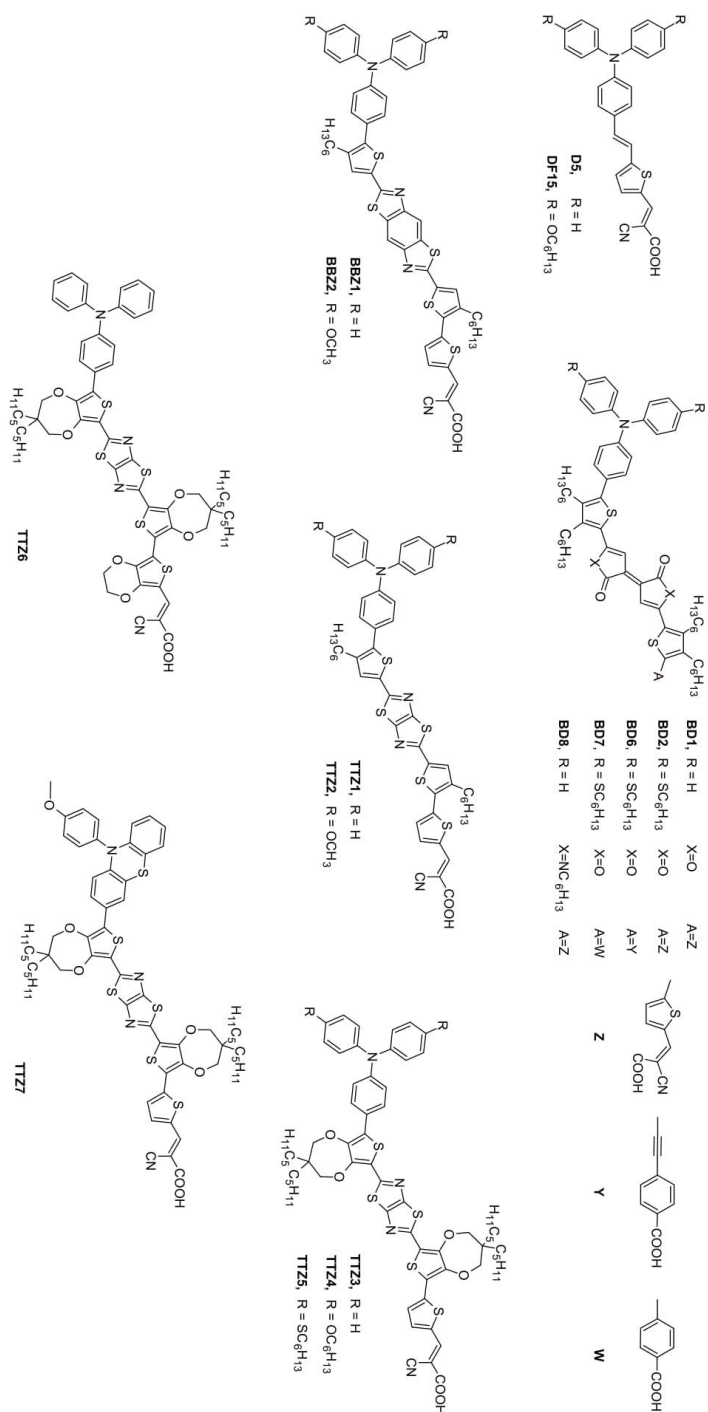
80
81      **Chart 1.** Investigated Set of Molecules

82  **2. Methods**

83    All QM calculations have been performed by means of density functional theory (DFT) and time-
84  dependent DFT (TDDFT) using the G09 program package [19]. The ground state redox potential have
85  been computed at the MPW1K/6-31+G* level of theory as free energy differences between the neutral
86  and oxidized state of these dyes $(G^0 - G^+)_{\text{solv}}$, following the procedure described by A. Pastore et al.
87  [15].
88    Neutral and oxidized state geometries of all dyes have been computed using the MPW1K [16,17]
89  functional in combination with 6-31G* and 6-31+G* basis set both in vacuo and in the presence of
90  dichloromethane as a solvent. Solvent effects have been added to the energies of the gas-phase
91  optimized molecules via PCM [18]. These effects are computed as energy differences between values
92  in solution and in gas-phase, both computed at the geometry optimized in solution.
93    -ε(HOMO) (minus the value of the HOMO energy) values have been evaluated both in gas-
94  phase and in DCM, for the neutral state of all dyes at their optimized geometry in DCM.
95    Vertical excitation energies ($E_{\text{exc}}$), absorption maxima ($\lambda_{\text{max}}$), and oscillator strengths (f) have
96  been computed at the time-dependent DFT (MPW1K/6-31+G*) level on all the optimized structures.
97  Again, the PCM was used to include the effect of the solvent. These results are shown in the
98  Supporting Information.

99

100  **3. Results and Discussion**

101    All the investigated dyes (see Chart 1) are based on fully conjugated D-π-A or D-A-π-A
102  structures, the latter having an auxiliary acceptor group in the central part of the molecule. D5 and
103  DF15 are triarylamine-thiophene derivatives bearing cyanoacrylic acid as anchoring group. The
104  heterocyclic benzobisthiazole- and thiazolothiazole-systems constitutes the central π scaffold of
105  BBZ1,2 and TTZ1-7 sensitizers, respectively. The last group of molecules (BD1,2,6,7,8) contains an
106  electron-poor *bis*-lactone moiety (Pechmann lactone) connected to thiophenes decorated with various
107  donor and acceptor groups. With the only exception of compound D5 [20], all the investigated dyes
108  have been designed, characterized and synthetized in our laboratories, as described in our previous
109  works [9,21–23].
110    The neutral ground state geometries of these dyes, computed at the MPW1K/6-31+G* level, are
111  shown in Fig. 2. All the dyes assume a largely planar structure along most of the conjugated system
112  with a deviation from coplanarity (ranging from 27° to 49°) between the triarylamine and the linked
113  thiophene. To assess the quality of the MPW1K/6-31+G* optimized structures, their vertical excitation
114  energies have been computed at the TDDFT level and the comparison between these results and
115  experimental values is shown in Table S1. The mean absolute error is about 0.06 eV, which clearly
116  indicates the accuracy of the optimized structures and the high degree of accuracy of MPW1K
117  functional in dealing with the excited states of the analyzed D-π-A or D-A-π-A dyes. Table S1 also
118  shows that the main electronic transition is, in all cases, a HOMO→LUMO transition with a smaller
119  contribution of a HOMO-1→LUMO transition. From the plot of the corresponding DFT frontier
120  molecular orbitals collected in Table S2 it is clear that the HOMO and LUMO are mostly localized on
121  the donor and acceptor unit, respectively, albeit still with a sizable contribution of the conjugated
122  scaffold.
123
124
125

63

126
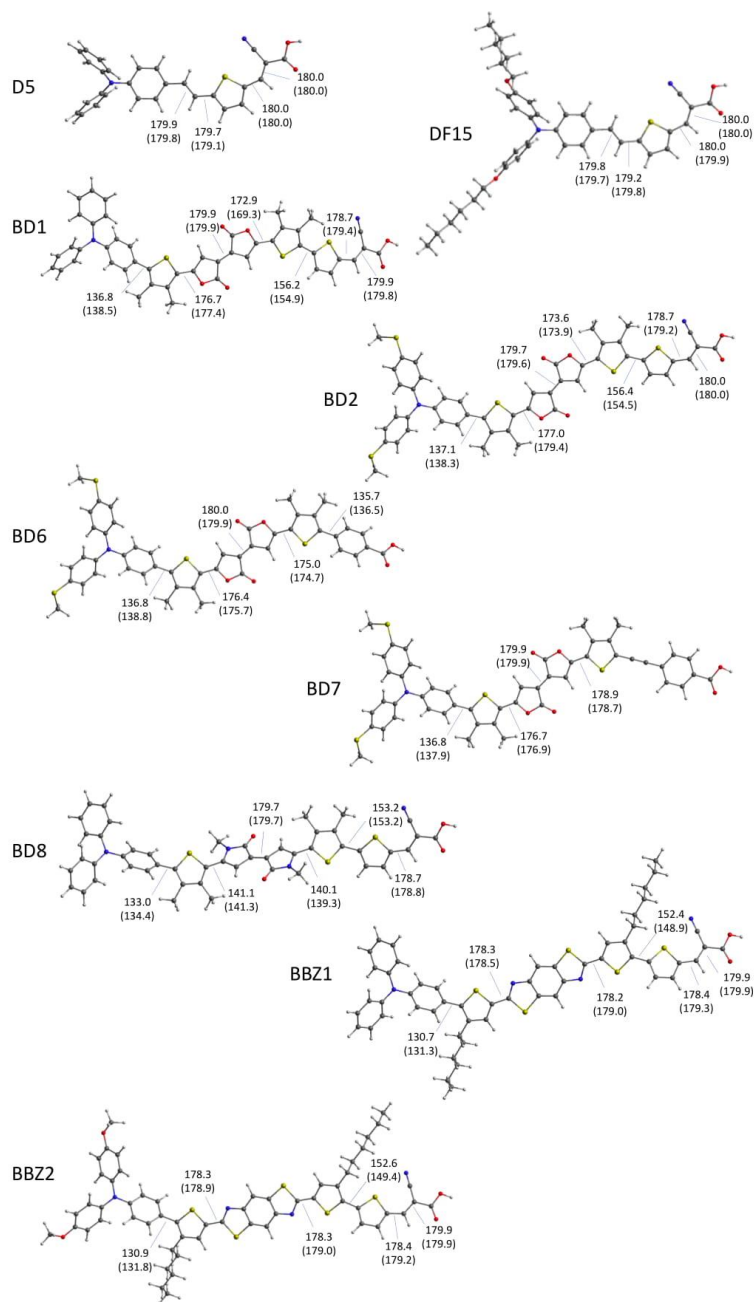
**Figure 2 (to be continued).** MPW1K/6-31+G* optimized geometries of all dyes computed in vacuo and in DCM (in brackets). Dihedral angles are given in degrees.

129

130
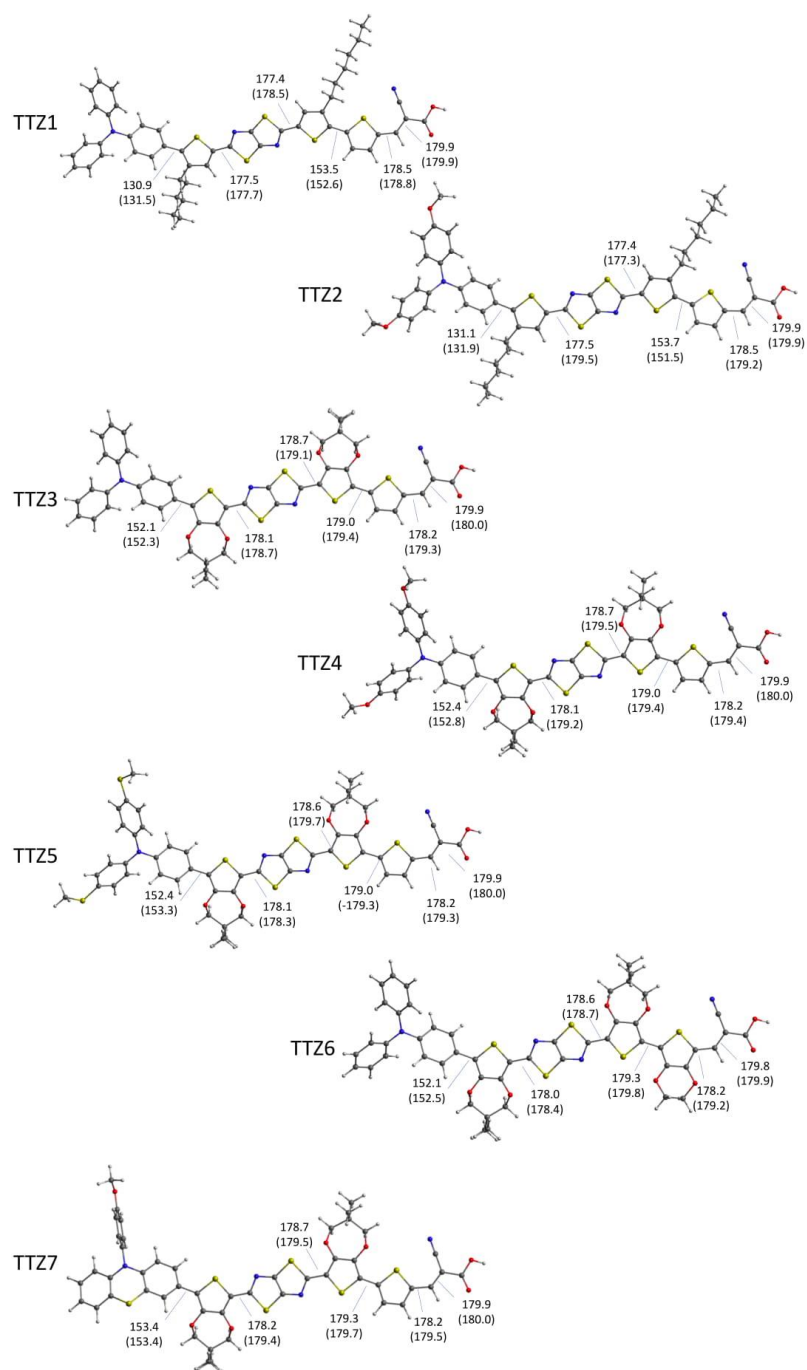
**Figure 2 (continued).** MPW1K/6-31+G* optimized geometries of all dyes computed in vacuo and in
DCM (in brackets). Dihedral angles are given in degrees.

133       Given the good performance of the MPW1K functional in reproducing the vertical excitation
134   energies (this work) and in computing excited state geometries and vertical emission energies [13],
135   the choice of MPW1K functional appears appropriate also to compute GSRP. Additionally, in a
136   previous paper, the MPW1K has been demonstrated to be by far the method that provided computed
137   GSRP closer to the experimental values [15].
138       The results of GSRP computed *vs* experimental $E_{S^+/S}$ values on all the investigated dyes are
139   shown in Fig. 3. The graph is built from raw data of Table S3 (GSRP[b-f]) which have been mainly
140   computed in terms of free energies at different levels of theory. The analysis of the computed values
141   leads to some interesting considerations. At a first glance, it's straightforward to observe that data
142   cover two distinct regions of the graph: GSRP values calculated in the gas-phase overestimate the
143   experimental value (black circles in the region above the diagonal, where y=x, i.e. calculated (y) =
144   experimental (x)), while GSRP values calculated in the presence of the solvent slightly underestimate
145   the experimental value (empty and filled red and blue circles, below the diagonal). The use of high-
146   quality basis sets in the calculation visibly improves the agreement between the calculated GSRP and
147   experimental potential values (red circles). On the other hand, the zero point energy (ZPE) correction
148   has a minor effect on the quality of the calculated GSRP (empty and filled sets of points, which nearly
149   overlap). From the quantitative point of view, the highest level of theory employed, i.e. computing
150   frequencies at the MPW1K/6-31+G* on neutral and oxidized state geometries optimized at the same
151   level (MPW1K/6-31+G*//MPW1K/6-31+G*) is the one that provides the most accurate values with a
152   mean absolute error (MAE) of 0.18 eV both including ZPE correction or avoiding it (empty and filled
153   red circles). Higher deviations from experiments are found applying the MPW1K/6-31+G*
154   combination on neutral and oxidized state geometries computed at the MPW1K/6-31G* level
155   (MPW1K/6-31+G*//MPW1K/6-31G*). Indeed, the MAE is about 0.32 eV, again both including ZPE
156   correction or not (empty and filled blue circles). The highest deviations from experiments are
157   provided by the GSRP calculations in terms of free energies using the MPW1K/6-31+G*//MPW1K/6-
158   31+G* level, including ZPE correction and in gas-phase (black circles). Interestingly, the linear best
159   fits of each GSRP[b-f] set of data, y = ax + b, are all almost parallel with slopes a ~ 1 and intercept b = 0.
160   Thus, we may conclude that, as a general tendency and whatever the level of sophistication of the
161   calculation method, the difference of the free energy values allows, at least, to correctly reproduce
162   the redox potential qualitative trend, while higher-level calculations with high-quality basis-sets in
163   the presence of the solvent are crucial to correctly reproduce the quantitative trend.
164       According to Koopmans' theorem, $-\varepsilon$(HOMO) values have also been computed as
165   approximation of GSRP both in gas-phase and in DCM giving a MAE of 0.50 and 0.56 eV,
166   respectively. The plot of $-\varepsilon$(HOMO) values *vs* the experimental $E_{S^+/S}$ values discloses an intriguing
167   behavior. When calculated in the gas phase, $-\varepsilon$(HOMO) values lie on a best-fit line parallel to the best
168   fits of the GSRP[b-f] sets (Fig. 3, grey triangles, slope a ~ 1). In gas phase $-\varepsilon$(HOMO) values overestimate
169   the experimental data and nevertheless, possibly as an artifact due to error compensation, they seem
170   to be a better approximation of real data than the more sophisticated GSRP calculated in the gas phase
171   (Fig. 3, black circles). Instead, $-\varepsilon$(HOMO) values calculated in the presence of the solvent lie on a best-
172   fit line clearly divergent from the best fits of the GSRP[b-f] sets (grey asterisks, slope a ~ 0.7). In other
173   words, $-\varepsilon$(HOMO) calculated in the gas phase is a good approximation of the $S^+/S$ free energy
174   difference, while the same is not true in solution. Thus, for the investigated molecules in the gas-
175   phase Koopmans' theorem is valid, i.e. the frozen-orbital condition is verified, the orbitals of the
176   charged and neutral species are nearly identical and orbital relaxation is not expected. On the
177   contrary, based on the same considerations, in solution Koopmans' theorem seems to be not reliable
178   for the description of these molecules and their oxidation is expected to be accompanied by orbital
179   relaxation.
180
181
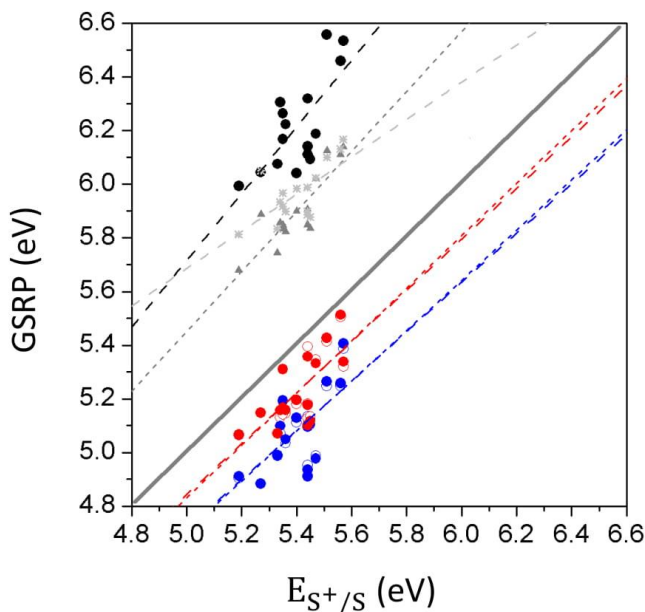
182
183 **Figure 3.** Computed GSRP values (GSRP[b-f] in Table S3) *vs.* experimental $E_{S+/S}$ values. The y=x
184 diagonal is reported as a reference. Black circles: MPW1K/6-31+G*//MPW1K/6-31+G* values in gas-
185 phase including ZPE correction; empty blue circles: MPW1K/6-31+G*//MPW1K/6-31G* values in
186 DCM; MPW1K/6-31+G*//MPW1K/6-31G* values in DCM including ZPE correction; MPW1K/6-
187 31+G*//MPW1K/6-31+G* values in DCM; MPW1K/6-31+G*//MPW1K/6-31+G* values in DCM
188 including ZPE correction; grey triangles: -ε(HOMO) in gas-phase; grey asterisks: -ε(HOMO) in DCM.
189
190         Since the difference Δε=ε(HOMO)vac−ε(HOMO)solv broadly varies from ∼ 0 to a few hundreds of
191 meV, our hypothesis has been tested by further investigating three of the dyes, namely TTZ7 (a large
192 molecule with the larger Δε), BD2 (a large molecule with Δε ≈ 0) and D5 (a small molecule with Δε ≈
193 0). To probe the extent of the orbital relaxation, the HOMO of each neutral dye has been compared
194 with the spin-density surface calculated for its cation: orbital relaxation should produce visible
195 differences in the space localization of these two surfaces. In Figure 4 it is visible how, for D5 and
196 BD2, the HOMO of the neutral dye and the spin density of its cation have a very similar shape and
197 space distribution, both in the gas-phase and in DCM. Therefore, in this case, the orbital relaxation is
198 minimal and Koopmans' theorem is expected to be valid, either in gas phase or in solution. On the
199 other side, the HOMO of TTZ7 and the spin density of TTZ7+ have a similar shape and space
200 distribution in the gas-phase, while in solution the spin density is much more localized on the donor
201 region as an effect of the orbital rearrangement. Localization of the charge on a more restricted region
202 is possible because of the stabilizing interaction with the solvent. In this case, there are not the
203 favorable conditions to apply Koopmans' theorem. In general, charge localization is driven by the
204 presence of electron-withdrawing groups, facilitated by the larger size of the molecule and made
205 possible by the presence of the solvent, while its delocalization is favored by the relief of the
206 interelectronic repulsion and made possible by the presence of an efficient conjugation path.
207 Considering all these aspects, after having analyzed the conformation, the dimensions and the
208 presence of electron-withdrawing groups, for the moment it has not been possible to univocally
209 identify the reason why a more marked charge localization is observed only in some cases.
210 Reasonably this interesting aspect will require a dedicated study and may be the subject of a
211 subsequent work, but for the moment we will have to settle for this further caveat against the
212 uncritical use of Koopmans' theorem.

|  | Gas-phase | DCM |
|---|---|---|
| D5 | | |
| BD2 | | |
| TTZ7 | | |
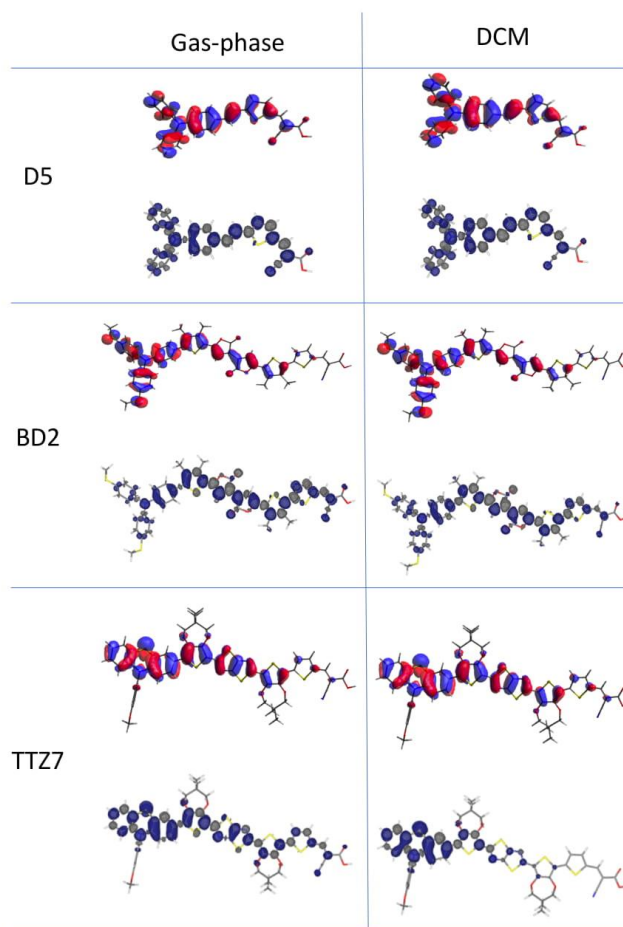


213
214 **Figure 4.** HOMO of the neutral species and the spin density of its cation for D5, BD2 and TTZ7
215 dyes.

216

217 Inspection of Fig. 5, which collects the computed GSRP vs dyes, reveals that, considering closely
218 related compounds with similar scaffolds, computed GSRPs and -$\varepsilon$(HOMO) reproduce the same
219 trends found for the experimental values. For example, in agreement with the experiments, GSRP
220 and -$\varepsilon$(HOMO) values of DF15 are lower in energy than those of D5, due to the presence of a stronger
221 hexyloxy-substituted donor group in DF15. Both dyes have more positive values than the redox
222 potential of the iodide/triiodide couple (4.77 eV)[24], as well as those of the most common Co-based
223 redox systems used in DSSC (4.85-5.04 eV)[25] suggesting that regeneration of the sensitizer is
224 feasible. Similar considerations apply to the Pechmann lactone containing molecules (BD1,2,6,7,8)
225 and to the benzobisthiazole- (BBZ1,2) and thiazolothiazole-systems (TTZ1-7). In particular, and again
226 in agreement with the experiments, the introduction of a stronger donor group (BD2 vs BD1) and the
227 substitution of the lactone moiety with the less electronwithdrawing lactam (BD8 vs BD1) lowers the
228 GSRP. Moreover, the substitution of the cyanoacrylic acid with a less electron-withdrawing acceptor
229 (BD6 and BD7 vs BD2) provides experimental ground state oxidation potentials similar to BD2. While
230 the computed GSRP and -$\varepsilon$(HOMO) values for BD6 and -$\varepsilon$(HOMO) value for BD7 are in line with
231 this observation, GSRPs of BD7 are instead predicted to be higher in energy although closer to the

232 experimental values. Concerning the benzobisthiazole- and thiazolothiazole- systems, the introduction
233 of electron-rich methoxy-substituents on TTZ2 and BBZ2 leads to a decrease in the ground-state
234 oxidation potentials compared to TTZ1 and BBZ1, which is also evident in the computational results.
235 In the series TTZ3-7, in line with experiments, the introduction of the electrondonating-alkoxy groups
236 on the triarylamine portion in TTZ4 and the presence of the terminal phenothiazine unit in TTZ7
237 resulted in lowering ground-state oxidation potential values. However, all BBZs and TTZs dyes have
238 ground-state oxidation potentials more positive than that of the iodide/triiodide couple, thus
239 assuring dye regeneration. The present results are consistent with the following final observations: i)
240 the frontier orbital approximations, according to Koopmans' theorem, might be used to reproduce
241 the trend of standard potentials in closely related families of compounds but cannot be used as a
242 method to predict quantitative values; ii) to obtain GSRPs with a certain degree of accuracy sufficient
243 to be comparable with experimental standard potentials, free energy cycle computations including
244 solvent effects need to be taken into account.

245
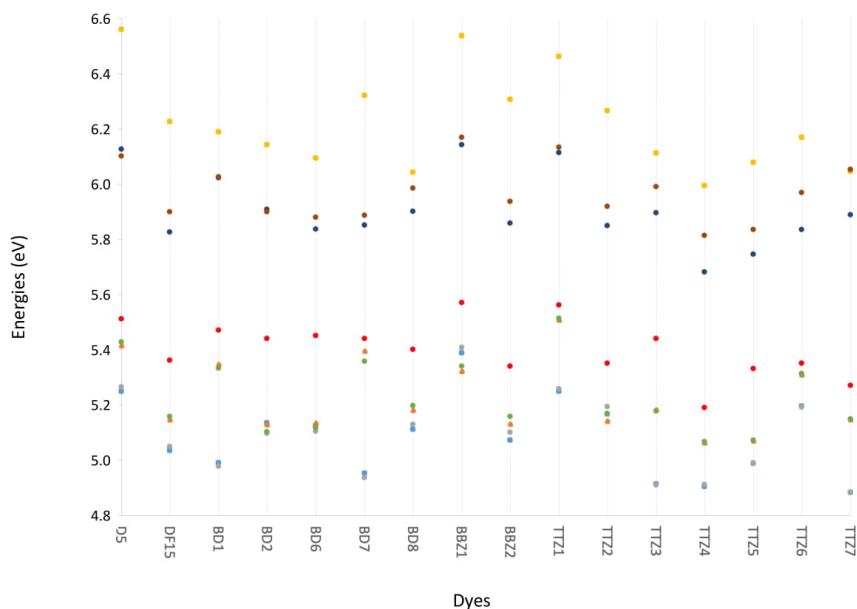


246

247 **Figure 5.** Experimental (red circles) and computed GSRP in solution of dye sensitizers computed at
248 different level of theory: MPW1K/6-31+G*//MPW1K/6-31G* (avion-blue squares); MPW1K/6-
249 31+G*//MPW1K/6-31+G* (orange triangles); MPW1K/6-31+G*//MPW1K/6-31G* including ZPE
250 correction (grey circles); MPW1K/6-31+G*//MPW1K/6-31+G* including ZPE correction (green circles).
251 MPW1K/6-31+G*//MPW1K/6-31+G* computed values for GSRP in gas-phase (yellow squares) and for
252 -ε(HOMO) in gas-phase (blue circles) and in DCM (brown circles) are also shown. The same solvent
253 (DCM) used in the experiments has been modeled.

254

## 4. Conclusions

256 The present study shows that, using the MPW1K functional in combination with an appropriate
257 basis set, it is possible to predict with a good level of accuracy the GSRP of a relatively large set of D-
258 π-A/D-A-π-A dyes having a medium to large size of the conjugated scaffold. Moreover, the
259 experimental trends in GSRP values of closely related compounds with similar scaffolds is well
260 reproduced. Thus, the employed strategy should help researchers to identify sensitizers that can

261 efficiently be used in DSSCs or in photocatalytic systems for the production of $H_2$, allowing them to
262 concentrate precious time and resources only on the preparation of the most promising candidates.
263

278 **References**

279 1. Hagfeldt, A.; Boschloo, G.; Sun, L.; Kloo, L.; Pettersson, H. Dye-Sensitized Solar Cells. *Chem Rev* **2013**,

280 *110*, 159–184.

281 2. Lee, C.P.; Li, C.T.; Ho, K.C. Use of organic materials in dye-sensitized solar cells. *Mater. Today* **2017**,

282 *20*, 267–283.

283 3. Gong, J.; Sumathy, K.; Qiao, Q.; Zhou, Z. Review on dye-sensitized solar cells (DSSCs): Advanced

284 techniques and research trends. *Renew. Sustain. Energy Rev.* **2017**, *68*, 234–246.

285 4. Dessì, A.; Monai, M.; Bessi, M.; Montini, T.; Calamante, M.; Mordini, A.; Reginato, G.; Trono, C.;

286 Fornasiero, P.; Zani, L. Towards Sustainable H2 Production: Rational Design of Hydrophobic

287 Triphenylamine-based Dyes for Sensitized Ethanol Photoreforming. *ChemSusChem* **2018**, *11*, 793–

288 805.

289 5. Bettucci, O.; Skaltsas, T.; Calamante, M.; Dessì, A.; Bartolini, M.; Sinicropi, A.; Filippi, J.; Reginato, G.;

290 Mordini, A.; Fornasiero, P.; et al. Combining Dithienosilole-Based Organic Dyes with a

291 Brookite/Platinum Photocatalyst toward Enhanced Visible-Light-Driven Hydrogen Production. *ACS*

292 *Appl. Energy Mater.* **2019**, *2*, 5600–5612.

71

293    6.    Zhang, X.; Peng, T.; Shuaishuai, S. Recent advances in dye-sensitized semiconductor systems for

294        photocatalytic hydrogen production. *J. Mater. Chem. A Mater. energy Sustain.* **2016**, *4*, 2365–2402.

295    7.    Cecconi, B.; Manfredi, N.; Montini, T.; Fornasiero, P.; Abbotto, A. Dye-Sensitized Solar Hydrogen

296        Production: The Emerging Role of Metal-Free Organic Sensitizers. *European J. Org. Chem.* **2016**,

297        *2016*, 5194–5215.

298    8.    De Angelis, F.; Fantacci, S.; Selloni, A. Alignment of the dye's molecular levels with the TiO2band

299        edges in dye-sensitized solar cells: A DFT-TDDFT study. *Nanotechnology* **2008**, *19*, 15–17.

300    9.    Dessì, A.; Calamante, M.; Mordini, A.; Peruzzini, M.; Sinicropi, A.; Basosi, R.; Fabrizi de Biani, F.;

301        Taddei, M.; Colonna, D.; Di Carlo, A.; et al. Organic dyes with intense light absorption especially

302        suitable for application in thin-layer dye-sensitized solar cells. *Chem. Commun.* **2014**, *50*, 13952.

303    10.    Zani, L.; Reginato, G.; Mordini, A.; Calamante, M.; Peruzzini, M.; Taddei, M.; Sinicropi, A.; Parisi, M.L.;

304        Fabrizi de Biani, F.; Basosi, R.; et al. An unusual thiazolo[5,4-d]thiazole sensitizer for dye-sensitized

305        solar cells. *Tetrahedron Lett.* **2013**, *54*, 3944–3948.

306    11.    Pastore, M.; Fantacci, S.; Angelis, F. De Modeling Excited States and Alignment of Energy Levels in

72

307    Dye- Sensitized Solar Cells : Successes , Failures , and Challenges. *J. Phys. Chem. C* **2013**, *117*, 3685–

308    3700.

309 12.    Castellucci, E.; Monini, M.; Bessi, M.; Iagatti, A.; Bussotti, L.; Sinicropi, A.; Calamante, M.; Zani, L.;

310    Basosi, R.; Reginato, G.; et al. Photoinduced excitation and charge transfer processes of organic dyes

311    with siloxane anchoring groups: A combined spectroscopic and computational study. *Phys. Chem.*

312    *Chem. Phys.* **2017**, *19*, 15310–15323.

313 13.    Bernini, C.; Zani, L.; Calamante, M.; Reginato, G.; Mordini, A.; Taddei, M.; Basosi, R.; Sinicropi, A.

314    Excited state geometries and vertical emission energies of solvated dyes for DSSC: A PCM/TD-DFT

315    benchmark study. *J. Chem. Theory Comput.* **2014**, *10*, 3925–3933.

316 14.    Fantacci, S.; De Angelis, F. Ab Initio Modeling of Solar Cell Dye Sensitizers: The Hunt for Red Photons

317    Continues. *Eur. J. Inorg. Chem.* **2019**, *2019*, 743–750.

318 15.    Pastore, M.; Fantacci, S.; De Angelis, F. Ab Initio Determination of Ground and Excited State

319    Oxidation Potentials of Organic Chromophores for Dye-Sensitized Solar Cells. *J. Phys. Chem. C* **2010**,

320    22742–22750.

73

321    16.    Lynch, B.J.; Fast, P.L.; Harris, M.; Truhlar, D.G. Adiabatic Connection for Kinetics. *J. Phys. Chem. A*

322            **2000**, *104*, 4811–4815.

323    17.    Zhao, J.; Lynch, B.J.; Truhlar, D.G. Development and Assessment of a New Hybrid Density Functional

324            Model for Thermochemical Kinetics. *J. Phys. Chem. A* **2004**, *108*, 2715–2719.

325    18.    Tomasi, J.; Mennucci, B.; Cammi, R. Quantum Mechanical Continuum Solvation Models. *Chem. Rev.*

326            **2005**, *105*, 2999–3094.

327    19.    Frisch, M.J.; Trucks, G.W.; Schlegel, H.B.; Scuseria, G.E.; Robb, M.A.; Cheeseman, J.R.; Scalmani, G.;

328            Barone, V.; Mennucci, B.; Petersson, G.A.; et al. Gaussian 09, Revision C.01 2010.

329    20.    Hagberg, D.P.; Edvinsson, T.; Marinado, T.; Boschloo, G.; Hagfeldt, A.; Sun, L. A novel organic

330            chromophore for dye-sensitized nanostructured solar cells. *Chem. Commun.* **2006**, 2245–2247.

331    21.    Dessì, A.; Calamante, M.; Mordini, A.; Peruzzini, M.; Sinicropi, A.; Basosi, R.; Fabrizi de Biani, F.;

332            Taddei, M.; Colonna, D.; Di Carlo, A.; et al. Thiazolo[5,4-d]thiazole-based organic sensitizers with

333            strong visible light absorption for transparent, efficient and stable dye-sensitized solar cells. *RSC Adv.*

334            **2015**, 32657–32668.

74

335  22.  Dessì, A.; Consiglio, B.; Calamante, M.; Reginato, G.; Mordini, A.; Peruzzini, M.; Taddei, M.; Sinicropi,

336      A.; Parisi, L.; Fabrizi de Biani, F.; et al. Organic Chromophores Based on a Fused Bis-Thiazole Core and

337      Their Application in Dye-Sensitized Solar Cells. *Eur. J. Org. Chem.* **2013**, 1916–1928.

338  23.  Dessì, A.; Sinicropi, A.; Mohammadpourasl, S.; Basosi, R.; Taddei, M.; Fabrizi de Biani, F.; Calamante,

339      M.; Zani, L.; Mordini, A.; Bracq, P.; et al. New Blue Donor – Acceptor Pechmann Dyes: Synthesis,

340      Spectroscopic, Electrochemical, and Computational Studies. *ACS Omega 2019,* **2019**, *4*, 7614–7627.

341  24.  Boschloo, G.; Hagfeldt, A. Characteristics of the Iodide/Triiodide Redox Mediator in Dye-Sensitized

342      Solar Cells. *Acc. Chem. Res.* **2009**, *42*, 1819–1826.

343  25.  Feldt, S.M.; Gibson, E.A.; Gabrielsson, E.; Sun, L. Design of Organic Dyes and Cobalt Polypyridine

344      Redox Mediators for High-Efficiency Dye-Sensitized Solar Cells. *J. Am. Chem. Soc.* **2010**, 16714–

345      16724.

346

347

# Ground state redox potential calculations of organic dyes for DSSC and Visible-Light-Driven Hydrogen Production

**Sanaz Mohammadpourasl[1], Fabrizia Fabrizi de Biani[2], Carmen Coppola[1,3], Maria Laura Parisi[1,3,4], Lorenzo Zani[4], Alessio Dessì[4], Massimo Calamante[4], Gianna Reginato[4], Riccardo Basosi[1,3,4] and Adalgisa Sinicropi[1,3,4]***

[1] R²ES Lab, Department of Biotechnology, Chemistry and Pharmacy, University of Siena, 53100 Siena, Italy
[2] Department of Biotechnology, Chemistry and Pharmacy, University of Siena, 53100 Siena, Italy
[3] Center for Colloid and Surface Science (CSGI), 50019 Firenze, Italy
[4] Italian National Council for Research, Institute for the Chemistry of Organo Metallic Compounds (CNR-ICCOM), 50019 Firenze, Italy
[*] Correspondence: adalgisa.sinicropi@unisi.it

1

**Table S1:** TDDFT (MPW1K/6-31+G*//MPW1K/6-31+G*) absorption maxima ($\lambda^a_{max}$ (nm)), excitation energies ($E_{exc}$ (eV)), oscillator strenghts (f) and transition contributions (%). Solvent effects are included via PCM. The same solvents used in the experiments have been modeled. The experimental $\lambda^a_{max}$ and corresponding $E_{exc}$ are given in brackets.

| Dyes | Solvent (PCM) | $\lambda^a_{max}$ | $E_{exc}$ | f | Main transitions |
|------|---------------|-------------------|-----------|---|------------------|
| D5 | EtOH | 486 (427-474[a]) | 2.55 (2.90-2.62) | 1.4258 | HOMO -> LUMO (89%). HOMO-1 -> LUMO (7%) |
| DF15 | EtOH | 508 (494-530[b]) | 2.44 (2.51-2.34) | 1.4402 | HOMO -> LUMO (89%). HOMO-1 -> LUMO (7%) |
| BD1 | CHCl₃ | 652 (676[c]) | 1.90 (1.83) | 2.2304 | HOMO -> LUMO (85%). HOMO-1 -> LUMO (11%) |
| BD2 | CHCl₃ | 660 (681[c]) | 1.88 (1.82) | 2.2069 | HOMO -> LUMO (66%). HOMO-1 -> LUMO (31%) |
| BD6 | CHCl₃ | 624 (651[c]) | 1.98 (1.90) | 1.8282 | HOMO -> LUMO (69%). HOMO-1 -> LUMO (29%) |
| BD7 | CHCl₃ | 645 (666[c]) | 1.92 (1.86) | 2.0600 | HOMO -> LUMO (69%). HOMO-1 -> LUMO (29%) |
| BD8 | CHCl₃ | 603 (608[c]) | 2.05 (2.04) | 1.6577 | HOMO -> LUMO (78%). HOMO-1 -> LUMO (13%) |
| BBZ1 | THF | 442 (446[d]) | 2.80 (2.78) | 2.4243 | HOMO -> LUMO (19%). HOMO-1 -> LUMO (61%) |
| BBZ2 | THF | 447 (455[d]) | 2.77 (2.72) | 2.3036 | HOMO -> LUMO (28%). HOMO-1 -> LUMO (52%) |
| TTZ1 | THF | 472 (472[d]) | 2.63 (2.63) | 2.2867 | HOMO -> LUMO (37%). HOMO-1 -> LUMO (23%) |
| TTZ2 | THF | 479 (476[d]) | 2.59 (2.60) | 2.1922 | HOMO -> LUMO (36%). HOMO-1 -> LUMO (24%) |
| TTZ3 | THF | 503 (510[e]) | 2.47 (2.43) | 2.4603 | HOMO -> LUMO (54%). HOMO-1 -> LUMO (32%) |
| TTZ4 | THF | 511 (518[e]) | 2.43 (2.39) | 2.3851 | HOMO -> LUMO (49%). HOMO-1 -> LUMO (37%) |
| TTZ5 | THF | 507 (510[e]) | 2.45 (2.43) | 2.4426 | HOMO -> LUMO (43%). HOMO-1 -> LUMO (42%) |
| TTZ6 | THF | 507 (521[e]) | 2.44 (2.38) | 2.4839 | HOMO -> LUMO (56%). HOMO-1 -> LUMO (32%) |
| TTZ7 | THF | 500 (513[e]) | 2.48 (2.42) | 2.4593 | HOMO -> LUMO (56%). HOMO-1 -> LUMO (31%) |

[a] D5 in ethanol: 441 nm (2.81 eV); methanol: 444 nm (2.79 eV); methanol + acid (protonated): 474 nm (2.62 eV); acetonitrile (deprotonated): 427 nm (2.90 eV). See Ref. [1]
[b] DF15 in ethanol: 494 nm; CH₂Cl₂: 530 nm. See Refs. [2,3]
[c] See Ref. [4]
[d] See Ref. [5]
[e] See Refs [6,7]

2

**Table S2 (to be continued):** DFT frontier molecular orbitals for all dyes obtained at MPW1K/6-31+G* level in vacuo.
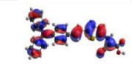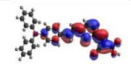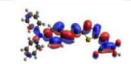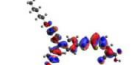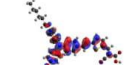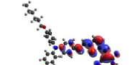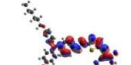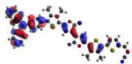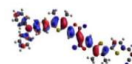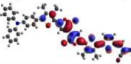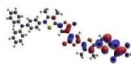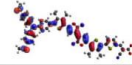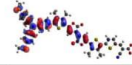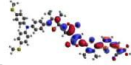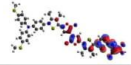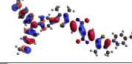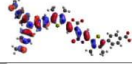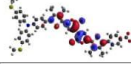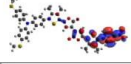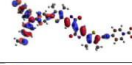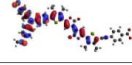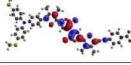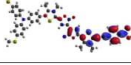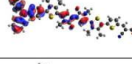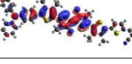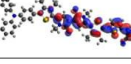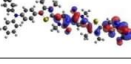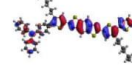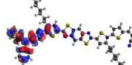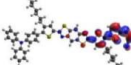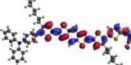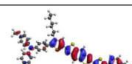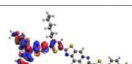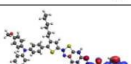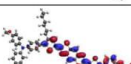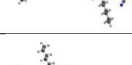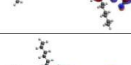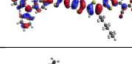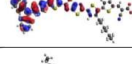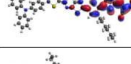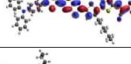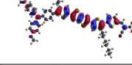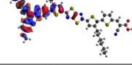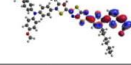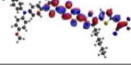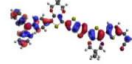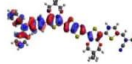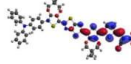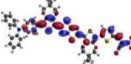
| Dyes | HOMO-1 | HOMO | LUMO | LUMO+1 |
|---|---|---|---|---|
| D5 | | | | |
| DF15 | | | | |
| BD1 | | | | |
| BD2 | | | | |
| BD6 | | | | |
| BD7 | | | | |
| BD8 | | | | |
| BBZ1 | | | | |
| BBZ2 | | | | |
| TTZ1 | | | | |
| TTZ2 | | | | |
| TTZ3 | | | | |
| TTZ4 | | | | |

3

**Table S2 (continued):** DFT frontier molecular orbitals for all dyes obtained at MPW1K/6-31+G* level in vacuo.
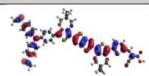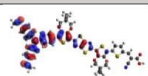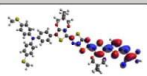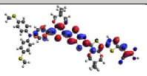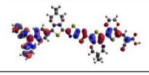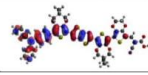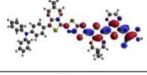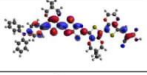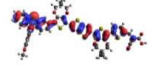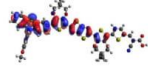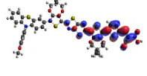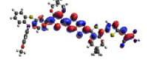
| Dyes | HOMO-1 | HOMO | LUMO | LUMO+1 |
|------|--------|------|------|--------|
| TTZ5 | | | | |
| TTZ6 | | | | |
| TTZ7 | | | | |

4

**Table S3:** Experimental ($E_{S+/S}$), computed **GSRP** (eV) and **-ε(HOMO)** of all investigated dyes.

| Dyes | $E_{S+/S}$[a] | GSRP[b] | GSRP[c] | GSRP[d] | GSRP[e] | GSRP[f] | -ε(HOMO)[g] | -ε(HOMO)[h] |
|------|------|------|------|------|------|------|------|------|
| D5 | 5.51 | 6.56 | 5.25 | 5.41 | 5.26 | 5.43 | 6.13 | 6.10 |
| DF15 | 5.36 | 6.22 | 5.03 | 5.15 | 5.05 | 5.16 | 5.82 | 5.90 |
| BD1 | 5.47 | 6.19 | 4.99 | 5.35 | 4.98 | 5.33 | 6.02 | 6.02 |
| BD2 | 5.44 | 6.14 | 5.13 | 5.13 | 5.10 | 5.10 | 5.91 | 5.90 |
| BD6 | 5.45 | 6.09 | 5.12 | 5.13 | 5.10 | 5.12 | 5.84 | 5.88 |
| BD7 | 5.44 | 6.32 | 4.95 | 5.39 | 4.94 | 5.36 | 5.85 | 5.89 |
| BD8 | 5.4 | 6.04 | 5.11 | 5.18 | 5.13 | 5.20 | 5.90 | 5.98 |
| BBZ1 | 5.57 | 6.53 | 5.39 | 5.32 | 5.41 | 5.34 | 6.14 | 6.17 |
| BBZ2 | 5.34 | 6.31 | 5.07 | 5.13 | 5.10 | 5.16 | 5.86 | 5.94 |
| TTZ1 | 5.56 | 6.46 | 5.25 | 5.51 | 5.26 | 5.51 | 6.11 | 6.13 |
| TTZ2 | 5.35 | 6.26 | 5.17 | 5.14 | 5.19 | 5.17 | 5.85 | 5.92 |
| TTZ3 | 5.44 | 6.11 | 4.91 | 5.18 | 4.91 | 5.18 | 5.89 | 5.99 |
| TTZ4 | 5.19 | 5.99 | 4.90 | 5.06 | 4.91 | 5.07 | 5.68 | 5.81 |
| TTZ5 | 5.33 | 6.08 | 4.99 | 5.07 | 4.99 | 5.07 | 5.74 | 5.83 |
| TTZ6 | 5.35 | 6.17 | 5.19 | 5.31 | 5.19 | 5.31 | 5.83 | 5.97 |
| TTZ7 | 5.27 | 6.05 | 4.88 | 5.15 | 4.88 | 5.15 | 5.89 | 6.05 |
| | | | | | | | | |
| MAE[i] | | 0.82 | 0.32 | 0.18 | 0.32 | 0.18 | 0.50 | 0.56 |

[a] The 4.420 value for the NHE half-reaction was added to the experimental $E_{S+/S}$ values [8–10].
[b] Computed at the MPW1K/6-31+G*//MPW1K/6-31+G* level of theory including ZPE correction in gas-phase.
[c] Computed at the MPW1K/6-31+G*//MPW1K/6-31G* level of theory without ZPE correction.
[d] Computed at the MPW1K/6-31+G*//MPW1K/6-31+G* level of theory without ZPE correction
[e] Computed at the MPW1K/6-31+G*//MPW1K/6-31G* level of theory including ZPE correction
[f] Computed at the MPW1K/6-31+G*//MPW1K/6-31+G* level of theory including ZPE correction
[g] Computed at the MPW1K/6-31+G* level of theory or the neutral species in gas-phase
[h] Computed at the MPW1K/6-31+G* level of theory for the neutral species in DCM
[i] Mean Absolute Error

5

**References**

1.  Pastore, M.; Fantacci, S.; De Angelis, F. Ab Initio Determination of Ground and Excited State Oxidation Potentials of Organic Chromophores for Dye-Sensitized Solar Cells. **2010**, 22742–22750.
2.  Franchi, D.; Calamante, M.; Reginato, G.; Zani, L.; Peruzzini, M.; Taddei, M.; Fabrizi, F.; Biani, D.; Basosi, R.; Sinicropi, A.; et al. A comparison of carboxypyridine isomers as sensitizers for dye- sensitized solar cells : assessment of device ef fi ciency and stability. *Tetrahedron* **2014**, *70*, 6285–6295.
3.  Bettucci, O.; Franchi, D.; Sinicropi, A.; di Donato, M.; Foggi, P.; Fabrizi De Biani, F.; Reginato, G.; Zani, L.; Calamante, M.; Mordini, A. Tailoring the Optical Properties of Organic D- π -A Photosensitizers : Effect of Sulfur Introduction in the Acceptor. **2019**, 812–825.
4.  Dessì, A.; Sinicropi, A.; Mohammadpourasl, S.; Basosi, R.; Taddei, M.; Fabrizi de Biani, F.; Calamante, M.; Zani, L.; Mordini, A.; Bracq, P.; et al. New Blue Donor − Acceptor Pechmann Dyes: Synthesis, Spectroscopic, Electrochemical, and Computational Studies. **2019**.
5.  Dessì, A.; Consiglio, B.; Calamante, M.; Reginato, G.; Mordini, A.; Peruzzini, M.; Taddei, M.; Sinicropi, A.; Parisi, L.; Fabrizi De Biani, F.; et al. Organic Chromophores Based on a Fused Bis-Thiazole Core and Their Application in Dye-Sensitized Solar Cells. **2013**, 1–14.
6.  Dessì, A.; Calamante, M.; Mordini, A.; Peruzzini, M.; Sinicropi, A.; Basosi, R.; Fabrizi De Biani, F.; Taddei, M.; Colonna, D.; Di Carlo, A.; et al. Organic dyes with intense light absorption especially suitable for application in thin-layer dye-sensitized solar cells. *Chem. Commun.* **2014**, *50*.
7.  Dessì, A.; Calamante, M.; Mordini, A.; Peruzzini, M.; Sinicropi, A.; Basosi, R.; Fabrizi De Biani, F.; Taddei, M.; Colonna, D.; Di Carlo, A.; et al. Thiazolo[5,4-d]thiazole-based organic sensitizers with strong visible light absorption for transparent, efficient and stable dye-sensitized solar cells. **2015**, 32657–32668.
8.  Kelly, C.P.; Cramer, C.J.; Truhlar, D.G. Single-Ion Solvation Free Energies and the Normal Hydrogen Electrode Potential in Methanol , Acetonitrile , and Dimethyl Sulfoxide. **2007**, 408–422.
9.  Zanello, P.; Fabrizi De Biani, F.; Nervi, C. *Inorganic Electrochemistry: Theory. Practice and Application*; RSC Publishing, 2011;
10. Fawcett, W.R. The Ionic Work Function and its Role in Estimating Absolute Electrode Potentials. *Langmuir* **2008**, *24*, 9868.

6

# Combined LCA and Green Metrics Approach for the Sustainability Assessment of an Organic Dye Synthesis on lab scale

**Maria Laura Parisi[1,2,3,$], Alessio Dessì[3,$], Lorenzo Zani[3], Simone Maranghi[1,2], Sanaz Mohammadpourasl[1,2,4], Massimo Calamante[3,4], Alessandro Mordini[3,4], Riccardo Basosi[1,2,3], Gianna Reginato[3]\* and Adalgisa Sinicropi[1,2,3]\***

[1]R[2]ES Lab, Department of Biotechnology, Chemistry and Pharmacy, University of Siena, 53100 Siena, Italy.
[2]Center for Colloid and Surface Science-CSGI, 50019 Sesto Fiorentino, Firenze, Italy
[3]National Research Council, Institute for the Chemistry of OrganoMetallic Compounds (CNR-ICCOM), 50019 Sesto Fiorentino, Firenze, Italy
[4]Department of Chemistry "U. Schiff", University of Florence, Via della Lastruccia 13, 50019 Sesto Fiorentino, Italy
$These authors contributed equally to this work

**\* Correspondence: Gianna reginato gianna.reginato@iccom.cnr.it (G.R.); Adalgisa Sinicropi adalgisa.sinicropi@unisi.it (A.S.)**

## Abstract

New generation photovoltaic devices have attracted much attention in the last decades since they can be efficiently manufactured employing abundant raw materials and with less-energy intensive processes. In this context, the use of powerful environmental assessment is pivotal to support the fine-tuning of solar cells fabrication and hit the target of manufacturing effective sustainable technological devices. In this work, a mass-based green metrics and life cycle assessment combined approach is applied to analyze the environmental performances of an innovative synthetic protocol for the preparation of organic dye **TTZ5**, which has been successfully proposed as a sensitizer for manufacturing dye sensitized solar cells. The new synthetic strategy, which is based on the C-H activation process, has been compared with the previously reported synthesis employing classic Suzuki-Miyaura cross-coupling chemistry. Results highlight the contribution of direct energy consumption and purification operations in organic syntheses at lab scale. Furthermore, they demonstrate the usefulness of the environmental multifaceted analytic tool and the power of life cycle assessment to overcome the intrinsic less comprehensive nature of green metrics for the evaluation of organic synthesis protocols.

## 1 Introduction

In order to match the target of the EU Renewable Energy Directive (EU, 2018) and the Circular Economy Action Plan (EC COM(2019) 190 final, 2019), the research and development activity on photovoltaics (PV) should cope in looking for more eco-friendly manufacturing solutions. Since PV devices are known to be an emission-free technology during their operative phase, the major efforts in terms of sustainability should result in minimizing the environmental impact associated with the production of the cell and module components and the end-of-life phase (Bravi et al., 2010).

This matter is of paramount importance especially for innovative PV, and particularly for the so-called last generation technologies, that stand out for the use of materials alternative to traditional semiconductors. In recent years, relevant results have been obtained in this field in terms of efficiency and technological advancement(A.T. Kearney Energy Transition Institute, 2017), thanks to a lively and very productive research activity developed at lab scale(Polman et al., 2016; Luceño-Sánchez et al., 2019). In this context, the adoption of an eco-design approach becomes essential to pursue the improvement of the eco-profile of products(Maranghi et al., 2019; Parisi et al., 2019) and the environmental sustainability assessment offers a powerful tool to achieve this goal. The panorama of environmental sustainability assessment methods offers a wide range of possibilities (Sheldon, 2016b, 2018). Above all, a multivariate approach combining mass-based green metrics and life cycle assessment (LCA) affords an extremely useful tool for evaluating the environmental impact of processes, as already demonstrated in the bulk and fine chemicals production, pharmaceutical and nanotechnology sectors (Eckelman et al., 2008; Gałuszka et al., 2012; Li et al., 2012; F. et al., 2015; Sheldon, 2016a).

The concurrent use of these different tools allows to combine the versatility and practicality of green metrics with the detailed environmental screening that can be obtained through the implementation of an all-encompassing assessment like LCA. Indeed, in such a way it is possible to take in consideration relevant information such as resource efficiency and energy requirements together with all of the possible hotspots associated to the investigated systems.

Although this combined approach is quite often implemented at the industrial R&D level(Cespi et al., 2019), its application at lab scale for product and processes eco-design is not so diffused(Pini et al., 2019). Indeed, notwithstanding the increasing and recognised importance of Life Cycle Thinking (LCT) approaches also for laboratory scale procedures (Allen et al., 201AD), the application of the LCA methodology requires the compiling of a comprehensive inventory of data that, when appropriate information can be found, is always a laborious and very time-demanding procedure.

So far, examples of such combined sustainability assessment are absent in the scientific literature concerning the synthesis of innovative materials for PV. For instance, in a recent work by Grisorio et al. (Grisorio et al., 2015), a green metrics analysis has been applied for the evaluation of the environmental sustainability of an innovative chemical process used to prepare a solar cell component, but not in the perspective of a LCT approach.

In this work, a mass-based green metrics and LCA combined approach is applied to obtain a gate-to-gate assessment on two new alternative synthetic protocols, specifically designed to scale-up the production of the organic dye **TTZ5** (Figure 1), and compare their environmental performances with those of its original preparation (Dessì et al., 2014). Compound **TTZ5**, bearing a thiazolo[5,4-*d*]thiazole (TzTz) ring as its central unit, has been successfully employed as a sensitizer for the preparation of photocatalysts for hydrogen production (Dessì et al., 2018)and the manufacturing of dye sensitized solar cells (DSSCs) (Dessì et al., 2014, 2015).This innovative photovoltaic technology dates back to 1991 and was proposed as a more versatile and cheaper alternative to silicon based photovoltaic (PV) devices. Indeed, DSSCs proved to be more competitive in terms of ease of production, reduction in the use of hazardous substances, manufacturing costs and raw materials availability compared with other photovoltaic devices(Hagfeldt et al., 2010; Gong et al., 2017). However, the efficiency of these devices is strongly dependent on the sensitizer.(Parisi et al., 2013, 2014) From this perspective, dye **TTZ5**, when used in thin film DSSCs (photoanode thickness approx. 5.5 µm) drew great attention(Dessì et al., 2014) showing efficiencies up to 7.71%, which are superior to the Ru-based sensitizer **Z907** ($\eta$ 5.51%) measured in the same conditions, and approaching the 11.9% record efficiencies registered for champion DSSCs(NREL, 2019). For these reasons, **TTZ5** is particularly suitable for application in transparent and opaque thin-layer cells (Dessì et al., 2014), which are a common choice for the application in Building Integrated Photovoltaic (BIPV) systems.

PAGE \* Arabic \* MERGEFORMAT 4

Figure 1

## 2    Materials and methods

### 2.1    Synthetic approach

In the last years, **TTZ5** has found application as a photosensitizer in the photocatalytic hydrogen production(Dessì et al., 2018) and in transparent thin-layer DSSCs(Dessì et al., 2014), which are very attractive for the production of colored, transparent modules to be applied in building-integrated photovoltaics. However, fulfilling this aim would require the preparation of large-scale panels, in turn demanding the development of a reliable and sustainable gram-scale preparation of the dye. The original synthesis of **TTZ5** required three main synthetic operations to obtain the key intermediate aldehyde **6**: *a)* the preparation of thiazolothiazole-based spacer **1** (Scheme S1), *b)* the preparation of boronic ester **3**, containing the donor group (Scheme S2) and *c)* the introduction of the donor and the acceptor moieties through two sequential Suzuki-Miyaura cross-couplings (Scheme 1). Finally, the anchoring group cyanoacrylic acid was introduced following the well-established Knoevenagel condensation protocol on aldehyde **6** (Dessì et al., 2014). The undeniable Achilles' heel of the old synthetic approach, which hampered the scale-up of **TTZ5**, was the desymmetrization of thiazolothiazole-based spacer **1**: following a straightforward double electrophilic iodination, the Suzuki-Miyaura coupling of diiodide **2** with boronic ester **3** proved troublesome, since the reaction had to be stopped before the complete conversion of the starting material **2**, in order to minimize the second coupling with the residual carbon-iodine bond in compound **4**. Moreover, undesired dehalogenation of both the starting material **2** and the product **4** decreased the yield, making the chromatographic purification difficult. As a result, only a small amount of the final compound could be obtained in pure form.

Scheme 1

In order to design a more sustainable and scalable synthetic procedure of dye **TTZ5**, we decided to change our approach to the functionalization of building block **1**. Our choice was to move from a classic Suzuki-Miyaura cross-coupling to the exploitation of a direct arylation protocol. In this case, in fact, the formation of a new carbon-carbon bond could be performed avoiding the use of any preformed organometallic reagent and reducing the number of the synthetic steps (Zani et al., 2019). Inspired by Liu's work about the C-H functionalization of a central heteroaromatic core with different electron-rich and electron-poor bromides (Lu et al., 2017), we initially explored the single direct arylation of starting material **1** with the electron-poor bromide **7** (Scheme 2). Application of Liu's reaction conditions, which consisted in using an excess amount of the starting material, $Pd(OAc)_2$ as pre-catalyst, the bulky electron-donating phosphine CataCXium® A as ligand, pivalic acid as the acid additive, inexpensive $K_2CO_3$ as the base and *N*,*N*-DMF as the solvent at 110 °C, allowed to isolate pure intermediate **8** with 28% yield.

Scheme 2

Unfortunately, part of the starting material **1** decomposed under these conditions and just a small fraction of its excess could be recovered at the end of the reaction. Despite that, the simple change of *N,N*-DMF with a less polar solvent such as toluene and a reduction of the reaction temperature to 85 °C allowed to minimize undesired side-reaction and to employ just a stoichiometric amount of thiazolothiazole **1**. Under these conditions, a 70% conversion of the starting material **1** could be achieved, leading to a 40% yield of the desired aldehyde **8** as a pure product. Disappointingly, when the same conditions were tested to introduce the donor group by reaction with bromide **9**, no conversion to product **6** was observed. To achieve this transformation, a quantitative electrophilic bromination of intermediate **8** and a subsequent Stille-Migita cross-coupling with stannane **10** proved necessary, affording the desired product in 82% yield. Accordingly, following this C-H activation/Stille-Migita cross-coupling route, the desired advanced intermediate **6** could be isolated in a two steps sequence, with an overall yield of 33%, leading to a good improvement in terms of yield and selectivity compared to the original synthetic strategy. In addition, application of this route allowed to scale-up the preparation of compound **6** to a quantity of approx. 1.3 g, much higher than that obtained with the original synthetic sequence.

However, the sustainability of the whole process appeared still limited by the employment of the tin-containing reagent (**10**) and the use of quite harsh conditions: clearly the possibility to perform two subsequent C-H activation processes would be largely preferred. To reach this goal, we decided to explore a different approach, inspired by those previously reported for the direct arylation-based synthesis of D-π-A dyes for DSSCs (Lin et al., 2015; Lu et al., 2017), and consisting in the reversal of the order in the introduction of the donor and acceptor groups (Scheme 2). Thus, the direct arylation of the starting material **1** was first performed with donor bromide **9** and then the resulting intermediate **11** was reacted with electron-poor bromide **7**.

The first step of the synthesis was indeed accomplished using the same reaction conditions mentioned above, with a slight increase of the temperature and using an excess of the starting material **1**. The reaction proceeded smoothly, with a complete conversion of donor bromide **9**; unfortunately, however, a complete chromatographic separation of product **11** and unreacted starting material **1** was almost impossible, hampering the isolation of pure **11**. Despite that, such 1:1 mixture of **11** and **1** could be successfully reacted with electron-poor bromide **7** to give, under the usual conditions, pure compound **6**, which was isolated after chromatographic purification. Unfortunately, the excess of reagent **1** used in the first step could not be recovered at the end of the second step, since it underwent a double direct arylation with bromide **7**. The overall yield of this C-H activation route was 29%, comparable to the previous C-H activation/Stille-Migita route in terms of yield, although a larger amount of starting material **1** was consumed.

Scheme 3

Finally, to overcome the problem of purification of intermediate **11** and trying to minimize the presence of unreacted **1**, we decided to test a *one-pot* direct arylation protocol (Scheme 3), aiming to obtain compound **6** directly from the starting material **1** and to avoid the isolation of any intermediate. To achieve this goal, an optimization of the reaction conditions was carried out using different Pd catalyst and conditions. Thus, using tri-*tert*-butylphosphine as a ligand no conversion of the starting material **1** was obtained, while using tricyclohexylphosphine or CataCXium® A provided the desired product **6** with yields of 13% and 19% respectively. Finally, we found that, for the introduction of the donor group, acetic acid was superior to pivalic acid, since it reduced the relevance of possible side-reactions such as a partial oligomerization of **1**.

Following this optimized *one-pot* C-H activation route, compound **6** was thus obtained in 26% yield after purification (isolated amount: 0.24 g). Clearly, from a practical point of view, despite the overall yield of this process was a bit lower than the previous ones, the possibility of accessing intermediate **6** in a single synthetic step, without using stoichiometric organometallic reagents and avoiding expensive and time-consuming purification procedures, makes this route more intriguing especially for large scale application (see Table 1).

Table 1

## 2.2 Environmental sustainability assessment

As anticipated in the introduction, an important aim of this work is the calculation of the eco-profile of the photosensitizer **TTZ5** produced via the three above-mentioned alternative synthetic routes, to assess if an environmental sustainability improvement can be obtained while looking for scalability of the manufacturing procedure. A generic PV module production process is synthetically represented in Figure 2: it starts from the acquisition of raw materials, encompassing the fabrication process of all the components and it ends with the assembling phase.

Figure 2

The implemented approach is a gate-to-gate analysis exclusively focused on the manufacturing phase of the DSSC photosensitizer, using both green metrics and LCA calculations. The reason of this choice arises from the necessity of evaluating exclusively the obtained improvements (if present) derived from the change of reaction strategies for the production of target molecule **TTZ5**. The foreground system includes the original synthesis and the two new alternative synthetic routes to obtain **TTZ5**. An overview of the process is sketched in the figure, where the three routes are distinct with different colors (Compounds **13**, **14**, **15**, **16**, **18**, **19** are numbered according to the synthetic procedure described in ref. (Dessì et al., 2014), see Scheme S1-S2).
In the following sub-sections, some methodological details are given.

PAGE \* Arabic \*
MERGEFORMAT 3

### 2.2.1 Green metrics

*E-factor:* The E-factor (EF) represents the quantity of waste generated (i.e. anything except the product) to produce 1 unit of the target product. Work-up substances, auxiliaries and solvents are incorporated in the definition of waste. The following equation express the value of EF:

$$EF = \frac{\sum_i \quad m(raw\ material_i) - m_p}{m_p}$$

A higher EF means more waste and, consequently, greater negative impact. The ideal EF is zero. Lower EF have been shown to correlate well with reduced manufacturing costs which is a reflection of lower process materials input and output, reduced cost of hazardous and toxic waste disposal, improved capacity utilization and reduced energy demand. In this work, since the main purpose is a lab-scale application, EF is calculated in g/g to suitably quantify discards in laboratory synthesis.

*Overall Yield:* The overall yield has always been a pillar of calculations on reaction efficiency. Considered as a "classical metrical measure" like selectivity, its relevance persists also in green metrics assessment. An implicit consideration of the overall yield is included in the EF calculation, since higher yields result in less disposal (inferior mass of byproducts, major incorporation of reactants into the target product, etc.).

*Price Estimate:* In order to evaluate whether more environmentally benign syntheses provide a real financial benefit, estimation on the global price of product becomes remarkable. Calculating the cost of production of a target molecule involves incorporation of all the expenses related to the implemented raw materials. To achieve this objective, commercially available chemical prices were collected. In order to draw the attention on advantages due to waste prevention, costs related to recovered materials were subtracted to the "total waste price". At this point, to assess the price of the product per gram, the "total waste price" is divided by the grams of obtained product. In case one of the reactants was not commercially available, but derived from a previous synthesis, its costs were incorporated into the reaction path price by adding to the "total price of waste". This enables a "conditional cost estimate", namely a price evaluation specific for the conditions of a synthesis (costs of reactants and their relative usage, spared materials and so on) allowing the exact appraising of financial burden on synthetic approaches and potential improvements in the perspective of a possible industrial scalability.

*Eco-scale:* Eco scale is a semiquantitative laboratory scale tool to estimate the eco-sustainability of chemical reactions based on yield, price, safety conditions, technical setup, temperature/time and ease of workup/purification. The usefulness of this tool in up-scaled processes is not significant because relative weights of the six proposed categories may differ for industrial purposes. The ideal Eco Scale value is 100, representing an "ideal reaction where a substrate A undergoes a reaction with the inexpensive reactant B at room temperature to give the product in 100% yield with a minimal risk for the operator and the environment". For this assessment the original approach of Van Aken and coworkers (Van Aken et al., 2006) was adopted. Thus, penalty points are assigned according to a specific ranking for each category and then subtracted by the ideal value of 100 to obtain the Eco scale rate. Eco Scale values higher than 75 are associated to an excellent performance; values between 75 and 50 are considered acceptable, while Eco Scale scores minor than 50 are assigned as inadequate.

### 2.2.2 LCA

According to the ISO 14040 family standards (International Organization for Standardization, 2006; Standardization, 2006) and the more completely elaborated ILCD Handbook Guidelines (European Commission, 2010a), an attributional approach was implemented for the LCA calculation on **TTZ5** synthesis. The functional unit chosen in this study is 1 gram of the target product. The same unit has been employed for the calculation of the green metrics. No allocation procedure was required since all of the environmental burdens were attributed to the final product of the process, i.e. 1 g of **TTZ5**. Data life cycle inventory (LCI) was built based on lab primary data. When needed, meta-data (conveniently customized to generate datasets for reactants, auxiliaries and solvents) and secondary data were taken from the Ecoinvent Database v. 3.4 (Wernet et al., 2016). Equipment and instruments are not included in the system modelling as capital goods, but they are accounted for in terms of energy requirement for their functioning. The life cycle impact assessment (LCIA) method employed is the ILCD 2011 Midpoint+ method (version 1.0.9, May 2016), developed by the Joint Research Centre - European Commission (European Commission, 2010b). that allows to obtain single scores results expressed as Eco-Points (Pt). The Cumulative Energy Demand (CED) method (version 1.09, August 2014) is employed to quantify the use of the direct and indirect energy requirement during all the life cycle phases of the system expressing the results in units of Mega Joule (MJ) (Frischknecht et al., 2007). LCA Calculations are performed with software Simapro v. 8.5.

### 3    Results and Discussion

Table 2 shows the EF values for intermediates and **TTZ5** generation for the C-H/Stille route and the *one-pot* C-H activation route, respectively. Data concerning the Suzuki-Miyaura route are reported for comparison (more details are available in the Supporting Information).

Table 2

The reported data clearly disclose the general trend of EF growing with increasing reactant complexity, and the contribution of water in its calculation. The three routes have in common five steps for the synthesis of thiazolothiazole **1** (from **13** to **1**, see Scheme S1), three steps for the preparation of the brominated triarylamine **9** (from **18** to **9**, see Scheme S2) and the last one for the synthesis of the final compound **TTZ5**, so they can be excluded from the direct comparison (gray background in Table 2). It is evident from the simple comparison of the final **TTZ5**-EF values that both the new C-H activation-based routes generated a much lower amount of waste than the original Suzuki-Miyaura protocol, with a three-to-four times decrease of the EF values. This EF-drop is due both to the smaller number of synthetic steps required by the new routes compared to the old one (one step less for the C-H/Stille route and three less for the *one-pot* C-H activation route) and the higher efficiency of the desymmetrization reaction (Compound **8** C-H/Stille Route – EF: 21307.58 g/g; Compound **6** *one-pot* C-H Activation Route – EF: 28873.89 g/g, to be compared with: Compound **4** Suzuki-Miyaura Route – EF: 49103.81 g/g). Moreover, the Suzuki-Miyaura route was penalized by a high increase of the EF for the transformation of compound **4** (49103.81 g/g) into compound **6** (94719.08 g/g) too. The same transformation was either included in the desymmetrization step of the *one-pot* C-H activation route or, at least, much more efficient in the C-H/Stille route.

Indeed, considering the evolution of water-including EF outcomes, the C-H/Stille route shows increasing values from 29.23 g/g of Compound **13** to 21740.55 g/g of Compound **8**, this latter being the highest one. This trend becomes comprehensible considering that the more synthetic steps are required for manufacturing a specific reactant, the more previous waste is involved in the final calculations. However, EFs are not only influenced by previous waste or mass of reactants, but also yields of reactions play an important role on material efficient consumptions, since these calculations are made on gram-of-target molecule basis. Accordingly, water-excluding EFs proved to decrease for compound **9** and **10**, compared to their previous intermediate (compounds **19** and **9**, respectively), despite the necessity of more complex reactants. This trend can be understood considering the high reaction yield obtained in both processes (98% and 100% efficiency, respectively). In fact, increasing yields correlate with larger amounts of product, which, in turn, translate in lowering of waste per gram. Compound **10** exacerbates this trend since the high yield is supported also by a lower depletion of previously synthetized reactant (which correlates with the reduction of previous waste).

As shown in Table 2, for the water-including EF values, water plays a relevant role in reducing efficiency in material preparation. Indeed, the EF of the *one-pot* C-H activation route approach demonstrated to be less influenced by water considerations. Divergence in EF values among the water-included and the water-excluded outcomes amplifies with the progressively increasing complexity of the molecules. Interestingly, results underline that even processes which do not involve depletion of water, like manufacturing of compounds **1** and **8**, exhibit dissimilar EFs. The reason arises from previous steps contribution in water consumption, proving again how EF, if suitably implemented, can represent an efficient instrument in molecular analysis recording memories of previous processes. The convergence of the EF values both in water inclusion and water exclusion for product **18**, instead, becomes obvious considering that water was not depleted in the process and the target molecule was produced only through commercially available reactants.

Finally, the EF values for **TTZ5** show a direct correlation with the high values obtained for intermediate **6**, since the final step of the synthesis is substantially identical for all routes. Regarding the overall yield for manufacturing **TTZ5** starting from compound **12** (Scheme S1), values of 4.90% and 3.75% are obtained for the C-H/Stille route and for the *one-pot* C-H activation route, respectively. In general, a significant improvement is obtained if compared to the original Suzuki-Miyaura route featuring a 0.81% overall yield. Comparing the two new synthetic protocols, the *one-pot* C-H activation route exhibits an inferior yield and higher EF values, despite an inferior number of reaction steps. The best explanation of this trend arises from the lower yield of production of the aldehydic precursor **6** using the *one-pot* C-H activation route (26%), in comparison with the overall yield of the conversion of thiazolothiazole **1** to precursor **6** using the C-H/Stille route (33%).

Concerning the overall financial burden in manufacturing **TTZ5**, it should be highlighted that costs are related not only to commercially available reactants, but also to intermediates which need to be previously synthetized. Table 3 reports the calculated overall costs for all synthetic routes. Details concerning the estimated cost of production of each intermediate are reported in the SI.

Table 3

The higher efficiency of the two new procedures resulted in a lower cost of the final product. Indeed, the cost of 3497.85 €/g calculated for the original process has been largely reduced to 850.11 and 1118.41 €/g for the C-H/Stille route and the one-pot C-H activation route, respectively. Again, this is related to the strong improvement of the Pd-catalyzed processes. Indeed, the most expensive steps in the previously reported synthesis were both the desymmetrization of diiodide **2** (cost of compound **4** – 1729.07 €/g) and the introduction of the acceptor moiety (cost of compound **6** – 3496.62 €/g), while desymmetrization of compound **1** was the most expensive step for both the C-H/Stille route and one-pot C-H activation route (800.70 and 1082.19 €/g, respectively). Furthermore, among all the reagents used to introduce the donor group, boronic ester **3** was the most expensive one (cost of compound **3**, 281.91 €/g *vs.* 88.03 €/g for Compound **9** and 75.25 €/g for Compound **10**).

Comparing the two optimized procedures, avoiding the use of reagent **10** and the preparation of compound **8** should have contributed, in the *one-pot* C-H activation route, to decrease the overall price of **TTZ5.** However, synthesis of the aldehydic precursor **6** in such route involves significant expenses due to the use of chromatographic purifications (costs for silica cartridge, petroleum ether and toluene amount to 78.92 €/g with the solvent contributing the most). Conversely, producing compound **6** from intermediates **10** and **8**, as in the C-H/Stille synthesis, involved major costs due to the high-price of production of these reactants, while compound **9** proved to be more economical. Starting material **1** was prepared following Scheme S1 from inexpensive reagents **13** and **14**, in turn prepared from commercially available very simple starting materials. On the other hand, compound **18** (Scheme S2), despite being obtained from commercially available chemicals, was responsible for a higher cost, mainly due to the need to isolate it through dedicated purification procedures.

Despite the general trend observed, that costs rise when more complex intermediates are used, this was not observed in the case of compound **19** and **10**. In this case, the simpler compound **19** (95.75 €/g) appears more expensive than compound **10** (75.25 €/g)(see SI), due to the fact that the latter is prepared by means of very efficient reaction steps and using inexpensive reagents.

Finally, most of the calculated costs of compounds **1** and **8** are due to the use of not commercially available precursors, which need to be prepared and purified by chromatographic procedures (41.06 €/g and 82.64 €/g represent the total cost of purification procedures for compounds **1** and **8**, respectively). Therefore, the economic burden is brought about first by the amount and complexity of employed intermediates as reactants, secondly by chromatographic costs and only in minimal part by commercially available reactants expense (with rare exceptions). Solvents for washings also contribute in enhancing the price per gram of the target molecule.

Table 4 reports the Eco Scale calculation outcomes. According to the definition of this semi-quantitative tool, results show a less negative value of Eco Scale for the one-pot C-H activation route approach, which correlates with improved human health and ecological compatibility.

Table 4

Penalty points for any single intermediate are provided in the SI. Regarding the score of the original Suzuki-Miyaura route, it should be noted that it is highly affected by the very low overall efficiency of the whole process, despite the penalty points pertaining to compound **2**, **3** and **4** are lower than those calculated for compounds **8** and **10**. The enhancement of 95.42 points in Eco scale between the C-

PAGE \* Arabic \*
MERGEFORMAT 3

H/Stille route and the *one-pot* C-H activation route represents a very interesting outcome since many common synthetic steps are shared by the two processes. This means that, according to the sensitivity of this green metric, some improvements are actually achieved in the *one-pot* C-H activation path, resulting in a decreasing of penalty points due to the lower number of reaction steps used in that process. Shortening a reaction path usually implies a reduction in the need of possible hazardous chemicals, special technical setup, temperature adjustment protocols as well as workup and purification steps. A strong contribution in this case is due to the possibility of avoiding the preparation and use of compound **10**, which results in a reduction of penalty points of a value of 56.

Low penalty points are also found for the syntheses of products **9** and **14**. Accordingly, the procedures used require few reagents, no temperature changes (the processes are carried out at room temperature) and avoid chromatographic purification, the most environmentally impacting procedure. In the case of compound **9**, a great portion of penalties is due to the use of dry chloroform and *N*-bromosuccinimide, which are both toxic chemicals, while in the case of intermediate **14** penalties come mostly from the need of using diethyl ether, a toxic and highly flammable solvent, and of cooling the reaction mixture to 0°C. All these factors negatively affect the Eco-scale score. Conversely, production of compound **8** has an acceptable environmental impact, which is once again mostly due to an efficient chromatographic purification protocol.

The most polluting processes involve the production of compound **18**, **19**, **16**, **10** and **1**. Penalties on intermediate **18** arise from of the need of using some hazardous reagents such as toluene, 1-hexanethiol, ethyl acetate, which are toxic and flammable, and 1,10-phenanthroline and copper iodide, which are toxic and dangerous for the environment. For each of these substances, having a double hazard symbol, penalty points should be doubled, thus contributing with a value of 10. In the case of compound **19**, in addition to toluene and diethyl ether, also aniline needs to be used, which is again classified as toxic and dangerous for the environment. Need of purification by column chromatography also downgraded the sustainability of its preparation. The most environmental impacting chemical of all the procedures is a 1.6 M solution of *n*-butyllithium in hexane, which is toxic, flammable and dangerous for the environment, and is used to prepare compound **16,** thus contributing with 15 points to the overall penalties for such intermediate. The same solution was also used to prepare intermediate **10**, but in this case lower penalty point are found thanks to the elimination of purification steps. Finally, the impact found for compound **1** is mainly due to chromatographic purification steps, microwave irradiation and the need to use *n*-butanol and THF, which are both classified as toxic and flammable, as well as chloranil, which is toxic and dangerous for the environment.

The last step for the preparation of **TTZ5** has been purposely excluded in the above detailed analysis, since it is performed almost in the same way in all the three procedures. However, detailed analysis on **TTZ5** shows that most penalties do not arise from the specific conditions used in the Knoevenagel condensation, but rather from consideration on the overall yield of the synthetic sequence. Specifically, in both routes only 23 penalty points are calculated, which attests to a good Eco-scale value.

Finally, it should be considered that the lower impact of the *one-pot* C-H activation process derives not only from the lower number of reaction steps, but also from slight improvements in the synthesis of the precursor **6**, comprising optimization of work-up and purification methods, avoidance of temperature adjustments steps and use of a less complicated technical setup.

In summary, we can conclude that most of the penalties for **TTZ5** production arise from safety concerns due to the use of some hazardous reagent. This means that the substitution of some reagents with greener alternatives would mostly minimize ecotoxicological impact, according to the Eco scale

PAGE \\* Arabic \\*
MERGEFORMAT 4

metric. Further improvement of green metric should originate from a careful choice of purification processes, i.e. minimization of column chromatography procedures and reduction of the amount of washing solvents. Costs, on the other hand, do not affect sustainability to a large extent. In this context, a specific attention should be put in limiting special technical setup requirements, reaction time and temperature adjustments steps.

A deeper assessment of the environmental sustainability of the synthetic routes for **TTZ5** production has been accomplished through the implementation of LCA. Figure 3 reports the eco-profile single scores comparison for all the compounds generated via the two alternative synthetic routes and the original one. It is evident that the eco-profiles of reactants and compounds generated by the C-H/Stille route and the *one-pot* C-H activation route perform better than those obtained via the original Suzuki-Miyaura route. More in detail, the analysis of the diagrams immediately reveals the major issue affecting the *one-pot* C-H activation procedure: in order to obtain 1 gram of the final product **TTZ5**, the mass balance principle required in LCA calculation leads to the demand of larger quantities of reactants, chemicals and solvents. This is mainly due to the reaction yield of the penultimate step (26% for the formation of compound **6**), for which a higher global single score (15.69 mPt) is obtained compared to the corresponding result in the C-H/Stille Route (2.08 mPt) due to the need of a larger amount of aldehydic precursor. Furthermore, this trend, although less pronounced, is present along the whole compound series in the *one-pot* C-H activation path.

Figure 3

The analysis of any single contributions highlights that electricity, solvents and metals are the major responsible of the environmental burden on all the impact categories. For instance, concerning solvents, the largest contribution on the single score value is given by toluene, with a consumption of 37.4 kg/g for the Suzuki-Miyaura route, 9.13 kg/g for the *one-pot* C-H activation route and 5.25 kg/g for the C-H/Stille route. This outcome highlights an interesting aspect of the revision of the manufacturing path via a *one-pot* direct arylation protocol (see SI): removal of the synthetic step for the isolation of compound **8** allows saving 1.3 kg/g of toluene, but this positive effect is totally counterbalanced, and even surpassed, by the quantity of toluene required to produce compound **6** directly from **1**, via the *one-pot* C-H activation route, due to the column chromatography carried out for purification (1.5 kg/g). Similar considerations can be expressed concerning the use of catalysts (palladium complexes) that affects mainly the impact category Acidification: compared to the $4.12 \cdot 10^{-5}$ `kg of Pd consumed for the Suzuki-Miyaura route,` a consumption of $7.94 \cdot 10^{-5}$ kg is required for the *one-pot* `C-H activation route, while the C-H/Stille route performs even better, as only` $4.04 \cdot 10^{-5}$ kg of metal are necessary.

Another important insight that can be derived from LCA calculation is the amount of direct and indirect energy consumption relative to the **TTZ5** production. In Figure 4, the CED indicator is used to show differences in terms of energy consumption between the three alternative synthetic routes. In general, a substantial improvement in the CED indicator performance is obtained compared to the original Suzuki-Miyaura route.

Figure 4

PAGE \* Arabic \*
MERGEFORMAT 3

In particular, for the C-H/Stille route, a consumption of 246 MJ (68.33 kWh) of electricity is required per gram of final product, while the energy embedded in all raw materials used accounts for 924 MJ. For the *one-pot* C-H activation route, these values increase, with a value of 563 MJ (156.38 kWh) of electricity required per gram of final product and 1417 MJ of energy embedded in all raw materials employed (see SI). Concerning the direct energy consumption, in the *one-pot* C-H activation route a portion of almost 30% (22.7 kWh) is relative to the generation of compound **6** (which requires stirring at about 100°C for 48 hours). Thus, from the LCA calculations we can claim that the difference in terms of CED between the two reaction paths is almost completely due to the global requirement of electricity and solvent (mainly toluene) which are necessary for the production of intermediate **6**. Possibly, a positive effect could be obtained if, with the same experimental setup, a larger amount of reactants and auxiliaries could be used thus producing more **TTZ5** for each reaction cycle. Indeed, a simplified sensitivity analysis on direct energy consumption conducted on the penultimate step allowed to highlight that an improvement of almost 2.5 mPt in the global single score value could be obtained if the electricity requirement for the preparation of compound **6** could be decreased up to 15 kWh.

## 4    Conclusions

In this work, two innovative synthetic protocols for the preparation of organic dye **TTZ5**, which has been successfully employed as a sensitizer for manufacturing DSSCs, are reported. The procedures rely on two different approaches based on a C-H activation/Stille cross-coupling sequence or on a *one-pot* double C-H activation sequence, and have been optimized to allow the production of **TTZ5** in gram scale. A mass-based green metrics and LCA combined approach has been employed to investigate the environmental sustainability of those two alternative synthetic routes, compared to the original **TTZ5** synthesis based on a classic Suzuki-Miyaura cross-coupling.

The comparison of the green metrics and LCA results highlights how both the new procedures allowed to complete the synthesis of the dye **TTZ5** in a more sustainable way than the previous one, considering the inferior production of waste, the lower costs and a smaller environmental impact. Despite a higher number of steps, the C-H/Stille route revealed to be more sustainable than the *one-pot* C-H activation one: this outcome is mainly highlighted by EF values and global LCA single score results (23.97 mPt and 47.35 mPt for the C-H/Stille route and the *one-pot* C-H activation route, respectively), even if the employment of toxic and/or flammable reagents such as n-butyllithium and tin-containing materials raised its Eco-scale value (– 470.55 *vs.* – 375.13 for the C-H/Stille route and the *one-pot* C-H activation route, respectively). In particular, the application of LCA showed that the drawback of the *one-pot* C-H activation route procedure is represented by raw material inputs for the chromatography setup: even though the number of purification operations decreases, the use of larger quantities of solvents significantly influences the environmental profile of the process, which is also strongly affected by the electricity consumption. However, despite the differences in the environmental profile of the two procedures, the possibility of carrying out the complete functionalization of TzTz **1** in just one step through two consecutive C-H activation reactions makes the *one-pot* route more attractive, from a synthetic point of view, for a lab scale preparation of **TTZ5**. In addition, such approach allows the easy and versatile synthesis of new potential thiazolothiazole-based dyes, since a rapid screening of new substituents could be easily performed by changing the donor and/or acceptor groups. However, the

outcomes of the present study and, in particular, the most relevant LCA results should be carefully taken into account to guide the preparation of new photosensitizers.

The analysis performed in this work demonstrates the benefit connected with the use of LCA in environmental sustainability assessment for obtaining a trustworthy evaluation of the eco-profile of products and processes, also at lab scale. Indeed, the intrinsic less comprehensive nature of green metrics could in some cases represent a limiting factor, especially in detecting crucial issues concerning the use of resources and energy.

## 5     References

A.T. Kearney Energy Transition Institute (2017). Solar Photovoltaic.

Allen, D. T., Hwang, B.-J., Licence, P., Pradeep, T., and Subramaniam, B. (201AD). Advancing the use of sustainability metrics. *ACS Sustain. Chem. Eng.* 3, 2359–2360.

Bravi, M., Parisi, M. L., Tiezzi, E., and Basosi, R. (2010). International journal of heat &amp; technology: Life cycle assessment of advanced technologies for photovoltaic panels production. *Int. J. Heat Technol.* 28.

Cespi, D., Fabrizio, P., Esmeralda, N., Cucciniello, R., and Cavani, F. (2019). "LCA integration within sustainability metrics for chemical companies," in *Life Cycle Assessment In The Chemical Product Chain – Challenges, Methodological Approaches And Applications*, eds. S. Maranghi and C. Brondi (Springer).

Dessì, A., Calamante, M., Mordini, A., Peruzzini, M., Sinicropi, A., Basosi, R., et al. (2014). Organic dyes with intense light absorption especially suitable for application in thin-layer. *Chem. Commun.* 50, 13952–13955. doi:10.1039/c4cc06160h.

Dessì, A., Calamante, M., Mordini, A., Peruzzini, M., Sinicropi, A., Basosi, R., et al. (2015). Thiazolo[5,4-d]thiazole-based organic sensitizers with strong visible light absorption for transparent, efficient and stable dye-sensitized solar cells. *RSC Adv.* 5, 32657–32668. doi:10.1039/c5ra03530a.

Dessì, A., Monai, M., Bessi, M., Montini, T., Calamante, M., Mordini, A., et al. (2018). Towards Sustainable H2 Production: Rational Design of Hydrophobic Triphenylamine-based Dyes for Sensitized Ethanol Photoreforming. *ChemSusChem* 11, 793–805. doi:10.1002/cssc.201701707.

EC COM(2019) 190 final (2019). Circular Economy Action Plan. Available at: http://ec.europa.eu/environment/circular-economy/index_en.htm.

Eckelman, M. J., Zimmerman, J. B., and Anastas, P. T. (2008). Toward green nano: E-factor analysis of several nanomaterial syntheses. *J. Ind. Ecol.* 12, 316–328. doi:10.1111/j.1530-9290.2008.00043.x.

EU (2018). Directive (EU) 2018/2001 of the European Parliament and of the Council on the promotion of the use of energy from renewable sources. *Off. J. Eur. Union* 2018, 82–209. Available at: https://eur-lex.europa.eu/legal-content/EN/TXT/PDF/?uri=CELEX:32018L2001&from=EN.

European Commission (2010a). *International Reference Life Cycle Data System (ILCD) handbook: Framework and Requirements for Life Cycle Impact Assessment Models and Indicators*. doi:10.2788/38719.

European Commission (2010b). *International Reference Life Cycle Data System (ILCD) handbook: Framework and Requirements for Life Cycle Impact Assessment Models and Indicators*. doi:10.2788/38719.

F., R., Sheldon, R. A., and H., S. C. (2015). Overcoming Barriers to Green Chemistry in the

PAGE \* Arabic \* MERGEFORMAT 3

Pharmaceutical Industry - The Green Aspiration Level$^{TM}$ Concept. *Green Chem.* 17, 752–768.

Frischknecht, R., Jungbluth, N., Althaus, H.-J., Bauer, C., Doka, G., Dones, R., et al. (2007). Implementation of Life Cycle Impact Assessment Methods. ecoinvent report No. 3, v2.0. Swiss Centre for Life Cycle Inventories. 1–151. Available at: https://www.ecoinvent.org/files/201007_hischier_weidema_implementation_of_lcia_methods.pdf.

Gałuszka, A., Migaszewski, Z. M., Konieczka, P., and Namieśnik, J. (2012). Analytical Eco-Scale for assessing the greenness of analytical procedures. *TrAC - Trends Anal. Chem.* doi:10.1016/j.trac.2012.03.013.

Gong, J., Sumathy, K., Qiao, Q., and Zhou, Z. (2017). crossmark. *Renew. Sustain. Energy Rev.* 68, 234–246. doi:10.1016/j.rser.2016.09.097.

Grisorio, R., Marco, L. De, Baldisserri, C., Martina, F., Serantoni, M., Gigli, G., et al. (2015). Sustainability of Organic Dye-Sensitized Solar Cells: The Role of Chemical Synthesis. doi:10.1021/acssuschemeng.5b00108.

Hagfeldt, A., Boschloo, G., Sun, L., Kloo, L., and Pettersson, H. (2010). No Title. *Chem. Rev.* 110, 6595–6663.

International Organization for Standardization (2006). ISO 14040:2006 - Environmental management - Life cycle assessment - Principles and framework.

Li, G. C., Anastas, P., and Sheldon, R. A. (2012). Green Chemistry themed issue Fundamentals of green chemistry : efficiency in reaction design w z. doi:10.1039/c1cs15219j.

Lin, P. H., Lu, T. J., Cai, D. J., Lee, K. M., and Liu, C. Y. (2015). Connecting Direct C-H Arylation Reactions with Dye-Sensitized Solar Cells: A Shortcut to D-A-π-A Organic Dyes. *ChemSusChem* 8, 3222–3227. doi:10.1002/cssc.201500993.

Lu, T. J., Lin, P. H., Lee, K. M., and Liu, C. Y. (2017). End-Capping Groups for Small-Molecule Organic Semiconducting Materials: Synthetic Investigation and Photovoltaic Applications through Direct C–H (Hetero)arylation. *European J. Org. Chem.* 2017, 111–123. doi:10.1002/ejoc.201601257.

Luceño-Sánchez, J. A., Díez-Pascual, A. M., and Capilla, R. P. (2019). Materials for photovoltaics: State of art and recent developments. *Int. J. Mol. Sci.* 20. doi:10.3390/ijms20040976.

Maranghi, S., Parisi, M. L., Basosi, R., and Sinicropi, A. (2019). Environmental Profile of the Manufacturing Process of Perovskite Photovoltaics: Harmonization of Life Cycle Assessment Studies. *Energies* 12, 3746. doi:10.3390/en12193746.

NREL (2019). Best Research-Cell Efficiency Chart. Available at: https://www.nrel.gov/pv/cell-efficiency.html.

Parisi, M. L., Maranghi, S., and Basosi, R. (2014). The evolution of the dye sensitized solar cells from Grätzel prototype to up-scaled solar applications: A life cycle assessment approach. *Renew. Sustain. Energy Rev.* 39. doi:10.1016/j.rser.2014.07.079.

Parisi, M. L., Maranghi, S., Sinicropi, A., and Basosi, R. (2013). Development of dye sensitized solar cells: A life cycle perspective for the environmental and market potential assessment of a renewable energy technology. *Int. J. Heat Technol.* 31.

Parisi, M. L., Maranghi, S., Vesce, L., Sinicropi, A., Di Carlo, A., and Basosi, R. (2019). Prospective Life Cycle Assessment of Third-Generation Photovoltaics at the Pre-Industrial Scale: A Long-Term Scenario Approach. *Renew. Sustain. Energy Rev.* submitted.

Pini, M., Rosa, R., Neri, P., and Ferrari, A. M. (2019). "LCA Application to Chemical Synthesis at Laboratory Scale," in *Life Cycle Assessment In The Chemical Product Chain – Challenges, Methodological Approaches And Applications*, eds. S. Maranghi and C. Brondi (Springer), in

PAGE \* Arabic \*
MERGEFORMAT 4

press.

Polman, A., Knight, M., Garnett, E. C., Ehrler, B., and Sinke, W. C. (2016). Photovoltaic materials: Present efficiencies and future challenges. *Science (80-. ).* 352. doi:10.1126/science.aad4424.

Sheldon, R. A. (2016a). Green chemistry and resource e ffi ciency : towards a green economy. 3180–3183. doi:10.1039/c6gc90040b.

Sheldon, R. A. (2016b). The E factor 25 years on: the rise of green chemistry and sustainability. *Green Chem.* 19, 18–43. doi:10.1039/c6gc02157c.

Sheldon, R. A. (2018). Metrics of Green Chemistry and Sustainability: Past, Present, and Future. *ACS Sustain. Chem. Eng.* 6, 32–48. doi:10.1021/acssuschemeng.7b03505.

Standardization, I. O. for (2006). ISO 14044:2006 Environmental management -- Life cycle assessment -- Requirements and guidelines.

Van Aken, K., Strekowski, L., and Patiny, L. (2006). EcoScale, a semi-quantitative tool to select an organic preparation based on economical and ecological parameters. *Beilstein J. Org. Chem.* 2, 1–7. doi:10.1186/1860-5397-2-3.

Wernet, G., Bauer, C., Steubing, B., Reinhard, J., Moreno-Ruiz, E., and Weidema, B. (2016). The ecoinvent database version 3 (part I): overview and methodology. *Int. J. Life Cycle Assess.* doi:10.1007/s11367-016-1087-8.

Zani, L., Dessì, A., Franchi, D., Calamante, M., Reginato, G., and Mordini, A. (2019). Transition metal-catalyzed cross-coupling methodologies for the engineering of small molecules with applications in organic electronics and photovoltaics. *Coord. Chem. Rev.* doi:10.1016/j.ccr.2019.04.007.

## 6    Author Contributions

M.L.P, A.D., L.Z., A.M., R.B., G.R. and A.S. contributed conception and design of the study; M.L.P. S.M and S.M. performed the green metrics and LCA analysis, A.D., M.C. and L.Z. performed the synthesis, M.L.P, A.D., and A.S. wrote the first draft of the manuscript. All authors contributed to manuscript revision, read and approved the submitted version.

## 7    Acknowledgments

## 8    Supplementary Material

The Supplementary Material for this article can be found online at:

PAGE \* Arabic \* MERGEFORMAT 3

**Table 1. Comparison of the three alternative routes for the preparation of TTZ5 in terms of yield, number of steps and required chromatographic purifications.**

| *Route* | Yield (%)[a] | N° Steps[a] | N° chromatographic purifications[a] |
|---|---|---|---|
| Suzuki-Miyaura | 9% | 4 (+1)[b] | 2 (+1)[b] |
| C-H/Stille | 32% | 3 (+1)[b] | 2 |
| One-pot C-H Activation | 25% | 2 | 1 |

[a] From compound **1** to final product **TTZ5**. [b] In comparison with the *One-pot* C-H Activation Route, one step more is necessary for the preparation of the organometallic reagents (boronic ester **3** and stannane **10** for Suzuki-Miyaura Route and C-H/Stille Route, respectively).

**Table 2. EF results for the C-H/Stille route and the one-pot C-H activation route procedures compared to the original Suzuki-Miyaura route**

| *Product* | Suzuki-Miyaura Route | | C-H/Stille Route | | One-pot C-H Activation Route | |
|---|---|---|---|---|---|---|
| | EF Water Excluded | EF Water Included | EF Water Excluded | EF Water Included | EF Water Excluded | EF Water Included |
| Compound 13 | 27.31 | 29.23 | 27.31 | 29.23 | 27.31 | 29.23 |
| Compound 14 | 47.92 | 52.09 | 47.92 | 52.09 | 47.92 | 52.09 |
| Compound 15 | 562.50 | 600.02 | 562.50 | 600.02 | 562.50 | 600.02 |
| Compound 16 | 1906.86 | 2000.38 | 1906.86 | 2000.38 | 1906.86 | 2000.38 |
| Compound 1 | 7773.36 | 7971.50 | 7773.36 | 7971.50 | 7773.36 | 7971.50 |
| Compound 2 | 6354.72 | 6513.72 | - | - | - | - |
| Compound 8 | - | - | 21307.58 | 21740.55 | - | - |
| Compound 18 | 405.79 | 405.79 | 405.79 | 405.79 | 405.79 | 405.79 |
| Compound 19 | 1950.84 | 2018.41 | 1950.84 | 2018.41 | 1950.84 | 2018.41 |
| Compound 9 | 1817.77 | 1962.55 | 1817.77 | 1962.55 | 1817.77 | 1962.55 |
| Compound 3 | 5712.83 | 6509.90 | - | - | - | - |
| Compound 4 | 49103.81 | 50238.93 | - | - | - | - |
| Compound 10 | - | - | 1583.55 | 2271.85 | - | - |
| Compound 6 | 94719.08 | 96737.07 | 19080.93 | 20240.26 | 28873.89 | 29630.56 |
| TTZ5 | 93815.76 | 96384.21 | 20654.34 | 26505.92 | 28924.85 | 30250.26 |

**Table 3. TTZ5 price estimate results for the C-H/Stille route and the one-pot C-H activation route procedures compared to the original Suzuki-Miyaura route**

| *Product* | Suzuki-Miyaura Route | | C-H/Stille Route | | One-pot C-H Activation Route | |
|---|---|---|---|---|---|---|
| | *Synthetic step total cost (€)* | *Compound cost (€/g)* | *Synthetic step total cost (€)* | *Compound cost (€/g)* | *Synthetic step total cost (€)* | *Compound cost (€/g)* |
| TTZ5 | 2413.52 | 3497.85 | 586.58 | 850.11 | 771.70 | 1118.41 |

**Table 4. Eco Scale results the original Suzuki-Miyaura route, the C-H/Stille route and the one-pot C-H activation route**

| *Synthetic Route* | Eco Scale Rate |
|---|---|
| Suzuki-Miyaura | −474.59 |
| C-H/Stille | −470.55 |
| One-pot C-H activation | −375.13 |
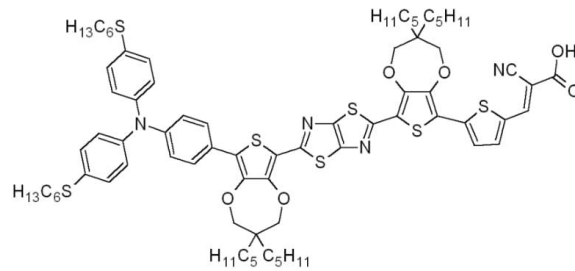
Figure 1. Structure of dye TTZ5
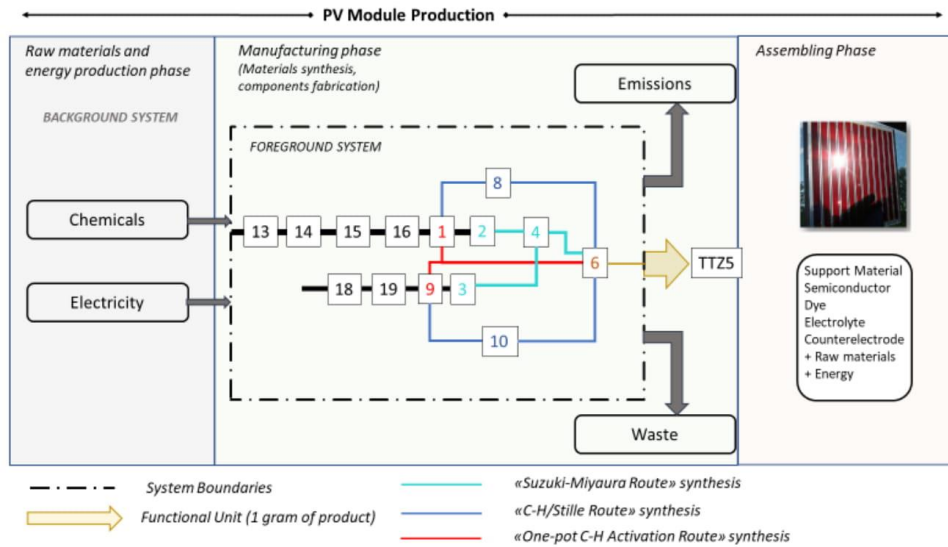


**Figure 2. PV module production process: sketch of the synthetic routes and system boundaries of this study**
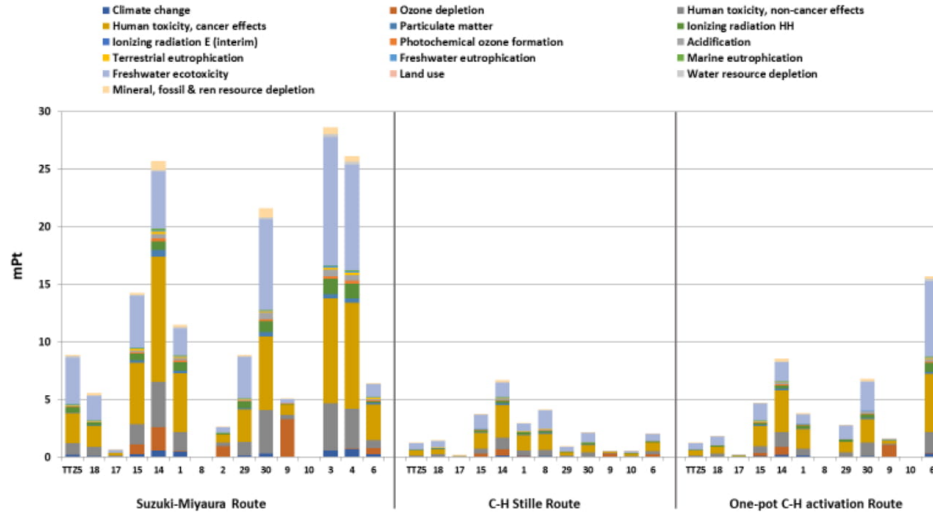
**Figure 3. Single score results for the original and the two new procedures (LCIA method: ILCD 2011 Midpoint+ V1.10 / EC-JRC Global, equal weighting)**
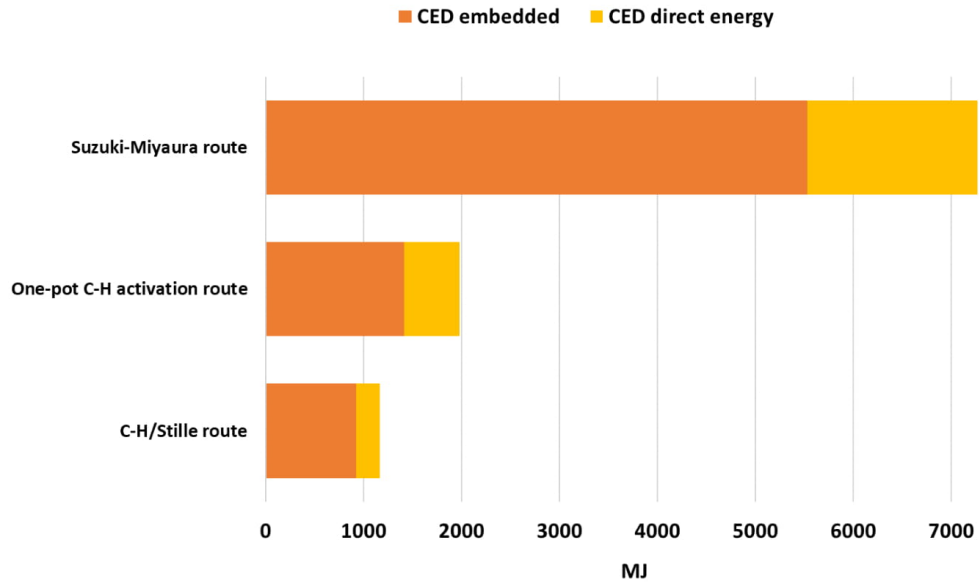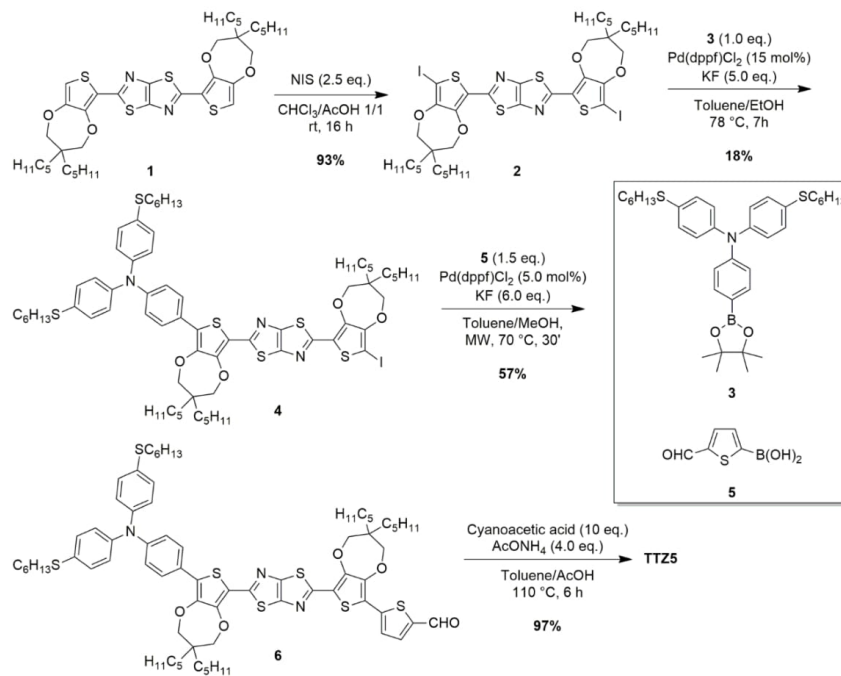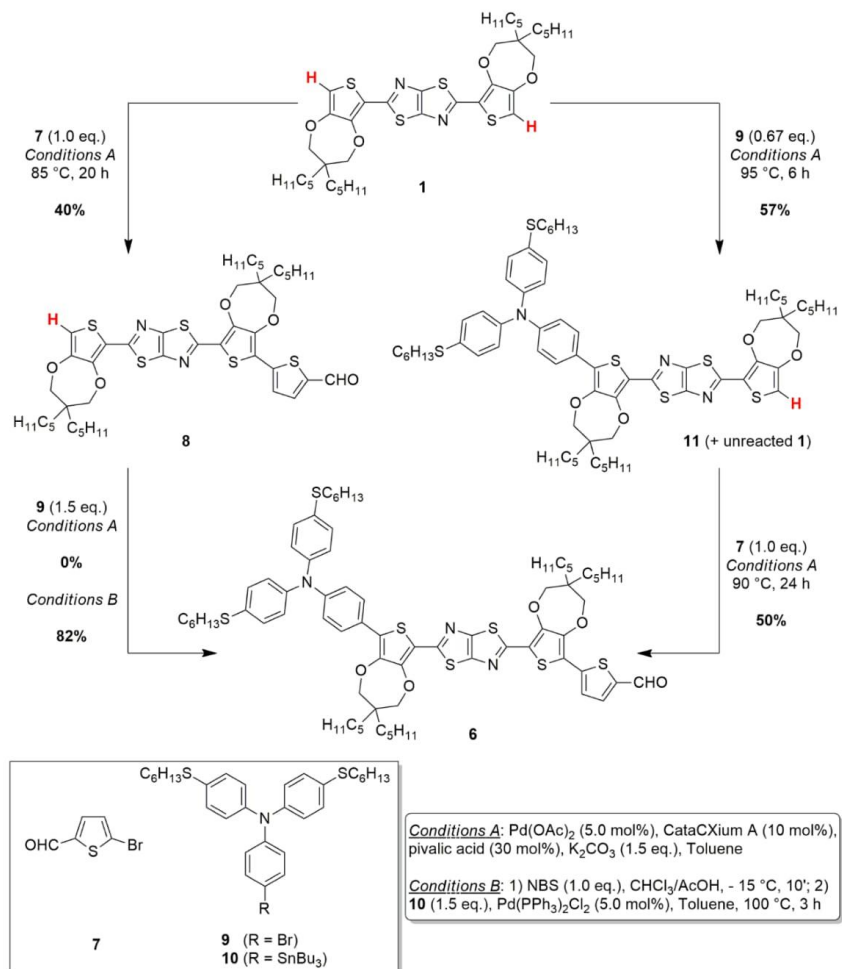


**Figure 4. CED indicator results for the original and revised procedures**
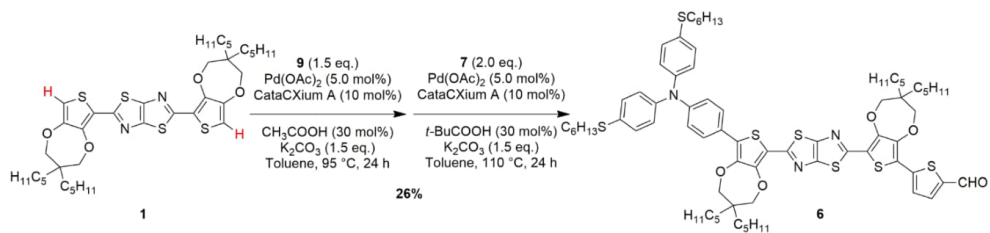
PAGE  \* Arabic  \*
MERGEFORMAT 3

Scheme 1. Functionalization of TzTz **1** with donor and acceptor groups through Suzuki-Miyaura cross-couplings.

Scheme 2. C-H activation/Stille-Migita route (on the left) and C-H activation route (on the right) for the conversion of the starting material **1** to the advanced intermediate **6**.

Scheme 3. *One-pot* C-H activation route for the conversion of the starting material **1** to the advanced intermediate **6**.